EXAMINATION OF PLANT WATER STRESS AND GROUNDWATER RECHARGE IN THE MOUNT LOFTY RANGES: AN ISOTOPIC PERSPECTIVE

Xiang Xu

Submitted as a requirement in full

for the degree of

Doctor of Philosophy

in the

School of the Environment

Flinders University of South Australia

Adelaide, South Australia

October 2014

To my husband

Guoqiang

TABLE OF CONTENTS

LIST OF TABLES

LIST OF FIGURES

SUMMARY

Climate change may impact both water resources and terrestrial ecosystem structures. For a better understanding of the hydrological and ecological responses to future climate change, it is important to know how recharge relates to climate conditions, how vegetation uses rain water of strong seasonal variation, and how much stress vegetation experienced under current climate conditions. This dissertation is to examine these issues from isotopic perspective based on a study area with a strong hydroclimatic gradient induced by topographic relief.

Upland catchments usually are not only composed of bedrock aquifers, thick fracture-rock vadose zone and thin soil, but also vegetation cover. Experiments were performed on two contrasting hillslopes in a native vegetated catchment – Mount Wilson, to study plant responses to environmental conditions (primarily water stress). Significant seasonal variations in leaf $\delta^{13}C$ are observed for both studied C_3 tree genus up to 1.7‰ for *Eucalyptus* Leucoxylon and up to 2.7‰ for *Acacia Pycnantha.* Temporally, the linear correlation coefficients between leaf $\delta^{13}C$ and aridity index (PET/P) can be as high as 0.45. Spatially the correlation coefficient is 0.34 for *E*ucalyptus species. This result suggests that PET/P may be applied to quantify the relationship between leaf $\delta^{13}C$ and plant water stress.

Stable isotope water composition of precipitation is of importance as input characterization to trace recharge sources of groundwater. In vegetated catchments, the input water isotopic composition is altered from precipitation. Based on one year throughfall monitoring for both ^{18}O and *d*-excess at two vegetated surfaces in Kuitpo Forest, South Australia, the results indicate that isotopic alteration can be significant in densely vegetated catchments and is important for hydrograph separation studies, but can be negligible for tracing groundwater recharge sources.

Water isotopic composition is also used to examine how vegetation uses rain water in a typical Mediterranean climate. One-year monitoring of $\delta^{18}O$ and $\delta^{2}H$ in twig water is applied to understand the root zone moisture replenishment. The response of $\delta^{18}O$ and $\delta^{2}H$ of twig water to the rain events indicates that landscape water storage capacity of winter rain is important for plant growth and survival during dry summer. The results of the $\delta^{18}O$ and $\delta^{2}H$ of groundwater had a mean value -5.1‰ and -27.5‰ respectively and that of throughfall in the wet season had a mean value -5.1(±1.7)‰ and -23.4(± 13.3)‰ correspondingly. They indicate that groundwater recharge is dominated by events in the wet season.

Extended from this small catchment, water isotopic composition is used to examine groundwater recharge seasonality over the whole Mount Lofty Ranges. Based on this understanding, an improved storage-discharge relationship-based method (SQR) is proposed to estimate groundwater recharge for mountainous catchments. Net catchment recharge estimates varies between 1.3 mm/year and 13.5 mm/year. Especially, recharge estimates from catchment Onkaparinga River at Hahndorf using SQR method is (7.0 mm/year) close with that from the independent chloride mass balance estimation (3 mm/year). Good correlation between annual direct water-table recharge and aridity index suggests that this method can be used to examine dynamic responses of groundwater recharge to the climate conditions in mountainous regions.

DECLARATION

I certify that this thesis does not incorporate without acknowledgment any material previously submitted for a degree or diploma in any university; and that to the best of my knowledge and belief it does not contain any material previously published or written by another person except where due reference is made in the text.

ACKNOWLEDGEMENTS

I have received assistance from so many people and agencies during my four-year study of Ph.D. Without their help, this dissertation would not have been possible.

First, I want to acknowledge my supervisor, Dr. Huade Guan for his time, effort, patience and care to shape all the chapters in this dissertation. Especially, I am kind of lost in the first two years of study but Huade never gave me up. I have learned from coding to think critically from Huade. Dr. Grzegorz Skrzypek gave me many useful suggestions about the sampling design and sample analysis. Without his help, chapter 2 and chapter 4 could not be finished. Dr. Craig T. Simmons has triggered my thoughts to think more broadly in research. Dr. John Hutson taught me a lot soil related knowledge. Dr Hoori Ajami who is the author proposed the method for recharge estimation, has helped me so much to finish the chapter 5.

Thanks to Daniel Jardine, Douglas Ford, Sara Lock, Gail Jackson, and Jodie Walker to help me and teach me to do isotope analysis in different kinds of materials. I have bothered these people so much to solve the unexpected problems in using different laboratory equipment. Thanks to Bill Drury, Wayne Peacock for their technical support of rain water collectors.

I would like to acknowledge Post-Doctoral Fellow Hugo Gutierrez-Jurado and Yuting Yang and my fellow students in our group, Hailong Wang, Zijuan Deng, Robert Andrew, Yunquan Wang and Saeedeh Gharib Choobary for the assistance of field work and the happy time we shared with each other. Thanks to Langdon Badger for the access to the field site of Mount Wilson. Thanks to Ashleigh Pitman from Willunga Environment Centre provided identification of the tree species. Thanks to Peter Baylis from Department for Water who gave me the permission of groundwater sampling.

Thanks to my parents for their selfless love in the past 27 years. Thanks to my friend Dongmei Han for taking care of me so much in the fourth year. Thanks to all the people who spend time with me in the four-year study in Adelaide.

Thanks to China Scholarship Council for the financial aid. This dissertation study was supported by National Centre for Groundwater Research and Training, School of the Environment of Flinders University of South Australia.

Adelaide

15 Oct 2014

CHAPTER 1 INTRODUCTION

1.1 Introduction

Climate changes may cause alterations of water resources (Vörösmarty *et al*., 2000) and terrestrial ecosystem structures (Walther *et al*., 2002). There is a likely increase in the global severity of hydrological droughts in the 21st century from the results of a global multi-model experiment (Prudhomme *et al*., 2014). For a better understanding of the hydrological and ecological responses to climate change, it is important to know how recharge relates to climate conditions, how vegetation uses rain water of strong seasonal variation, and under how much stress vegetation experiences under current climate conditions. Therefore, the aim of this dissertation is to 1) examine the responses of recharge to climate conditions with an improved method for groundwater recharge estimation, 2) quantify vegetation water stress and 3) trace root water-uptake with an origin from precipitation based on cases in upland catchments in this study. Isotopic methods are used to examine all these issues.

Upland catchments in mountain areas provide significant freshwater to adjacent lowland basins (Manning and Solomon 2005; Viviroli *et al*., 2007; Wilson and Guan, 2004). They are important sources of water for both human activities including irrigation and grazing, and environmental services such as reservation of native vegetation (UN, 1998). Because of their importance for sustainable water resources supply and a better environmental resources management, these catchments have gained a broad range of studies to understand hydrological processes and their interactions with vegetation.

One of the biggest unknowns in hydrological components in the upland catchments is groundwater recharge. Due to complex hydrogeological and hydrometeorological conditions and limited observational data (Green *et al*., 2011; Manning and Solomon, 2005; Taylor *et al*., 2012), it has long been a challenge to estimate groundwater recharge in

mountain catchments (Cook *et al*., 2003; Flint *et al*., 2002; Scanlon *et al*., 2006; Wilson and Guan, 2004). Different methods such as groundwater models and tracer based approaches like chloride mass balance (CMB) can be applied to estimate groundwater recharge for these catchments. However, scarcity of observation wells and hydrogeological complexities of bedrock aquifers have caused practical difficulties to apply groundwater models. In areas of significant vegetation cover changes, the most commonly used tracer-based method CMB likely becomes inapplicable. In addition (Guan *et al*., 2013), spatial variability related uncertainties have degraded the reliability of tracer based techniques. These techniques often lump the recharge over a relatively long period, resulting recharge estimation too coarse to reveal the dynamic response to interannual climate variability. Therefore, an alternative method which is relatively easy to use and representative across a catchment is needed.

Moreover, these catchments usually are not only composed of bedrock aquifers, thick vadose zone made of fracture rock and thin soil but also (plantation and native) vegetation cover (Wilson and Guan, 2004). Vegetation, which is an inherent element and relies on water sources of upland catchments, its responses to climate conditions like water stress and its effects on hydrological processes cannot be neglected.

Improved understanding of linkage between vegetation and environment may lead to improvement of groundwater recharge estimation (Sandvig and Phillips, 2006). It is necessary to study the plant responses to water stress when drought induced tree mortality has been found all around the world (Allen *et al*., 2010). Accumulating effects on plant photosynthesis from environmental conditions which is usually the water availability, can be related to carbon isotope ratio $^{13}C/^{12}C$ of leaves (expressed as leaf $\delta^{13}C$), particularly for C_3 species. Previous studies suggest that leaf $\delta^{13}C$ is correlated with mean annual precipitation over a range of climate conditions with mean annual precipitation from

100 to about 2000 mm (Diefendorf *et al*., 2010; Cernusak *et al*., 2011; Miller *at al*., 2001; Schulze *et al*., 1998; Schulze *et al*., 2006; Sterwart *et al*., 1995; Turner *et al*., 2008; Wang *et al*., 2010). The relationship has been used for paleoclimate reconstruction. However, this relationship appears to be weak in Europe and northern Australia indicating the complexity in the relationship between leaf $\delta^{13}C$ and climate conditions. This calls for more detailed examination of using leaf $\delta^{13}C$ for water stress quantification. What is the seasonal variability of leaf $\delta^{13}C$? What is the effect of topography on leaf $\delta^{13}C$? Is there an alternative index instead of precipitation that can be used to quantify the relationship between leaf $\delta^{13}C$ and plant water stress?

A better quantification of groundwater recharge requires a good understanding of groundwater recharge mechanisms. The oxygen isotope ratio $^{18}O/^{16}O$ (expressed as $\delta^{18}O$) and hydrogen isotope ratio $^{2}H/^{1}H$ (expressed as $\delta^{2}H$) of precipitation is often used as input characterization to trace recharge sources of groundwater, hydrograph separation, and paleoclimate reconstruction. Comparing $\delta^{18}O$ and $\delta^{2}H$ of groundwater with that of possible water sources and local meteoric water line becomes the standard way to understand the main sources of groundwater recharge (Clark and Fritz, 1997; Guan *et al*., 2009). However, it has not been well understood that how much precipitation isotopic composition is altered by vegetation canopy when throughfall rather than precipitation is the main water inputs in vegetated area, and how this alteration varies with different vegetation covers.

$\delta^{18}O$ and $\delta^{2}H$ of stem or twig of the plants are commonly applied in previous studies to trace sources of plant water use (e.g. Dawson and Ehleringer, 1993; Ehleringer and Dawson, 1992) and partition evapotranspiration (e.g. Brunel *et al*., 1997; Yepez *et al*., 2005; Good *et al*., 2014). Meanwhile, $\delta^{18}O$ and $\delta^{2}H$ of twig (or stem) water which reflect the mixed isotopic compositions from different water sources can be applied to understand details of root zone moisture replenishment and groundwater recharge. The simple

assumption that no fractionation happens in $\delta^{18}O$ and $\delta^{2}H$ during root water uptake has been verified in several laboratory and field experiments (Wershaw *et al*., 1966; White *et al*., 1985; Zimmermann *et al*., 1967). However, significant hydrogen isotope fractionation during root water uptake was observed by both Lin and Sternberg (1993) and Ellsworth and Williams (2007). This controversy poses a question on whether $\delta^{2}H$ can be used to trace plant water use.

As one important water source area, the Mount Lofty Ranges of South Australia provide about 60% of water requirements to support a population of 101,000 in 160 towns and 25,000 hectares of irrigated agriculture from the report of South Australian Government (www.environment.sa.gov.au). Furthermore, native vegetation, which is also supported by water source of the Mount Lofty Ranges, is vital for the health and prosperity of the ecosystems, communities and natural resource-based industries. Thus the aim of this dissertation is to investigate environmental stress (particularly water stress) on native vegetation, vegetation precipitation use, and groundwater recharge characteristics using isotopic tracers. This dissertation is going to answer the following research questions in upland catchments using the Mount Lofty Ranges as an example. Seasonal and inter-event variability of rain isotopic composition in this area (Guan et al. 2009, 2013), provides a good tool to trace how rain contributes to vegetation water use and groundwater recharge. Specific scientific questions are:

1) Is leaf $\delta^{13}C$ relevant to and can be used as an indicator for the water stress on typical native vegetation in South Australia?

2) How does vegetation cover, including both plantation and native vegetation, alter $\delta^{18}O$ and $\delta^{2}H$ in throughfall? Is this modification significant in terms of using $\delta^{18}O$ and $\delta^{2}H$ to study groundwater recharge sources, hydrograph separation and paleoclimate reconstruction?

3) How do trees use precipitation water in a native vegetation catchment with a Mediterranean climate? What does this imply for root-zone moisture replenishment and groundwater recharge?

4) How can we quantify groundwater recharge of upland catchments using the existing observation data, e.g. daily streamflow records?

More specifically, in Chapter 2, we study plant water stress based on one year monitoring data of $\delta^{13}C$ of the native tree species on two contrasting hillslopes of Mount Wilson, a typical native vegetated catchment in the Mount Lofty Ranges. From the investigation, we have observed significant seasonal variations of leaf $\delta^{13}C$ of two species, *Eucalyptus leucoxylon* and *Acacia pycnantha*, and spatial variations due to slope orientations and varying local hydrological conditions. To better quantify the relationship between leaf $\delta^{13}C$ and plant water stress temporally and spatially, we apply aridity index, which is the ratio of potential evapotranspiration to precipitation (PET/P), instead of precipitation that has been commonly used.

In chapter 3, we investigate the isotopic composition of throughfall that may have been altered by canopy in two typical vegetation surfaces, pine plantation and native eucalyptus forest including *Eucalyptus camaldulensis*, *Eucalyptus leucoxylon* and *Eucalyptus baxteri* in the Kuitpo Forest in the Mount Lofty Ranges. From this study, we synthesize a conceptual framework to understand the mechanisms leading to alteration of precipitation isotopic composition due to vegetation cover. The framework serves as a useful tool for studying canopy interception isotopic effects through intra-event selection, partial evaporation and inter-event selection. We also evaluate the significance of throughfall isotopic variations in the studies of groundwater recharge sources, hydrograph separation and paleoclimate reconstruction.

In chapter 4, we examine seasonal plant water use and its response to rain events using $\delta^{18}O$ and $\delta^{2}H$ of twig with an experiment on the two contrasting hillslopes in the Mount Wilson catchment. In this study, I monitored the water stable isotopic composition of the twigs monthly for one year. From the results, winter rain provides most moisture for tree water use. These results also indicate that landscape water storage capacity of winter rain is important for plant growth and survival during dry summer. I also generalized two typical patterns of $\delta^{18}O$ and $\delta^{2}H$ of tree water use with or without hydrogen fractionation by root water uptake. By taking advantages of the comparisons between the two hillslopes of contrasting aspects with one-year monitoring $\delta^{18}O$ and $\delta^{2}H$ of throughfall and twig water, the extremely low slope of the twig water line suggested that except for evaporation other process (e.g. hydrogen fractionation) may happen during the root water uptake.

Based on the understanding of groundwater recharge gained from the above water isotopic study, in chapter 5, an improved method based on the storage-discharge relationship is proposed for groundwater recharge estimation in six upland catchments of the Mount Lofty Ranges. The improvement from the original model includes that groundwater discharge in dry seasons is considered in the improved method to estimate net catchment recharge, and net subsurface lateral outflow from the catchment is considered in the water balance equation. We compare the results from this improved method with that from chloride mass balance (CMB) method. We also examine dynamic responses of groundwater recharge to the climate conditions in the study area.

In chapter 6, the main results and findings are summarized. The role of $\delta^{13}C$, $\delta^{18}O$ and $\delta^{2}H$ in ecohydrological studies are discussed. Future work following this dissertation is recommended.

References

Allen, C.D., A.K. Macalady, H. Chenchouni, D. Bachelet, N. McDowell, M. Vennetier, T.

Kitzberger, A. Rigling, D.D. Breshears, E.H. Hogg, P. Gonzalez, R. Fensham, Z. Zhang, J. Castro, N. Demidova, J-H. Lim, G. Allard, S.W. Running, A. Semerci, N. Cobb., 2010. A global overview of drought and heat-induced tree mortality reveals emerging climate change risks for forests. *Forest Ecol. Manag*. 259: 660–684.

Brunel, J-P., G.R. Walker, J.C. Dighton, B. Monteny., 1997. Use of stable isotopes of water to determine the origin of water used by the vegetation and to partition evaporatranspiration. A case study from HAPEX-Sahel. *J. Hydrol.* 188-189: 466-481.

Cernusak, L.A., L.B. Hutley, J. Beringer, J,A.M. Holtum, B.L. Turner, 2011. Photosynthetic physiology of eucalytptsalong a sub-continental rainfall gradient in northern Australia. *Agric. For. Meteorol.* 151: 1462-1470.

Clark, I.D., P. Fritz., 1997. Environmental Isotopes in Hydrogeology. CRC Press/Lewis Publishers, pp 35-60.

Cook, P. G., 2003. A guide to regional groundwater flow in fractured rock aquifers, Seaview Press, Adelaide.

Dawson, T.E., J.R. Ehleringer., 1993. Isotopic enrichment of water in the 'woody' tissues: Implications for plant water source, water uptake, and other studies which use the stable isotopic composition of cellulose. *Geochim. Cosmochim. Acta*. 57: 3487-3492.

Diefendorf, A.F., K.E. Mueller, S.L. Wing, P.L. Koch, K.H. Freeman, 2010. Global patterns in leaf ^{13}C discrimination and implications for studies of past and future climate. *Proc. Natl. Acad. Sci.*107 (13): 5738-5743.

Ehleringer, J.R., Dawson, T.E., 1992. Water uptake by plants: pespectives from stable isotope composition. *Plant Cell Environ*. 15: 1073-1082.

Ellsworth, P.Z., D.G. Williams., 2007. Hydrogen isotope fractionation during water uptake by woody xerophytes. *Plant Soil.* 291: 93-107.

Flint, A.L., L.E. Flint, E. M. Kwicklis, J.T. Fabryka-Martin, G.S. Bodvarsson., 2002. Estimating recharge at Yucca Mountain, Nevada, USA: comparison of methods. *Hydrogeol J.* 10:180–204.

Green, T. R., M. Taniguchi, H. Kooi, J. J. Gurdak, D. M. Allen, K. M. Hiscock, H. Treidel, A. Aureli., 2011. Beneath the surface of global change: Impacts of climate change on groundwater. *J. Hydrol*. 405(3-4), 532-560.

Good, S. P., K. Soderberg, K. Guan, E. G. King, T. M. Scanlon, K. K. Caylor., 2014. δ^2H isotopic flux partitioning of evapotranspiration over a grass field following a water pulse and subsequent dry down. *Water Resour. Res.* 50: 1410–1432. DOI: 10.1002/2013WR014333.

Guan, H., C.T. Simmons, A.J. Love., 2009. Orographic controls on rain water isotope distribution in the Mount Lofty Ranges of South Australia. *J. Hydrol.* 374: 255–264.

Guan, H., Zhang, X., Skrzypek, G., Sun, Z., Xu, X., 2013. Deuterium excess variations of rainfall events in a coastal area of South Australia and its relationship with synoptic weather systems and atmospheric moisture sources. *J. Geophys. Res.*: Atmospheres, 118(2): 1123-1138.

Lin, G., L. da S. L. Sterngerg., 1993. Hydrogen isotopic fractionation by plant roots during water uptake in coastal wetland plants. In: Ehleringer, J.R., Hall, A.E., Farquhar, G.D. (eds), Stable isotopes and plant carbon-water relations. Academic Press Inc., New York, pp 497-510.

Manning, A. H., D. K. Solomon., 2005. An integrated environmental tracer approach to characterizing groundwater circulation in a mountain block. *Water Resour. Res.* 41(12), n/a-n/a.

Miller, J.M., Williams, R.J., Farquhar, G.D., 2001. Carbon isotope discrimination by a consequence of *Eucalyptus* species along a subcontinental rainfall gradient in Australia. *Funct. Ecol*. 15: 222-232.

Prudhomme, C., I. Giuntoli, E. L. Robinson, D.B. Clark, N.W. Arnell, R. Dankers, B.M. Feketee, W. Franssenf, D. Gerten, S.N. Goslingh, S. Hagemanni, D.M. Hannah, H. Kim, Y. Masaki, Y. Satoh, T. Stacke, Y. Wada, D. Wisser, 2014. Hydrological droughts in the 21st century, hotspots and uncertainties from a global multimodel ensemble experiment. *Proc. Natl. Acad. Sci.*111 (9): 3262-3267.

Sandvig, R. M., and F. M. Phillips., 2006. Ecohydrological controls on soil moisture fluxes in arid to semiarid vadose zones. *Water Resour. Res*. 42, W08422.

Scanlon, B. R., K. E. Keese, A. L. Flint, L. E. Flint, C. B. Gaye, W. M. Edmunds, I. Simmers., 2006. Global synthesis of groundwater recharge in semiarid and arid regions, *Hydrol. Process.* 20(15), 3335-3370.

Schulze, E.-D., Turner, N.C., Nicolle, D., Schumacher, J., 2006. Leaf and wood carbon isotope ratios, specific leaf areas and wood growth of Eucalyptus species across a rainfall gradient in Australia. *Tree Physiol*. 26: 479-492.

Schulze, E.-D., Williams, R.J., Farquhar, G.D., Schulze, J.L., Miller, J.M., Walker, B.H., 1998. Carbon and nitrogen isotope discrimination and nitrogen nutrition of trees along a rainfall gradient in northern Australia. *Aust. J. Plant Physiol.* 25: 413-425.

Stewart, G.R., Turnbull, M.H., Schmidt, S., Erskine, P.D. 1995. ^{13}C Natural abundance in plant communities along a rainfall gradient: a biological integrator of water availability. *Aust. J. Plant Physiol.* 22: 51-55.

Taylor, R. G., B. Scanlon, P. Döll, M. Rodell, R. van Beek, Y. Wada, L. Longuevergne, M. Leblanc, J. S. Famiglietti, M. Edmunds, L. Konikow, T.R. Green, J. Chen, M. Taniguchi, M.F.P. Bierkens, A. MacDonald, Y. Fan, R.M. Maxwell, Y. Yechieli, J.J. Gurdak, D.M. Allen, M. Shamsudduha, K. Hiscock, P.J-F. Yeh, I. Holman, H. Treidel., 2012. Groundwater and climate change, *Nat. Clim. Change.* 3: 322-329.

Turner, N.C., Schulze, E.-D., Nicolle, D., Schumacher, J., Kuhlmann, I., 2008. Annual rainfall does not directly determine the carbon isotope ratio of leaves of *Eucalyptus* species. *Physiol. Plantarum*. 132: 440-445.

UN., 1998. Proclamation of the International Year of the Mountains, Report on the 1998 UN General Assembly Meeting, New York. URL: http://www.mtnforum.org.

Viviroli, D., H. H. Dürr, B. Messerli, M. Meybeck, R. Weingartner., 2007. Mountains of the world, water towers for humanity: Typology, mapping, and global significance. *Water*

Resour. Res. 43(7), n/a-n/a.

Viviroli, D., R. Weingartner, B. Messerli., 2003. Assessing the hydrological significance of the world's mountains. Mt. Res. Dev., 23(1), 32– 40.

Vörösmarty, C.J., P. Green, J.,Salisbury, R.B. Lammers., 2000. Global water resources: vulnerability from climate change and population growth. *Science*. 289(5477): 284-288.

Walther, G.R., E. Post, P. Convey, A. Menzel, C. Parmesan, T.J. Beebee, J.M. Fromentin, O. Hoegh-Guldberg, F. Bairlein., 2002. Ecological responses to recent climate change. *Nature*. 416(6879):389-395.

Wang, L., P. D'Odorico, L. Ries, S.A. Macko., 2010. Patterns and implications of plant-soil $\delta^{13}C$ and $\delta^{15}N$ values in African savanna ecosystems. *Quat. Res.* 73, 77-83.

Wilson, J. L., H. Guan., 2004. Mountain-block hydrology and mountain-front recharge., in Groundwater Recharge in a desert Environment: The southweatern United States, edited by J. F. Hogan, F. M. Phillips and B. R.Scanlon, pp. 113-137, American Geophysical Union, Washington, D.C.

Yepez, E. A., T.E. Huxman, D.D. Ignace, N.B. English, J.F. Weltzin, A.E. Castellanos, D.G. Williams., 2005. Dynamics of transpiration and evaporation following a moisture pulse in semiarid grassland: A chamber-based isotope method for partitioning flux components. *Agric. For. Meteorol.*132: 359–376.

CHAPTER 2 LEAF $\delta^{13}C$ OF NATIVE SPECIES ON TWO CONTRASTING HILLSLOPES IN SOUTH AUSTRALIA AND ITS ASSOCIATION WITH WATER STRESS[1]

2.1 Introduction

Carbon isotope ratio $^{13}C/^{12}C$ of leaves (expressed as leaf $\delta^{13}C$) has been demonstrated as a useful indicator to reveal accumulating effects of environmental conditions on plant photosynthesis. This ratio is determined by both physiological and physical processes. During photosynthesis, the overall carbon fractionation of C_3 plant leaves is primarily controlled by the diffusion of CO_2 containing ^{13}C and ^{12}C in the air (O'Leary, 1981; Hesterberg and Siegenthaler, 1991) and carboxylation in the CO_2 fixation (e.g. Schmidt *et al*., 1978; Guy *et al*., 1987). These two processes are related to a negative gradient of intercellular and ambient CO_2 mole fractions (CO_2 absorption) through the regulation of stomata openness, which also controlling leaf water loss through transpiration. Environmental factors that influence stomatal conductance will impact both CO_2 and water vapour exchange and isotopic fractionation of carbon between a leaf and its environment. This forms the basis that the leaf $\delta^{13}C$ can potentially work as an indicator of environmental conditions, especially water stress (Farquhar et al., 1989).

Generally, local availability of soil water (Farquhar and Sharkey, 1982) and potential evapotranspiration (PET) plays the key role in determining leaf $\delta^{13}C$ (Cernusak *et al*., 2013; O'Leary, 1981), although solar irradiance (e.g. Pearcy, 1988), salinity (e.g. van Groenigen and Kessel, 2002), temperature (e.g. Evans and von Caemmerer, 2013; Skrzypek et al., 2007) and nutrient availability (e.g. Cernusak *et al*., 2007) can also influence leaf $\delta^{13}C$. The solar irradiance effects on leaf $\delta^{13}C$ are difficult to be separated from those due to leaf-to-air vapour pressure deficit in the field (Farquhar *et al*., 1989). Salinity stress usually occurs

[1] This work was presented at *the 9th IsoEcol Conference*, 2014.

in irrigated agroecosystems or vegetation relies on saline water sources. The influence of temperature on $\delta^{13}C$ has not been studied broadly along temperature gradients and various factors were reported for different genus. However, in general $\delta^{13}C$ seems to be decreasing with an increase of temperature. For example, Evans and von Caemmerer (2013) shows that when leaf temperature increases from 15 to 40 ℃ carbon fractionation associated with photorespiration decreases only by 1.6‰ in tobacco. On the other hand significantly higher values were also reported varying from -1.0 to -2.4‰/°C (Smith et al., 1973; Troughton and Card, 1975). The most consistent pattern was observed in lower plants with less complicated metabolism such as mosses (Skrzypek *et al.*, 2007). Thus temperature effect may have to be considered as important factor controlling $\delta^{13}C$. However, this signal can be overwritten by other more pronounced environmental variables.

At the large scale, previous studies suggest that leaf $\delta^{13}C$ is correlated mainly with mean total annual precipitation over a range of climate conditions with mean annual precipitation from 100 to about 2000 mm as shown in Figure 2.1 (data from Diefendorf *et al*., 2010; Cernusak *et al*., 2011; Miller at al., 2001; Schulze *et al*., 1998; Schulze *et al*., 2006; Sterwart *et al*., 1995; Turner *et al*., 2008). However, this relationship appears to be weak in Europe and northern Australia.

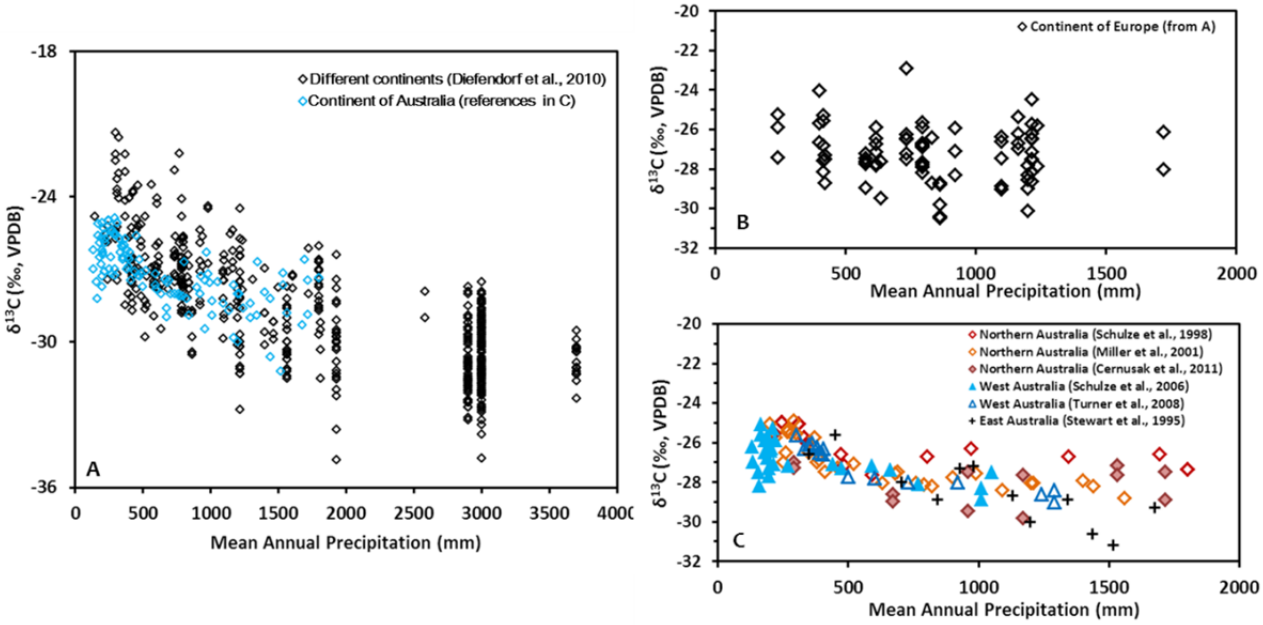

Figure 2.1 Pool leaf $\delta^{13}C$ of various tree genera vs. mean annual total precipitation for Europe, North America, Asia, Oceania and Southern Africa (summarized by Diefendorf et al., 2010) as shown as black diamonds while those for Australia (Cernusak et al., 2011; Miller et al., 2001; Schulze et al., 1998; 2006; Stewart et al., 1995; Turner et al., 2008) are shown as blue diamonds in panel A. More specifically, continent of Europe and Australia are shown in panel B and C respectively. Leaf $\delta^{13}C$ values generally decrease with increased precipitation except that of continent of Europe and Northern Australia.

Several possible effects and trends can be overlooked in large scale studies. First, in some studies (e.g. Diefendorf *et al.*, 2010; Cernusak *et al.*, 2011) several genera and even families were pooled together, what may dim otherwise possible stronger trends for individual species (Farquhar *et al.*, 1989). Second, many of these studies were based on one-time sampling procedure disregarding possible seasonal and inter-annual variability, which has likely diluted the correlation between leaf $\delta^{13}C$ and precipitation. Only a few studies have reported seasonal variations in leaf $\delta^{13}C$ (e.g. Ehleringer *et al.*, 1992; Gao *et al.*, 2006). Third, precipitation alone may not be the best option to represent plant water stress which is controlled by both supply (soil moisture) and demand (PET) at the same time. In some situation, local precipitation is not necessarily the sole water source for plants. Turner *et al.* (2008) suggest that annual precipitation does not directly determine leaf $\delta^{13}C$ of Eucalyptus species based on two samplings along a southeast to northeast

transect from Perth to the centre of Australia. Third, topography can induce changes of environmental conditions such as water availability and solar irradiance on the local scale. Therefore, there is a need to investigate leaf $\delta^{13}C$ continuously with simultaneous monitoring of environmental factors contributing to plant water stress over a range of hydroclimatic conditions.

In the present study, we performed experiments on a native vegetation catchment with two contrasting hillslopes, the north facing slope (NFS, more sunny on Southern Hemisphere) and the south facing slope (SFS, more shady), across a 'V' shape valley in South Australia. The two contrasting slopes provide a range of environmental conditions to examine the influencing factors in leaf $\delta^{13}C$. One-year leaf $\delta^{13}C$ of two tree species, *Eucalyptus* (*E.*) *leucoxylon* and *Acacia* (*A.*) *pycnantha* have been monitored monthly in this native vegetation catchment. We also collected two transects across the catchment to capture the spatial variations of leaf $\delta^{13}C$ after the dry season and the wet season. It is aimed to understand the seasonality of leaf $\delta^{13}C$ variations of the two tree species and spatial variations due to slope characteristics and varying local hydrological conditions. We also evaluate the correlation between leaf $\delta^{13}C$ and aridity index, which is the ratio of potential evapotranspiration to precipitation (PET/P), to check if this index is useful to quantify the relationship between leaf $\delta^{13}C$ and plant water stress.

2.2 Materials and methods

2.2.1 Study site

The study site is located in Mount Wilson (138.64˚ E, 35.21˚ S, 370 m a.s.l.) in the Mount Lofty Ranges of South Australia (Figure 2.2). This study site is characterized with a Mediterranean type climate, being cold and humid in winter and hot and dry in summer. Long-term average annual precipitation (1982-2013) is 716 mm dominated by winter rain events (http://www.bom.gov.au/climate/data/stations/). In this native vegetation site, there

are four main tree species: *Eucalyptus leucoxylon*, *Acacia pycnantha*, *Acacia notabilis* and *Eucalyptus viminalis cygnetensis*. Especially, *Eucalyptus leucoxylon* and *Eucalyptus viminalis cygnetensis* are the dominant species. A transect including ten trees is selected across two contrasting hillslopes, the north facing slope and the south facing slope to conduct our monitoring work with five trees on each slope. It would be more representative if we monitor more trees. Nevertheless, these ten trees, which include all the typical tree species of the study site, gradually covered the change of environmental conditions such as solar irradiance due to the two contrasting aspects of the hillslopes. One mast was installed on each hillslope to monitor net radiation above the canopy.

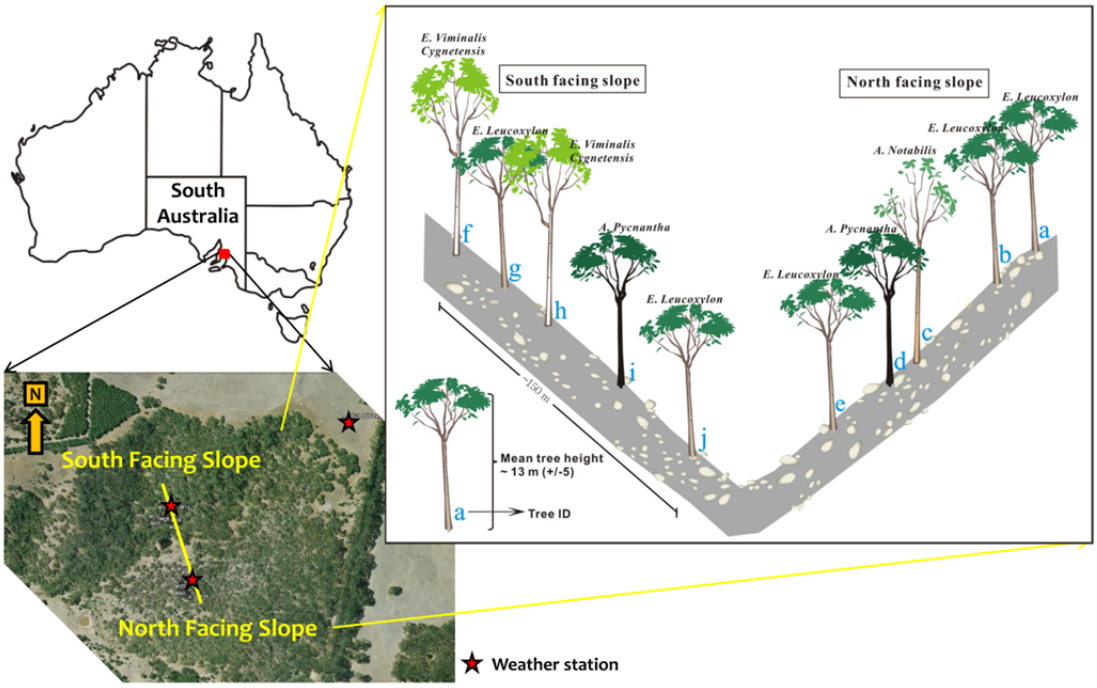

Figure 2.2 The study site and locations of ten sampling trees on the two contrasting hillslopes.

2.2.2 Field work and sample storage

The trees we chose were all around 13 m in height to avoid the uncertainty in data interpretation resulting from the tree height and age effect (e.g. McDowell *et al*., 2011). From 31 August 2012 to 2 September 2013, 16 batches (one batch refers to one time

sampling) of leaf samples have been collected. In every batch, samples were collected in four directions (east, south, west and north) for each tree except that the tree did not have a developed canopy in desired directions. Each sample for isotopic analysis was prepared from 10 to 20 leaves of the canopy in each direction. Leaf samples were sealed in zip-lock bags and stored in a cold ice chest box. In the lab, the samples were dried at 70 ˚C in an oven until a constant weight. Dry leaf samples were then grounded into powders and stored in plastic sealed jars.

2.2.3 Isotopic analysis

The grounded leaf samples were analysed in West Australian Biogeochemistry Centre at the School of Plant Biology, The University of Western Australia Perth for $\delta^{13}C$ using a continuous flow system consisting of a Delta V Plus mass spectrometer connected with a Thermo Flush 1112 via Conflo IV (Thermo-Finnigan/Germany). The measure δ-values were expressed with reference to VPDB (*Vienna PeeDee Belemnitella americana*) isotope reference scale using multi-point normalization technique and four standards NBS19, L-SVEC, NBS22 and USGS24 (Skrzypek *et al.*, 2010). The $\delta^{13}C$ was expressed in parts per thousand (‰, VPDB) (Skrzypek, 2013).

$$\delta^{13}C_{sample} = (\frac{R_{sample}}{R_{VPDB}} - 1) \times 1000‰ \quad (2.1)$$

where $\delta^{13}C_{sample}$ is delta notation of the sample, R_{sample} is $^{13}C/^{12}C$ ratio of the sample, and R_{VPDB} is the $^{13}C/^{12}C$ ratio of the standard VPDB. The external analysis error for $\delta^{13}C$ (1 standard deviation) is reported to be 0.10‰.

2.2.4 Calculation of potential evapotranspiration

PET lumps the demand control of plant water use and precipitation plays as an input control, thus aridity index (PET/P) is very likely to represent the environmental conditions than sums of precipitation only. It is easy to calculate from weather station data. To

quantify the relationship between leaf $\delta^{13}C$ and plant water stress, daily PET (mm day^{-1}) is calculated using Priestly-Taylor method (1972) as shown in equation (2.2).

$$\mathrm{PET} = \alpha \frac{\Delta}{\Delta + \gamma} \frac{R_n}{\lambda} \times \frac{10^3}{\rho} \quad (2.2)$$

where α is the Priestly-Taylor coefficient assumed to be 1.26; Δ (kPa $^{\circ}C^{-1}$) is the slope of the saturation vapour pressure-temperature relationship; γ (kPa $^{\circ}C^{-1}$) is the psychrometric constant; R_n (MJ m^{-2} day^{-1}) is the net radiation above the surface and λ is latent heat of vaporization, 2.45 MJ kg^{-1}; ρ is water density, 1.0×10^3 kg m^{-3}.

As it is known that leaf $\delta^{13}C$ is time-integrated signal, correspondingly the aridity index for each sampling batch is calculated using equation (2.3).

$$\mathrm{PET/P} = \sum_0^i \mathrm{PET} / \sum_0^i \mathrm{P} \quad (2.3)$$

where 0 refers to the date as starting point which is one month ahead from the first batch of the sampling and *i* refers to the date of the sampling batch of interest.

The way we do the calculation for this accumulation is because the beginnings of the accumulating periods of the leaf biomass are not even. Usually, we do not have the knowledge of how long ^{13}C has been stored in the leaf biomass. Therefore, we have tried three different ways to decode the life period of leaves using linear stepwise regression for time series data of leaf $\delta^{13}C$ and PET/P. The main uncertain parameter is which date should be used as the start point for calculation of the integrated values. First, we used the period between the two consecutive sample batches as the accumulation time for the latter sampling batch (*i*-1 to *i*). In average we have around 23-day sampling interval, and we set one month period for the first sampling batch. Second, we applied two-month (61 days) period prior to the sampling date for each sampling batch. In other words, we assumed

that accumulating time period is 61 days until we did sample collection. Third, we apply the integral method as we described in Equation (2.3). The first batch was collected on August 31st, 2012, the starting point (*i*=0) we use is August 1st, 2012.

2.2.5 Radiation inputs and topographic index

In order to quantify the relationship between leaf $\delta^{13}C$ and plant water stress spatially, daily PET* (mm day^{-1}) was calculated using equation (2.2) as well. Specifically, the net radiation we apply is calculated from the observation net radiation and the relationship (linear regression) between global radiation at tree location and that at the mast location. The global radiation is the sum of direct and diffuse radiation of all sun map and sky map sectors for different locations of the ten trees, respectively. Simply, we used solar radiation analysis tools in ArcGIS (ESRI Inc., 2003) to calculate the global radiation based on methods from the hemispherical viewshed algorithm (Rich 1990; Rich *et al*., 1994; Fu and Rich 2000; Fu and Rich 2002) with high resolution (1 m ×1 m) based on Digital Elevation Models (DEMs) of the study area. The daily global radiation data for each location of the trees were then extracted for linear regression to get relationship between the tree location and the mast location. The equation (2.3) was utilized for the calculation of spatially aridity index for each tree location.

Topographic index (Beven *et al*., 1984), which may potentially relate to the soil moisture conditions, was also calculated for each tree location as given in the following equation (2.4).

$$TI = \ln(\frac{A}{\tan \beta}) \quad (2.4)$$

Where *TI* is topographic index, *A* is the upslope contributing area per unit length of contour, and β is the topographic slope of the cell. *TI* is derived from DEMs based on topographic data using ArcGIS.

2.2.6 Statistical analysis

To evaluate the correlation between leaf $\delta^{13}C$ and environmental factors, stepwise linear regression was applied using IBM SPSS© software both in time and space. Analysis of variance (ANOVA) table including significance level was also obtained for each regression.

2.3 Results and discussion

2.3.1 Seasonal variations of leaf $\delta^{13}C$

The results of leaf $\delta^{13}C$ at the end of dry season (05/Mar/2013) and the end of wet season (02/Sep/2013) are shown in Figure 2.3 (lower panel) in comparison to the precipitation (upper panel in Figure 2.3). All leaf $\delta^{13}C$ of ten trees after wet season were all consistently lower than that after dry season except tree *i* where no significant change was observed. The difference in leaf $\delta^{13}C$ between the two batches for each tree can be as large as 1.2± 0.4‰, which shows significant seasonal variations.

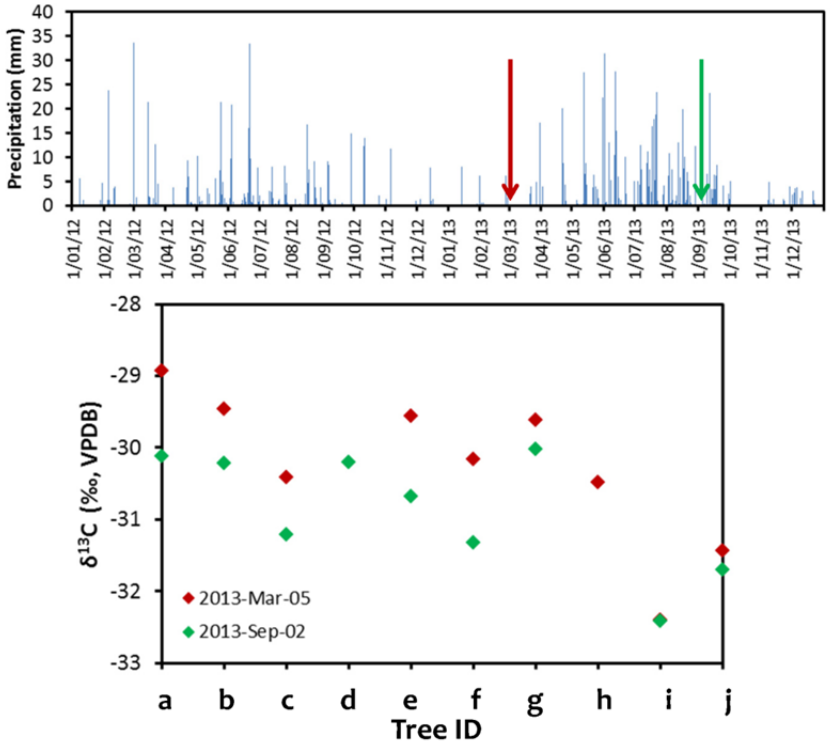

Figure 2.3 Daily precipitation from 1/Jan/2012 to 12/Dec/2013 of the Mount Wilson site (upper panel) and two sets of leaf $\delta^{13}C$ of the 10 sampling trees (lower panel) across the site on 05/Mar/2013 and 02/Sep/2013 separately.

We focus on tree *a*, *b*, *d* and *e* on NFS and tree *g*, *i* and *j* on SFS for more detailed time series analysis (Figure 2.4). Generally, leaf $\delta^{13}C$ has an increasing trend in the dry season and decreasing trend in the wet season except tree *j*. The timing of the turning of these two trends was also quite consistent among trees except for tree *i*.

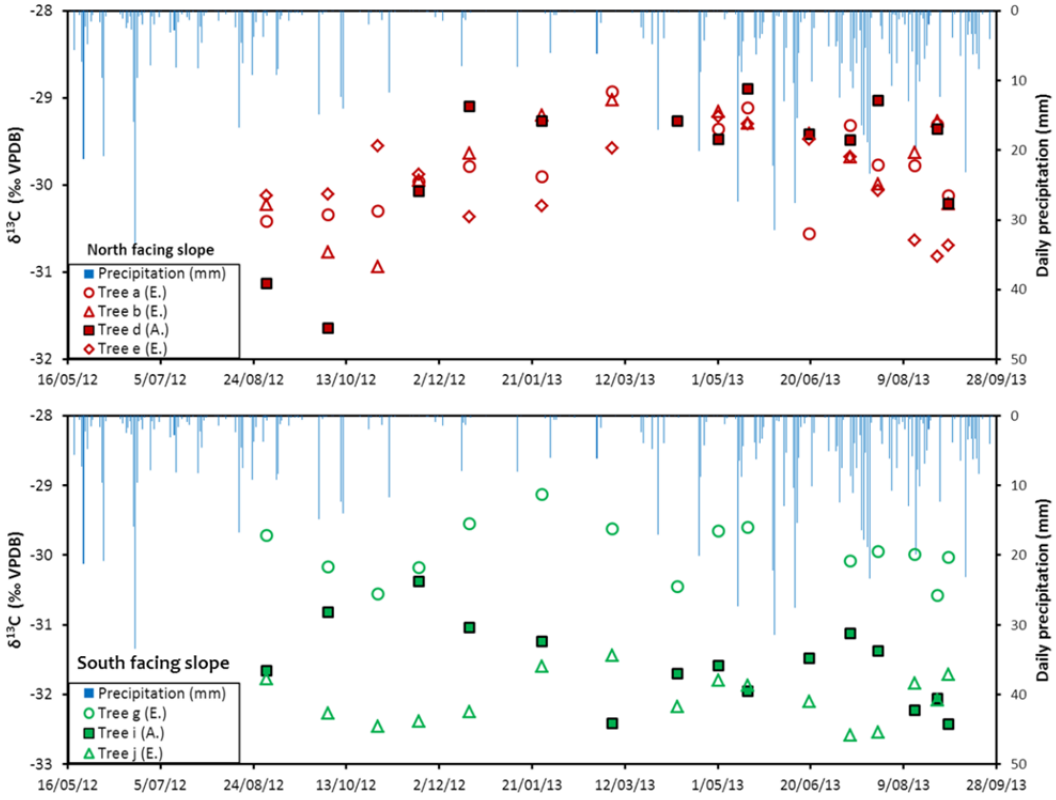

Figure 2.4 Time series data of leaf $\delta^{13}C$ of *Eucalyptus leucoxylon* and *Acacia pycnantha* on the two contrasting hillslopes.

The above results confirm that precipitation is important in determination of the seasonal variations of leaf $\delta^{13}C$ in general. However, it is not clear in what timescale the relationship between precipitation and leaf $\delta^{13}C$ is robust. If we focus on NFS only, a decrease in $\delta^{13}C$ (e.g. batch 5 to batch 6) can be found in the dry season and an increase (batch 9 to batch 10) can be seen in the wet season after rain events. The effects of precipitation on the seasonal variations of leaf $\delta^{13}C$ of SFS are not as clear as that of NFS. The two

contrasting hillslopes located no more than 200 meters one from another, precipitation is similar (observed throughfall data). For this reason, precipitation cannot be considered as the factor responsible for differences in $\delta^{13}C$ of leaves between the two slopes. Therefore, other factors arising from topography, such as soil moisture storage and solar irradiance, need to be considered. In general, the top part of the slopes receives more solar irradiation and tends to be dryer as shallow soil and regolith water infiltrate downhill keeping bottom of the valley wetter. An alternative index to sum of precipitation is needed to reveal the relationship between leaf $\delta^{13}C$ and plant water stress in this study.

The statistics of leaf $\delta^{13}C$ of each tree are summarized in Table 2.1. Leaf $\delta^{13}C$ shows a range of values from -32.6‰ to -28.9‰. The span from maximum and minimum $\delta^{13}C$ of leaves for each tree is 1.2‰ to 2.7‰, which is similar to some species like *Ambrosia dumosa*, *Bebbia juncea*, *Gutierrezia sarothrae etc*. in Sonoran Desert of Arizona (Ehleringer *et al*.,1992). Mean values of leaf $\delta^{13}C$ may smooth the leaf $\delta^{13}C$ variation of leaves as it is integrated over a certain period as discussed in section 2.2.4. Nevertheless, it is still useful to examine the systematic trend in observation. For instance, leaf $\delta^{13}C$ of wet season mean values are all consistently more negative than that of dry season although the difference is less than 1.1‰. Specifically, tree *i* and tree *e* have a smallest difference between seasons than other trees.

The observed leaf $\delta^{13}C$ values in this study are more negative (-30.4±1.1‰) in comparison to C_3 species (-26.4±1.4‰) presented on Figure 2.1 for similar precipitation regime (700-750 mm/year). This indicates that local baselines are importantly related to local conditions. Thus for detailed study trends, local conditions such as slope orientation needs to be considered except precipitation.

Table 2.1 Leaf $\delta^{13}C$ (in ‰) at the Mount Wilson site from 31/Aug/2012 to 02/Sep/2013.

Site	Tree ID	Tree species	Leaf $\delta^{13}C$ range (‰)	Mean (±SD)	Dry season* mean (±SD)	Wet season* mean (±SD)	Annual global radiation ($\times 10^6$ Wh/m^2)	Topographic Index (*TI*)
North facing slope	*a*	*E. Leucoxylon*	-30.6 ~ -28.9	-29.8 (±0.5)	-29.5 (±0.5)	-29.9 (±0.4)	1.281	5.55
	b	*E. Leucoxylon*	-30.9 ~ -29.0	-29.7 (±0.6)	-29.3 (±0.3)	-30.1 (±0.6)	1.270	4.06
	c	*A. Notabilis*	-	-	-30.4	-31.2	1.262	5.78
	d	*A. Pycnantha*	-31.6 ~ -28.9	-29.7 (±0.8)	-29.2 (±0.1)	-30.1 (±1.1)	1.260	4.21
	e	*E. Leucoxylon*	-30.8~ -29.2	-30.0 (±0.5)	-30.1 (±0.4)	-30.2 (±0.5)	1.282	4.36
South facing slope	*f*	*E. viminalis cygnetensis*	-	-	-30.2	-31.3	0.934	5.70
	g	*E. Leucoxylon*	-30.6 ~ -29.1	-29.9 (±0.4)	-29.4 (±0.3)	-30.1 (±0.3)	0.806	5.66
	h	*E.viminalis cygnetensis*	-	-	-30.5	-	0.785	5.43
	i	*A. Pycnantha*	-32.4 ~ -30.4	-31.6 (±0.6)	-31.6 (±0.7)	-31.7 (±0.6)	0.809	5.65
	j	*E. Leucoxylon*	-32.6 ~ -31.4	-32.0 (±0.3)	-31.8 (±0.4)	-32.1 (±0.4)	0.775	3.95

*Dry Season is from Nov to Mar and Wet Season is from Jun to Oct. Tree *c*, tree *f* and tree *h* have twice sampling only.

2.3.2 Spatial variations of leaf $\delta^{13}C$

Trees on SFS had more negative leaf $\delta^{13}C$ than trees on NFS. This relative difference can be as large as 3.4‰ (Figure 2.4 and Table 2.1). Moreover $\delta^{13}C$ of trees on SFS start decreasing earlier in the wet season than that on NFS. This is in agreement with expected pattern as the trees on more shady SFS are subject to shorter water stress period due to lower evaporative demand and therefore more negative $\delta^{13}C$ values.

Tree *i* on SFS and tree *d* on NFS are both *Acacia pycnantha*. They are located about 100 meters apart from another (Figure 2.2) at a similar elevation, but had a leaf $\delta^{13}C$ difference by almost 2‰. Leaf $\delta^{13}C$ was similar for tree *i* (*A. pycnantha*) and tree *j* (*E.leucoxylon*) on SFS. Tree *j* and tree *g* (both *E.leucoxylon*) on SFS had very different leaf $\delta^{13}C$ but almost the same pattern in the seasonal variations. In general, trees on NFS all have similar patterns and values in leaf $\delta^{13}C$ among them (Figure 2.4 and Table 2.1).

Both tree species and environmental related factors are possible to account for the differences in leaf $\delta^{13}C$ observed between the two slopes. However, it seems that environmental conditions are more important than the difference in species itself. Because different species on the same hillslope, e.g. tree *a* and tree *d* on NFS or tree *i* and tree *j* on SFS, show similar values and seasonal variations of leaf $\delta^{13}C$ through the monitoring year. Moreover, the same species on the same hillslope, e.g. tree *g* and tree *j*, show similar variations but very consistent different value (2.1 ± 0.3‰) of leaf $\delta^{13}C$ all over the year (Figure 2.4 and Table 2.1).

With better water availability, it is expected to have more negative leaf $\delta^{13}C$ as the better conditions for transpiration and photosynthesis. With less irradiance, it will also cause the decrease of leaf $\delta^{13}C$ as intercellular CO_2 pressure will increase at lower light levels (Farquhar *et al*., 1989; Pearcy, 1988). As it shown in Table 2.1, *TI* is calculated to serve as the indicator for soil moisture condition. The larger *TI* indicates potentially better soil

moisture condition at the same slope. It is very likely better water condition, while irradiance is less, at the bottom than at the top on both SFS and NFS, respectively. Therefore, more negative values of leaf $\delta^{13}C$ of tree *d*, tree *i* and tree *j* were observed at the bottom of the valley than that on the top (Table 2.1).

2.3.3 Time series of leaf $\delta^{13}C$ and aridity index

From the results of the three exercises we described in section 2.2.4, the third approach gave the best fitting results. As it shown in Table 2.2, the correlations between leaf $\delta^{13}C$ and PET/P are good based on the R-square (0.31±0.11) and p-value (0.02±0.03, 0.05 is the usual threshold value for significance) for trees on NFS. As we can tell from the regression equations, one unit change of PET/P can cause around 0.19‰ change on NFS and around 0.06‰ change (excluding tree *i*) on SFS in leaf $\delta^{13}C$. From our calculation, the integrated PET/P ranges from 1.3 to 7.5 on NFS and from 1.0 to 6.5 on SFS in the monitoring year. Hence, PET/P, which quantitatively reflects plant water stress, works well to quantify the correlation with leaf $\delta^{13}C$. In other words, if the main environmental control is water availability, PET/P can be a good index to correlate with leaf $\delta^{13}C$.

Table 2.2 Linear stepwise regression results for time series data of leaf $\delta^{13}C$ and aridity index for the two genera *Eucalyptus Leucoxylon* and *Acacia Pycnantha*.

Site	Tree ID*	Regression equations	R^2 (adjusted)	p-value
North facing slope	*a (E.)*	$\delta^{13}C = 0.16 \times (PET/P) - 30.4$	0.30	0.00
	b (E.)	$\delta^{13}C = 0.20 \times (PET/P) - 30.5$	0.44	0.00
	d (A.)	$\delta^{13}C = 0.27 \times (PET/P) - 30.8$	0.30	0.03
	e (E.)	$\delta^{13}C = 0.14 \times (PET/P) - 30.4$	0.18	0.06
South facing slope	*g (E.)*	$\delta^{13}C = 0.11 \times (PET/P) - 30.3$	0.13	0.1
	i (A.)	$\delta^{13}C = -0.04 \times (PET/P) - 31.4$	-0.07	0.73
	j (E.)	$\delta^{13}C = 0.10 \times (PET/P) - 32.3$	0.10	0.13

*Tree species are in brackets, E. for *Eucalyptus Leucoxylon* and A. for *Acacia Pycnantha*.

Trees on SFS showing much less significant (all $p > 0.05$) relations between PET/P and leaf $\delta^{13}C$ is consistent with our understanding that they suffered less water stress. PET/P on SFS is smaller than that on NFS throughout the monitoring year. This difference can be as large as 2 units. From the regression results of tree *i*, it seems that this plant has no water stress. With better moisture on SFS but much less irradiance than NFS and quite negative values in leaf $\delta^{13}C$ (Table 2.1), we may conclude that tree *i* mainly suffered irradiance stress while tree *g* and tree *j* suffered both irradiance stress and water stress.

2.3.4 Spatial leaf $\delta^{13}C$ and aridity index

Linear stepwise regression is also performed on the two batches of transect sampling to examine the spatial relations of leaf $\delta^{13}C$ and PET/P. In each regression, we use the re-calculated PET/P for the trees on each slope (Table 2.3). For example, for batch on March 5th 2013, PET/P values are the integrated ones to this date as we described in section 2.2.4. A very similar idea using monthly P/PET has been added to adjust the ratio of saturation vapour pressure of ambient air to the total atmospheric pressure ($e_{a,sat}/p_{total}$) for evaluating ecological adaption (Comstock and Ehleringer, 1992).

Table 2.3 Linear stepwise regression results for spatial variations of leaf $\delta^{13}C$ and aridity index including the two genera, *Eucalyptus* and *Acacia*.

Date	Regression equations	R^2 (adjusted)	p-value
2013-Mar-05	$\delta^{13}C = 0.84 \times (PET/P) - 35.8$	0.35	0.05
2013-Sep-02	$\delta^{13}C = 1.68 \times (PET/P) - 34.5$	0.20	0.13

As it shown in Table 2.3, the spatial correlations between leaf $\delta^{13}C$ and PET/P has p-value larger than or equals to the usual threshold value of 0.05 for the two batches. One possible reason for that is we only have ten pairs of data in each regression. Nevertheless, we can still have quantitatively understanding from the regression equations that one unit change

of PET/P may cause 0.84‰ to 1.68‰ change of leaf $\delta^{13}C$. This spatial change is much larger than temporal change in leaf $\delta^{13}C$ caused by PET/P for this plot scale study. Spatially, leaf $\delta^{13}C$ is affected by the combination of different environment conditions in different locations while temporally it is smoothed by time integration.

Table 2.4 Linear stepwise regression results for spatial variations of integrated aridity index (PET/P) and topographic index (*TI*) and leaf $\delta^{13}C$ of *Eucalyptus* and *Acacia* separately.

Genus	Regression	Constant (‰)	Topographic Index (*TI*)	PET/P	R^2	Adjusted R^2
	Coefficient	-34.0	0.60	0.24		
Eucalyptus	p-value	0.00	0.00	0.00	0.36	0.34
	Coefficient	-25.1	-1.10	0.13		
Acacia	p-value	0.00	0.00	0.12	0.68	0.65

In order to articulate the spatial relationship between leaf $\delta^{13}C$ and environmental water conditions, linear stepwise regressions were also conducted for the two genera Both topographic index and integrated aridity index were included in the exercise, with results shown in Table 2.4. It should be noticed that only two trees have been applied the regression analysis in genus *Acacia* while five trees were used in *Eucalyptus*. The relationship between spatial leaf $\delta^{13}C$ and PET/P may be buried by lack of data in *Acacia*. Thus we focus on the result of genus *Eucalyptus* in Table 2.4. *TI* has a coefficient of 0.60 and integrated PET/P has that value of 0.24. This suggests that the location of the trees which may relate to soil moisture conditions is very important to determine the spatial leaf $\delta^{13}C$. Integrated PET/P is also a key factor in this determination. Thus leaf $\delta^{13}C$ may be used as a good indicator for vegetation stress resulting from spatial variability of environmental conditions.

The larger dependence of spatial leaf $\delta^{13}C$ than temporal values on PET/P seems to be good news for the studies (e.g. Cernusak *et al*., 2011) looking at the behaviour of

ecosystem across complex climatic gradients using one time sampling plan. But without considering timing (seasonal variations) or the location (slope effects) will surely induce significant uncertainties from the results we reported. A careful sampling design is required to examine the relationship between leaf $\delta^{13}C$ and water availability over a regional climate gradient. Seasonal variations and slope aspects should be both kept in mind.

2.4 Conclusions and implications

Significant seasonal variations have been observed in leaf $\delta^{13}C$ for both studied C_3 tree genus up to 1.7‰ for *Eucalyptus leucoxylon* and up to 2.7‰ for *Acacia pycnantha*. On the two contrasting hillslopes, the difference in leaf $\delta^{13}C$ was also significant and on average between NFS and SFS was around 2‰. These results suggest that seasonal variations and slope topographic effect should be considered while examining the leaf $\delta^{13}C$ and ecosystem adaptions over a regional climate gradient.

Good correlations between temporal leaf $\delta^{13}C$ and aridity index was observed in location exposed to the higher water stress (NFS). In contrast, correlations for wetter slope SFS and downslope locations were not significant, suggesting that local soil conditions and position in the landscape can be more important than weather parameters. On the temporal axis, the correlation coefficients between leaf $\delta^{13}C$ and integrated aridity index can be as high as 0.44, and on the spatial axis, the correlation coefficients can be 0.36 for the examined *E*ucalyptus trees. These results suggest that PET/P may be a good indicator to quantify the relationship between leaf $\delta^{13}C$ and plant water stress.

References

Beven, K.J., Kirkby, M.J., Schofield, N., Tagg, A.F., 1984. A physically based flood forecasting model (TOPMODEL) for 3 UK catchments. *J. Hydrol.* 69: 119-143.

Cernusak, L.A., Hutley, L.B., Beringer, J., Holtum, J.A.M., Turner, B.L., 2011. Photosynthetic physiology of eucalytptsalong a sub-continental rainfall gradient in northern Australia. *Agric. For. Meteorol.* 151: 1462-1470.

Cernusak, L.A., Ubierna, N., Winter., K., Holtum, J.A.M., Marshall, J.D., Farquhar, G.D., 2013. Environmental and physiological determinants of carbon isotope discrimination in terriestrial plants. *New Phytol.* 200: 950-965.

Cernusak, L.A., Winter, K., Aranda, J., Turner, B.L., Marshall J.D., 2007. Transpiration efficiency of a tropical pioneer tree (Ficus insipida) in relation to soil fertility. *J. Exp. Bot.* 58: 3549-3566.

Comstock, J.P., Ehleringer, J.R., 1992. Correlating genetic variation in carbon isotopic composition with complex climatic gradients. *Proc. Natl. Acad. Sci.* 89: 7747-7751.

Diefendorf, A.F., Mueller, K.E., Wing, S.L., Koch, P.L., Freeman, K.H., 2010. Global patterns in leaf ^{13}C discrimination and implications for studies of past and future climate. *Proc. Natl. Acad. Sci.*107 (13): 5738-5743.

Ehleringer, J.R., Phillips, S.L., Comstock, J.P., 1992. Seasonal variation in the carbon isotopic composition of desert plants. *Funct. Ecol*. 6: 396-404.

ESRI Inc., 2003. ArcGIS 9.0. ESRI Inc., Redlands, CA.

Evans, J.R., von Caemmerer, S., 2013. Temperature response of carbon isotope discrimination and mesophyll conductance in tobacco. *Plant Cell Environ*. 36: 745-756.

Farquhar, G.D., Sharkey, T.D., 1982. Stomatal conductance and photosynthesis. *Annu. Rev. Aust. J. Plant Physiol.* 11: 539-552.

Farquhar, G.D., Ehleringer J.R., Hubick K.T., 1989. Carbon isotope discrimination and photosynthesis. *Annu. Rev. Plant Biol.* 40: 503-537.

Field, C., Mooney, H.A., 1986. The photosynthesis-nitrogen relationship in wild plants. In: Givnish, T. ed. *On the economy of plant form and function*. New York, NY, USA: Cambridge University Press, 25-55.

Fu, P., 2000. A Geometric Solar Radiation Model with Applications in Landscape Ecology. Ph.D. Thesis, Department of Geography, University of Kansas, Lawrence, Kansas, USA.

Fu, P., and P. M. Rich., 2000. The Solar Analyst 1.0 Manual. Helios Environmental Modeling Institute (HEMI), USA.

Fu, P., and P. M. Rich., 2002. A Geometric Solar Radiation Model with Applications in Agriculture and Forestry. *Comput. Electron. Agric.* 37:25–35.

Gao, T.P., Chen, T., Feng, H.Y., An. L. Z., Xu, S.J., Wang, X.L., 2006. Seasonal and annual variation of osmotic solute and stable carbon isotope composition in leaves of endangered desert evergreen shrub *Ammopiptanthus mongolicus*. *S. Afr. J. Bot.* 72: 570-578.

Guy, R.D., Fogel, M.F., Berry, J.A., Hoering, T.C., 1987. Isotope fractionation during oxygen production and consumption by plants. *Prog. Photosynth. Res.* III: 597-600.

Hesterberg, R., Siegenthaler, U., 1991. Production and stable isotopic composition of CO_2 in a soil near Bern, Switzerland. *Tellus*. 43B: 197-205.

McDowell, Bond, B.J., Dickman, L.T., Ryan, M.G., Whitehead, D., 2011. Relationships

between tree height and carbon isotope discrimination. In: Meinzer F.C., Lachenbruch, B., Dawson, T.E., eds. *Size- and age-related changes in tree structure and function*. New York, NY, USA: Springer, 255-285.

Miller, J.M., Williams, R.J., Farquhar, G.D., 2001. Carbon isotope discrimination by a consequence of *Eucalyptus* species along a subcontinental rainfall gradient in Australia. *Funct. Ecol*. 15: 222-232.

O'Leary M.H., 1981. Carbon isotope fractionation in plants. *Phytochemistry.* 20: 553-567.

Pearcy, R.W., 1988. Photosynthetic utilization of lightflecks by understory plants. *Aust. J. Plant Physiol.* 15: 223-238.

Priestley, C.H.B., Taylor, R.J., 1972. On the assessment of surface heat flux and evaporation using large-scale parameters. *Mon. Weather Rev.* 100 (2), 81-92.

Rich, P. M., R. Dubayah, W. A. Hetrick, and S. C. Saving., 1994. Using Viewshed Models to Calculate Intercepted Solar Radiation: Applications in Ecology. American Society for Photogrammetry and Remote Sensing Technical Papers, 524–529.

Rich, P. M., and P. Fu., 2000. Topoclimatic Habitat Models. Proceedings of the Fourth International Conference on Integrating GIS and Environmental Modeling.

Schmidt, H.L., Winkler, F. J., Latzko, E., Wirth, E., 1978. ^{13}C-Kinetic isotope effects in photosynthetic carboxylation reactions and δ^{13}C-values of plant material. *Isr. J. Chem*. 17: 223-224.

Schulze, E.-D., Turner, N.C., Nicolle, D., Schumacher, J., 2006. Leaf and wood carbon isotope ratios, specific leaf areas and wood growth of Eucalyptus species across a rainfall gradient in Australia. *Tree Physiol*. 26: 479-492.

Schulze, E.-D., Williams, R.J., Farquhar, G.D., Schulze, J.L., Miller, J.M., Walker, B.H., 1998. Carbon and nitrogen isotope discrimination and nitrogen nutrition of trees along a rainfall gradient in northern Australia. *Aust. J. Plant Physiol.* 25: 413-425.

Stewart, G.R., Turnbull, M.H., Schmidt, S., Erskine, P.D. 1995. ^{13}C Natural abundance in plant communities along a rainfall gradient: a biological integrator of water availability. *Aust. J. Plant Physiol.* 22: 51-55.

Turner, N.C., Schulze, E.-D., Nicolle, D., Schumacher, J., Kuhlmann, I., 2008. Annual rainfall does not directly determine the carbon isotope ratio of leaves of *Eucalyptus* species. *Physiol. Plantarum*. 132: 440-445.

Skyzypek, G., 2013. Normalization procedures and reference material selection in stable HCNOS isotope analyses-an overview. *Anal. Bioanal. Chem*. 405: 2815-2823.

Skrzypek G., Kałużny A., Wojtuń B, Jędrysek M.O., 2007. The carbon stable isotopic composition of mosses – the record of temperature variations. *Organic Geochemistry*. 38: 1770–1781.

Skrzypek G., Sadler R., Paul D., 2010. Error propagation in normalization of stable isotope data: a Monte Carlo analysis. *Rapid Commun. Mass Spectrom.* 24: 2697–2705.

Van Groenigen, J.W., van Kessel, C., 2002. Salinity-induced patterns of natural

abundance carbon-13 and nitrogen-15 in plant and soil. *Soil Sci. Soc. Am. J.* 66: 489-498.

CHAPTER 3 ISOTOPIC COMPOSITION OF THROUGHFALL IN PINE PLANTATION AND NATIVE EUCALYPTUS FOREST[2]

3.1 Introduction

Knowledge of the isotopic composition of precipitation is of importance for studies using isotopic composition as hydrological tracers to investigate the origin of groundwater (e.g. Ajami *et al*., 2011; Clark and Fritz, 1997; Frot *et al*., 2007), hydrograph separation (e.g. Goller *et al*., 2005; Hooper and Shoemaker, 1986; Kendall and McDonnell, 1993; Wels *et al*., 1991), and paleoclimate reconstruction (e.g. Darling, 2004; Steinman *et al*., 2012). A great number of studies on precipitation isotope and its applications in hydrological processes emerged in the last few decades (e.g. Rindsberger *et al*., 1990; Risi *et al*., 2008b; Risi *et al*., 2010; Rozanski *et al*., 1992; Rozanski *et al*., 1993; Soderberg et al., 2013; Uemura *et al*., 2012). However, in catchments with vegetation cover, major water stable isotope inputs are throughfall instead of precipitation. Interception loss refers to a part of precipitation evaporation from vegetation during or after rainfall while throughfall refers to the remaining part of precipitation may or may not contact the canopy and falls to the ground in vegetated area (Crockford and Richardson, 2000). Thus, it is necessary to know how much precipitation isotopic composition is altered by vegetation canopy, and how this alteration varies with different vegetation covers.

It is usually thought that throughfall isotopic composition is more enriched than the bulk precipitation (Pichon *et al*., 1996). This is because of the isotopic fractionation during partial evaporation of canopy intercepted water. There are two models based on partial evaporation concept, Saxena (1986) and Gat (2010), to predict isotopic compositions of throughfall. Saxena (1986) applied a Craig and Gordon (1965) type model to calculate

[2] A revised version of this chapter was published in *Journal of Hydrology* , with co-authors Huade Guan and Zijuan Deng.

isotopic composition of evaporate vapour while Gat (2010) used a Rayleigh type model to do the calculation. Because their focus is partial evaporation, certain assumption has to be made. For example, Gat (2010) gave the special solutions assuming the input isotopic signal of rain events is invariant, which is often not valid in reality.

However, Pichon *et al*. (1996) pointed out that the fractionation process in partial evaporation is not the only mechanism altering throughfall isotopic composition. This is supported by the fact that both enrichment and depletion of isotopic composition of throughfall have been reported in published studies. Saxena (1986) found that throughfall ^{18}O content was higher than open rainfall for most of the 24 summer rain events in a pine forest in Sweden, but depleted throughfall was observed for a few events. In DeWalle and Swistock (1994), Brodersen *et al*. (2000) and Kubota and Tsuboyama (2004), these two different effects were also observed. DeWalle and Swistock (1994) showed in one event under spruce, the throughfall isotope difference from precipitation can be as low as -0.65‰ and in another event that can be as high as 1.61‰ in terms of ^{18}O concentration. Similarly, Brodersen *et al*. (2000) showed that the difference under spruce can be as low as -1.48‰ and as high as 1.26‰. Kubota and Tsuboyama (2004) showed two events with depletion and four events with enrichment of ^{18}O in throughfall isotopic composition in comparison to that of bulk precipitation.

All these observations suggest that in addition to partial evaporation, other mechanisms should have contributed to the alteration of the throughfall isotopic composition from bulk precipitation. Because of canopy interception, part of rainfall (e.g. at the beginning or the end of the event) can be completely missing in the throughfall. If this missing part has different isotopic composition from the remaining rainfall, the throughfall isotopic composition can be different from the bulk rainfall. This mechanism is now referred to the selection process. Gat and Tzur (1967) first proposed that the selection process can affect

isotopic composition when part of the event evaporates totally from the canopy. Following this concept, Saxena (1986), DeWalle and Swistock (1994), Pichon *et al*. (1996), Gibson *et al*. (2000) showed their throughfall isotopic results to support the existence of selection process. Brodersen *et al*. (2000) summarized that the selection process is one important process responsible for the alteration of isotopic signal by canopy. Intra-event variation of precipitation isotopic composition is the key to understand the selection process. However, none of these studies have utilized the intra-event isotopic composition to examine this process. This is probably the reason why in some other studies like Liu *et al*. (2008) , Ikawa (2011) and Kato *et al*. (2013) the selection process is neglected. On the other hand, the selection process can also occur between events if small rainfall events are completely intercepted by canopy. This inter-event selection has not been clearly addressed in the previous studies. The isotopic amount effect, if present, is useful to examine this process.

In addition to δ^2H and $\delta^{18}O$, the secondary isotopic variable - deuterium excess which defined as $d = \delta^2 H - 8 \times \delta^{18} O$ (Dansgaard, 1964), is helpful to distinguish the selection proccesses from partial evaporation. This variable cancel out the covariation of oxygen and hydrogen isotopic compositions duing the equilibrium fractionation (Guan *et al.*, 2013). Selection processes have no effect on *d* while partial evaporation will decrease this variable. Such useful informmation has been applied in only a few throughfall studies. Using both $\delta^{18}O$ and *d*-excess to develop an operational framework will be useful to examine different processes responsible for the alteration of throughfall isotopic composition.

The objectives of this study are (i) to examine the isotopic composition of throughfall in two typical vegetation surfaces, pine plantation and native eucalyptus forest, in South Australia; (ii) to understand the mechanisms leading to alteration of precipitation isotopic composition due to vegetation cover using a synthesized conceptual framework; (iii) to

evaluate the significance of throughfall isotopic variations in the studies of groundwater recharge sources, hydrograph separation and paleoclimate reconstruction.

3.2 Study area

The study was conducted in Kuitpo Forest (138.68˚ E, 35.18˚ S, 335 m a.s.l.), 20 km east of Gulf St. Vincent and 30 km south of the central business district of Adelaide, South Australia (Figure 3.1). The study area is characterized with a Mediterranean type climate, being cold and humid in winter and hot and dry in summer. Long-term average annual precipitation (1971-2000) is 830 mm dominated by winter rain events, and monthly mean temperature (1975-1995) ranges from 8 ºC to 19.5 ºC (http://www.bom.gov.au/climate/data/). Three sites were selected including one bulk precipitation sampling site in open field (hereafter referred to as O site) and two throughfall sampling sites (Figure 3.1). One throughfall site is at a sampling plot under planted trees (hereafter referred to as P site). Another throughfall site is at a sampling plot under native eucalyptus trees (hereafter referred to as N site). The tree species at P site is *Pinus radiata and* at N site are *Eucalyptus camaldulensis*, *Eucalyptus leucoxylon* and *Eucalyptus baxteri.* More details of the study area can be found in Deng *et al*. (2013).

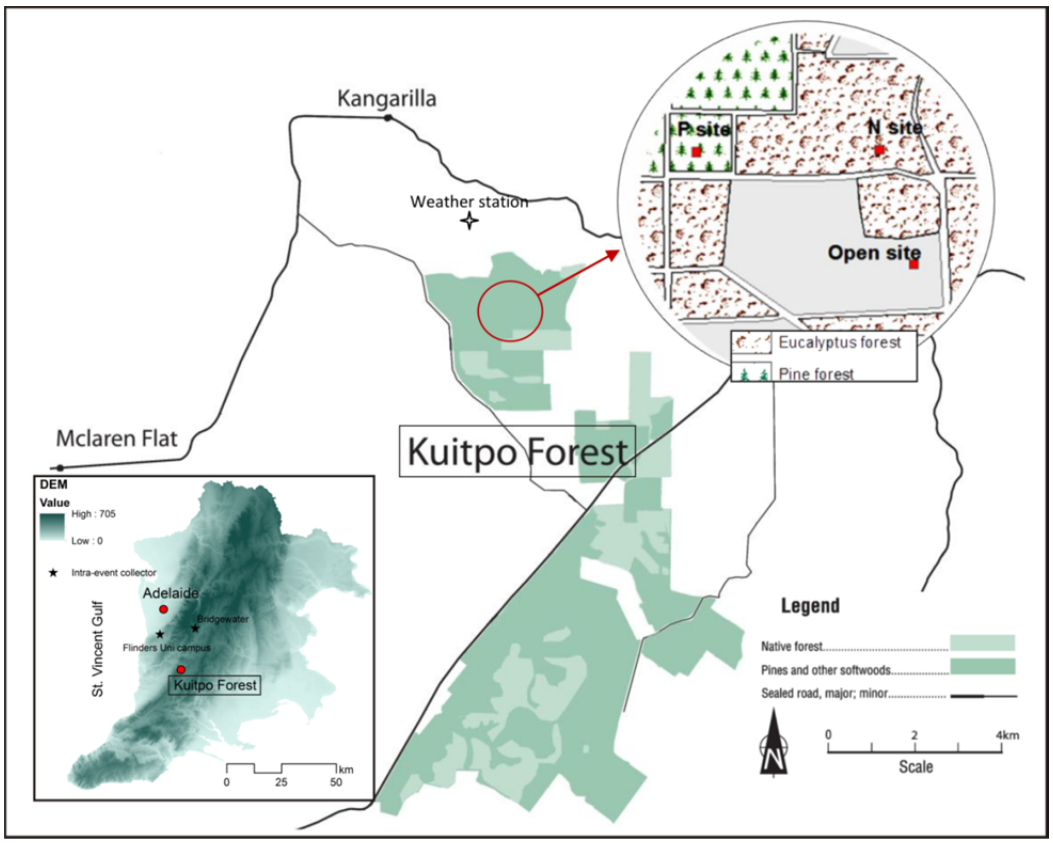

Figure 3.1 Study area at Kuitpo Forest, South Australia.

3.3 Methods

3.3.1 Field work

In the open field, four identical funnel collectors were placed to sample bulk precipitation. In each vegetation site, twenty collectors were placed randomly in a plot of 20 × 20 m^2. Each collector was made of 15 cm diameter funnel connected to a bottle of 1.5 L capacity. The funnel had coarse filters to stop leaf litter from falling into the bottle. The collector was held up in a plastic tube 55 cm above the ground to avoid dirt splashing into the funnels. To prevent water evaporation, each sampling bottle was filled with around 1 cm thick of liquid paraffin (Ajax Finechem Pty. Ltd., Adelaide) before being placed in the field. From September 29, 2009 to October 26, 2010, 17 batches of bulk precipitation and throughfall samples were collected. In every batch, 44 samples were collected with a roughly 18-day

interval depending on the event rainfall amount during the sampling period. For batch 10, overflow occurred.

Understanding of intra-event variation of isotopic composition is a starting point to understanding the isotopic composition of throughfall, thus more than 300 (34 events) intra-event rainwater samples were collected using automated sequential samplers at two sites: the Flinders University campus (elevation, 160 m a.s.l.) in Adelaide, and Bridgewater (elevation, 435 m a.s.l.) in the Mount Lofty Ranges (Figure 3.1) from 4 Sep. 2009 to 28 Feb. 2013. 289 samples (28 events) were collected on campus and the rest were collected at Bridgewater. Each sample was prescribed to collect a maximum of 2 mm, whereas a few were set to collect 1 mm during an event. Monthly rain isotope data collected at Global Network of Isotopes in Precipitation (GNIP) Adelaide site (#9467500, 34.97°S, 138.58°E, and 45 m above sea level) was also used for this study. The GNIP site monthly data covers a period between 1962 and 1984.

3.3.2 Isotopic analysis

Water samples were filtered with 0.45 μm filter paper (GN-6 Metrice Grid, Pall 186 Corporation) and kept in a cold room (4 ºC) before isotope analysis. Both ^{18}O and deuterium analysis of all samples were performed at Flinders Analytical Laboratory using L2130-*i* Cavity Ring-Down Spectroscopy (CRDS) Isotopic Water Analyzer (Picarro Inc., Santa Clara, CA, USA). Delta notation is used to express the stable isotope ratios of hydrogen and oxygen in precipitation and throughfall samples:

$$\delta(‰) = \left(\frac{R_{sample}}{R_{s\,\tan dard}} - 1 \right) \times 1000 \quad (3.1)$$

where R_{sample} and $R_{standard}$ represent the D/H or $^{18}O/^{16}O$ abundance ratios in sample and standard, respectively, and the standard refers to the Vienna Standard Mean Ocean Water (VSMOW). Four laboratory references have been applied to normalize the analysed

results to VSMOW values. The isotopic composition $\delta^{18}O$ and $\delta^{2}H$ of the four references are 0.95‰ and 7.40‰, -10.36‰ and -73.80‰, and -2.07‰ and -11.08‰ named as DESAL, EVIAN and SYNERGY, respectively. Precision (1σ) was reported to be 0.1‰ ($\Delta^{18}O$) for $\delta^{18}O$ and 1.0 ‰ ($\Delta^{2}H$) for $\delta^{2}H$ of our analysis results. The uncertainty (Δd) is calculated as $\Delta d = \left|\frac{\partial d}{\partial \delta^{2} H}\right| \Delta^{2} H + \left|\frac{\partial d}{\partial \delta^{18} O}\right| \Delta^{18} O$ with a value of 1.8‰.

3.3.3 Leaf area index

Leaf area index (LAI) was obtained with the hemispherical photography method at an overcast day (Zhang *et al.*, 2005). Each picture was taken vertically above each sampling point with a fish eye lens mounted to a Nikon D4000 at a stand height of 1.3 metres. The pictures were then processed with Gap Light Analyser (Frazer *et al.*, 1997) and the leaf area index was calculated according to Chen *et al*. (1991) for each zenith ring.

3.3.4 Calculation of mean isotopic composition

The volume-weighted mean value of precipitation and throughfall isotopes for each site were calculated as shown in equation (3.2).

$$\overline{\delta} = \frac{\sum_{i=1}^{n} \delta_i P_i}{\sum_{i=1}^{n} P_i} \qquad (3.2)$$

where δ_i and P_i are the isotopic composition of samples and water amount respectively at Open field, P site or N site, n is the total number of sample locations for each of the three sites, which is 4, 20 and 20 respectively.

3.4 Results and discussion

3.4.1 Isotopic composition of rainfall

Figure 3.2 shows 17 batches of isotopic composition of rainfall and throughfall. The trend of $\delta^{18}O$ in precipitation is reasonably consistent with that of GNIP monthly weighted mean

values except that 4 batches of collections are more enriched and one batch is much more depleted with ^{18}O in summer. On the other hand, *d*-excess of rainfall of nearly all 15 batches, are higher than GNIP data in the corresponding month especially in winter. This is likely because the study site (335 m a.s.l.) is higher in elevation than the GNIP site (45 m a.s.l.), thus tends to have a less degree of falling rain drops evaporation between the cloud base and the ground surface (hereafter referred to as sub-cloud evaporation).

The seasonal difference between summer and winter is quite obvious from the results in precipitation isotope and *d*-excess in the sampling period. $\delta^{18}O$ of precipitation is higher in summer than that in winter, while *d*-excess is lower in summer than that in winter. This seasonal pattern of both $\delta^{18}O$ and *d*-excess could be associated with the sub-cloud evaporation. Guan *et al*. (2013) reported that January and February rainfall, often associated with large trough synoptic weather patterns, could have very low $\delta^{18}O$, which has been observed in the GNIP data, but not in our throughfall samples. This is likely because that this weather pattern was less frequent than normal in the throughfall sampling year.

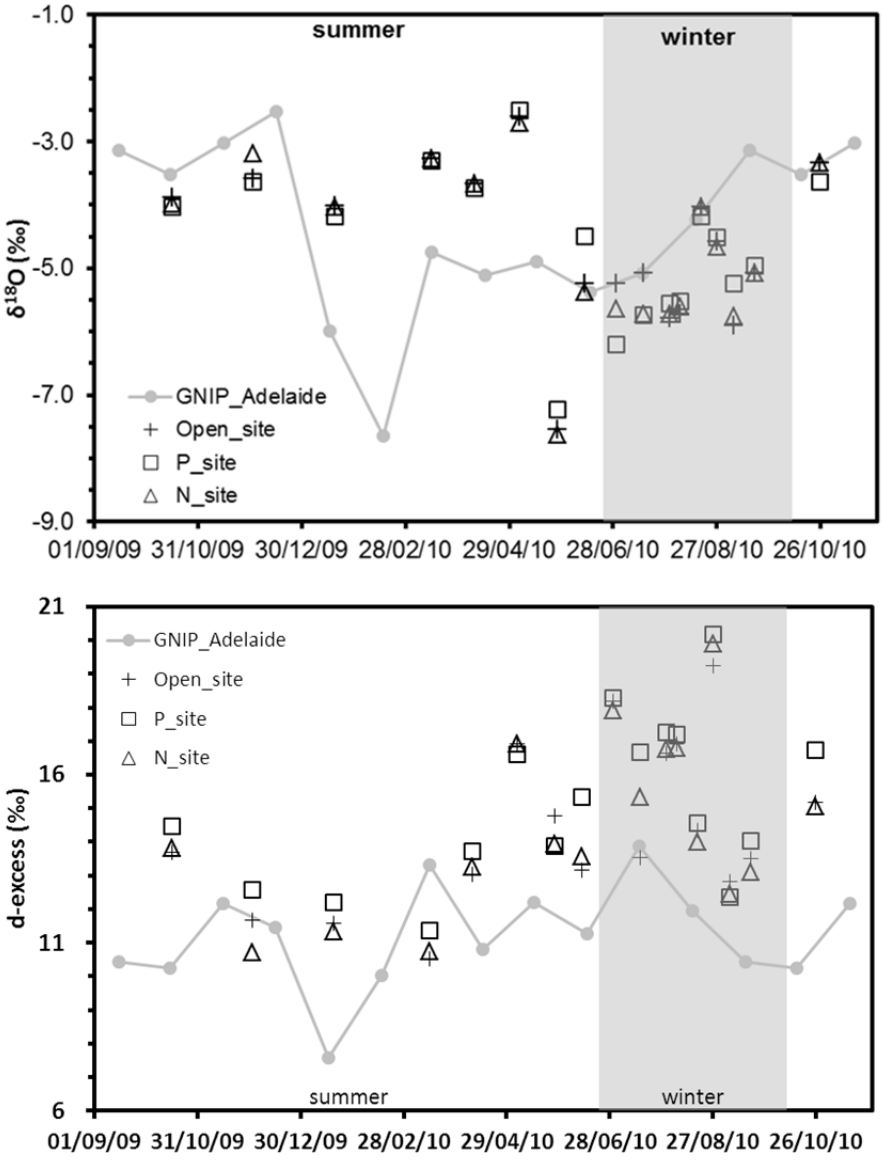

Figure 3.2 Isotopic composition of rainfall, throughfall at P site and N site respectively, and GNIP mean monthly data in Adelaide.

3.4.2 Isotopic composition of throughfall

The details of rainfall and throughfall isotopic composition and *d*-excess are showed in Table 3.1. For both P site and N site, $\delta^{18}O$ values of throughfall are depleted in half of all batches in comparison to that of precipitation. However, at P site, *d*-excess values are larger than that of precipitation while at N site *d*-excess values are smaller than that of precipitation for most batches.

Table 3.1 Climate characteristics and volume weighted mean of $\delta^{18}O$ and *d*-excess in the open site (O), the pine site (P) and the native vegetation site (N) in Kuipto Forest, South Australia. Air temperature and Relative humidity are mean daily values from the start day to the end day of the batch collection.

Batch No.	Sampling period		$\delta^{18}O$ (‰)			d-excess (‰)			P site		N site			Rain (mm)	Raining days	Air temperature (℃)	Relative humidity (%)
	Start	End	O	P	N	d_O	d_P	d_N	$\delta_P-\delta_O$	$d_P- d_O$		$\delta_N-\delta_O$	d_N-d_O				
2	29-Sep-09	16-Oct-09	-3.88	-4.03	-3.98	13.7	14.5	13.8	-0.14	0.8	a (c)	-0.10	0.1	-	58.9	9	13.0	63.3
3	16-Oct-09	2-Dec-09	-3.58	-3.64	-3.19	11.7	12.6	10.7	-0.06	0.9	a (c)	0.39	-1.0	b	60.8	14	23.2	44.9
4	2-Dec-09	18-Jan-10	-4.02	-4.19	-4.03	11.6	12.2	11.3	-0.16	0.6	a (c)	-0.01	-0.2	a	39.9	9	23.7	41.1
5	18-Jan-10	15-Mar-10	-3.27	-3.30	-3.27	10.5	11.4	10.7	-0.03	0.8	a (c)	0.00	0.2	a	30.0	11	24.2	42.4
6	15-Mar-10	9-Apr-10	-3.67	-3.74	-3.66	13.0	13.7	13.3	-0.07	0.7	a (c)	0.00	0.2	a	53.1	11	22.7	47.9
7	9-Apr-10	5-May-10	-2.62	-2.51	-2.71	16.9	16.6	16.9	0.10	-0.3	b	-0.09	0.0	-	39.0	12	17.7	60.2
8	5-May-10	27-May-10	-7.55	-7.22	-7.62	14.8	13.9	14.0	0.32	-0.9	b	-0.07	-0.8	a	42.0	12	15.3	60.9
9	27-May-10	12-Jun-10	-5.24	-4.49	-5.38	13.2	15.3	13.6	0.75	2.2	a	-0.14	0.4	a (c)	47.9	15	11.9	76.3
10*	12-Jun-10	30-Jun-10	-5.24	-6.20	-5.64	18.2	18.3	17.9	-0.96	0.1	a	-0.41	-0.3	a	91.2	10	11.7	69.4
11	30-Jun-10	16-Jul-10	-5.08	-5.74	-5.72	13.5	16.7	15.3	-0.65	3.1	a	-0.64	1.8	a	76.1	11	10.9	73.8
12	16-Jul-10	31-Jul-10	-5.78	-5.56	-5.73	16.6	17.3	16.8	0.23	0.6	a	0.05	0.1	-	26.5	11	11.2	77.6
13	31-Jul-10	6-Aug-10	-5.72	-5.53	-5.61	16.9	17.2	16.8	0.19	0.3	a	0.10	-0.1	-	61.3	5	8.4	78.0
14	6-Aug-10	18-Aug-10	-4.04	-4.19	-4.03	14.3	14.6	14.0	-0.15	0.2	a	0.00	-0.4	b	45.1	7	11.2	68.7
15	18-Aug-10	27-Aug-10	-4.57	-4.52	-4.67	19.2	20.2	19.9	0.05	1.0	a	-0.09	0.7	a	76.0	8	10.2	76.1
16	27-Aug-10	6-Sep-10	-5.90	-5.25	-5.76	12.8	12.4	12.4	0.65	-0.5	b	0.14	-0.4	b	65.2	6	10.9	76.5
17	6-Sep-10	18-Sep-10	-5.07	-4.96	-5.07	13.5	14.0	13.1	0.11	0.5	a	0.00	-0.4	b	49.9	6	12.3	69.6
18	18-Sep-10	26-Oct-10	-3.34	-3.64	-3.34	15.2	16.7	15.1	-0.30	1.5	a (c)	-0.01	-0.1	-	32.1	17	12.1	69.3

Shaded for summer collections and white for winter collections;
a, b and c are corresponding to the conceptual framework;
* refers to overflowed sample collection and - refers to the batch which is hard to classify from our conceptual framework due to isotopic analysis errors.

The lower $\delta^{18}O$ at both P site and N site than that at the open site are more frequent in summer than in winter. In summer, 6 out of 9 batches have lower $\delta^{18}O$ at P site as well as that at N site. In winter, the lower or higher $\delta^{18}O$ value than that of open precipitation does not show obviously patterns. But for batches 10 and 11, the depletions are consistent at both P site and N site.

From Figure 3.3, it shows that pine trees have larger canopy storage capacity than native eucalyptus trees. In other words, more interception loss happened at P site than at N site which is consistent with that the average LAI for P site is 2.11 and for N site is 0.56.

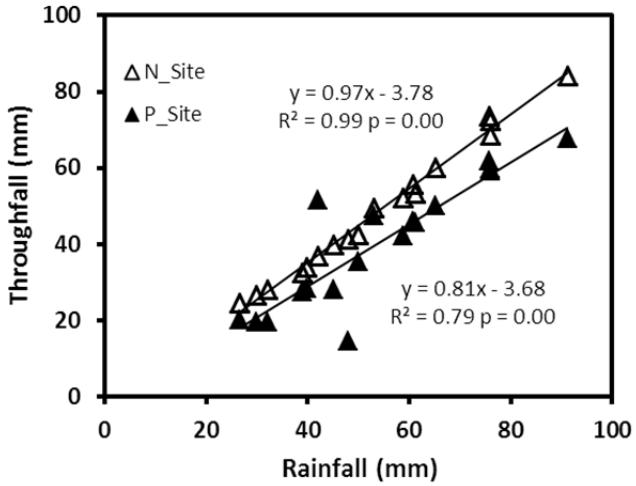

Figure 3.3 Relationships between throughfall and rainfall for 17 batches of sample collection in Kuitpo Forest, South Australia.

The results indicate more interception loss will not necessarily have higher $\delta^{18}O$ or smaller *d*-excess because throughfall collections could be resulted from partial evaporation, intra-event selection (complete evaporation of intercepted rain water), and inter-event selection (some small event being completely intercepted and evaporated). That $\delta^{18}O$ values of throughfall are depleted in most batches in comparison to that of precipitation make it invalid to apply Saxena's (1986) or Gat's (2010) model to estimate throughfall isotopes. Both of their models are mainly based on the theory of partial evaporation. When intra-

event selection happens, either depletion or enrichment can happen to throughfall but *d*-excess is likely to increase due to the information loss of relative low *d*-excess part, which is reasonable to explain our results. However, the situation is more complex when we had monthly sample collections. The isotopic information of some small events (rainfall smaller than canopy storage) is not reflected in throughfall collections. Due to the amount effect in summer that small events tend to have high $\delta^{18}O$ values and low *d*-excess, the inter-event selection process can easily cause a depletion of $\delta^{18}O$ values and an increase of *d*-excess values in throughfall.

3.4.3 Variations of $\delta^{18}O$ and *d*-excess of intra-events and the amount effect

The intra-event variations of $\delta^{18}O$ and *d*-excess at nearby locations are shown in Figure 3.4. Over all events for $\delta^{18}O$, there is on average a decreasing trend within each event. For *d*-excess, the value is low at the beginning and toward the end of a rainfall event, and is relatively stable in between.

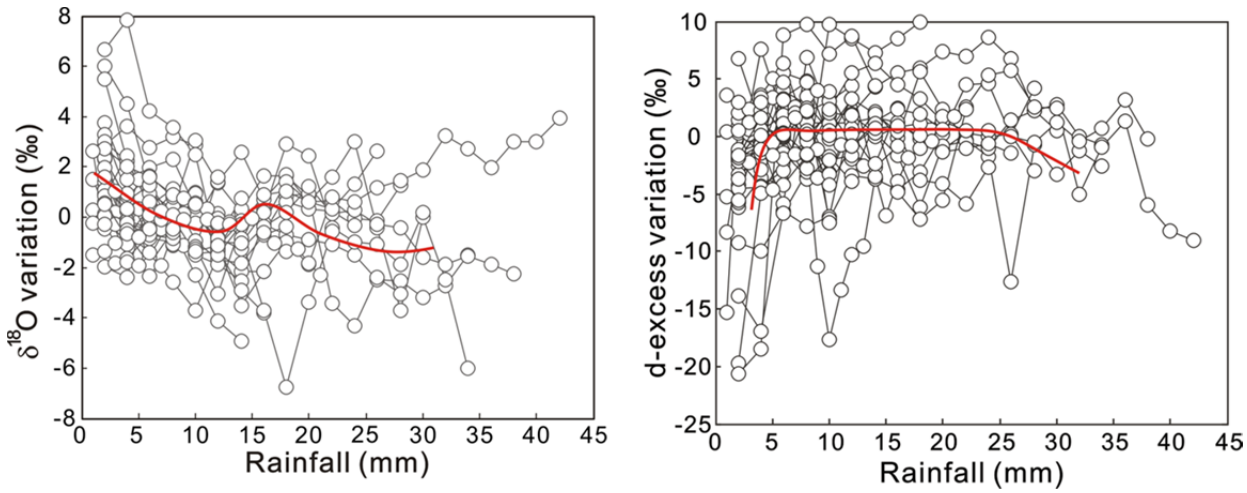

Figure 3.4 Intra-event variations of $\delta^{18}O$ and d-excess. $\delta^{18}O$ variation (d-excess variation) is calculated as the difference between $\delta^{18}O$ (*d*-excess) of each intra-event sample and the weighted mean $\delta^{18}O$ (*d*-excess) of the corresponding event. Red line is hand drawn.

The decreasing of $\delta^{18}O$ can be explained by the Rayleigh-type rainout process. The Rayleigh-type model described the process that rain drops condense continuously from

the limited vapour in isotopic equilibrium. The condensed rain drops become depleted in isotopic composition due to isotopic fractionation. This trend is also very similar to many other intra-event studies (e.g. Celle-Jeanton *et al*., 2004; Pionke and DeWalle, 1992; Yoshimura, 2003). Because the sub-cloud evaporation effect (Dansgaard, 1964; Gat, 1996) normally is strong at the beginning and the end of a rainfall event, *d*-excess has low values at these two stages. The intra-event variations of $\delta^{18}O$ and *d*-excess are useful to develop and examine a conceptual framework of isotopic composition of throughfall. Our generalized pattern (red line in Figure 3.4) is to capture the major characteristics of the variations of the intra-event isotopic composition although there are a few events do not follow the pattern.

$\delta^{18}O$ and *d*-excess of summer events and monthly samples are shown in Figure 3.5a and Figure 3.5b respectively. In summer season, the amount effect can be observed both in the events we collected and in long term records from GNIP monthly weighted mean data. Rainfall events of a larger size tend to have a lower $\delta^{18}O$ and a higher *d*-excess.

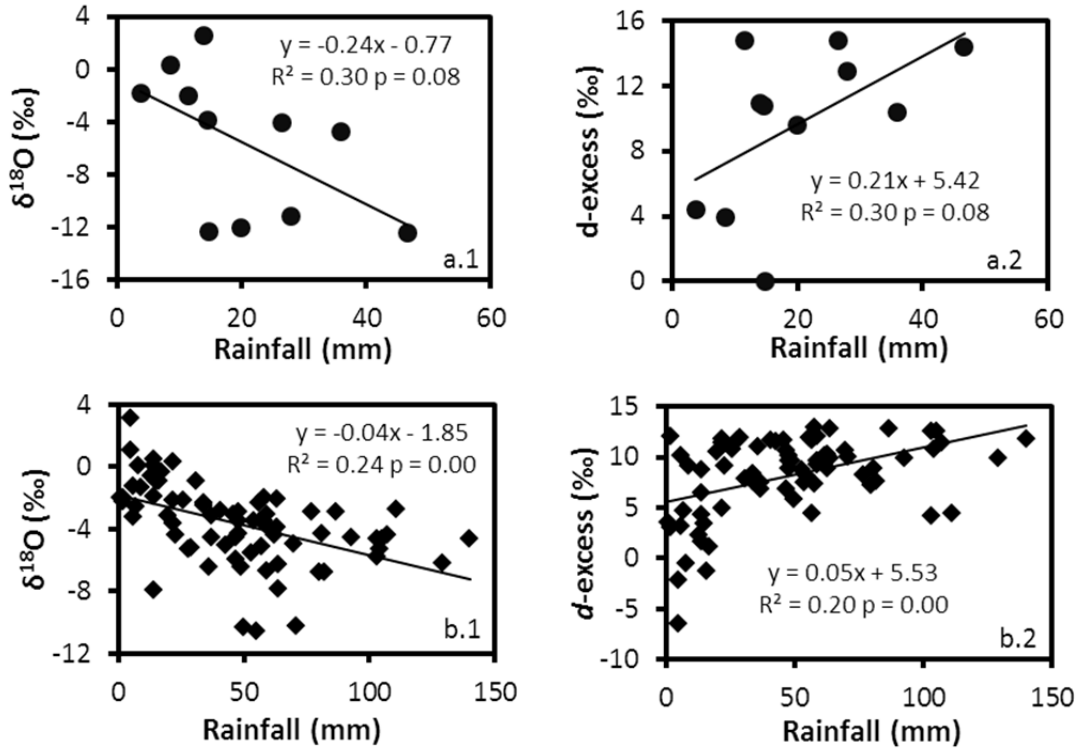

Figure 3.5 The amount effect on $\delta^{18}O$ and *d*-excess in summer. Event samples are collected during 2009-

2013 (Figure a) and GNIP data are monthly volume-weighted mean data from 1962 to 1984 (Figure b).

This phenomenon is consistent with Dansgaard (1964) who found that the amount effect is evident in summer time in mid-latitudes. One mechanism for the amount effect is that sub-cloud evaporation of the raindrops and/or the vapour mixing with surrounding moisture recondense to form the raindrops again (Lee and Fung, 2008; Risi *et al*., 2008a). Low relative humidity (or high vapour deficit), which is the case in summer in the study area (Table 3.1), can cause high sub-cloud evaporation. Another cause of the amount effect is Rayleigh fractionation in cloud vapour condensation. As water vapour condenses in rain clouds, heavier water isotopes become enriched in the liquid phase while the lighter isotopes remain in the vapour phase. Thus large rain events tend to have lighter isotopic composition (Dansgaard, 1964; Kendall and McDonnell, 1998). The amount effect in summer is another useful pattern to examine the mechanisms for isotopic composition of throughfall.

3.4.4 Conceptual framework of isotopic composition of throughfall

Three different dynamic processes may lead to the alteration of isotopic composition in throughfall from that of rainfall. The first one is that the water has no contact with canopy, without any isotopic alteration. The second one is that the water in contact with canopy partly evaporates with the residual contributing to throughfall. The last is that the water totally evaporates from the canopy without contribution to throughfall. In other words, the throughfall isotopic composition lies on the degree of evaporation, on what part of event rainfall being intercepted and evaporated. Based on the characteristics of event and intra-event isotopic composition in the study area, we develop the following conceptual framework to describe possible mechanisms influencing throughfall isotopic composition. The principles described here should apply for other areas although the details in throughfall isotopic composition in comparison to precipitation may vary if the event and

intra-event isotopic patterns are different from this study.

1. Intra-event selection process - Part of precipitation that is stored in canopy may evaporate totally which is more likely to happen in the beginning and the end of an event. Because the relative humidity is low at the beginning and rain water is lack in the end. In this case, throughfall isotopic composition selectively reflects part of precipitation. Since isotopic signature varies during one event, this process can lead to enrichment or depletion of heavy isotopes in throughfall, and more likely an increase in *d*-excess due to the 'disappearance' of low *d*-excess values in the beginning and the end of the event as shown in Figure 3.6a.

2. Partial evaporation in interception - The precipitation which reaches and is temporally stored in the canopy can partially evaporate. This leads to a heavy isotopic enrichment in throughfall and a decrease of *d*-excess because of isotopic fractionation as shown in Figure 3.6b.

3. Inter-event selection process - When we collect cumulative samples of multiple events, such as on the monthly time scale, events of a small size are intercepted totally thus do not contribute to throughfall. This process will depend on the time scale of sampling and can lead to either enrichment or depletion of heavy isotopes in throughfall. The depletion is more likely than enrichment as small events normally have a higher isotope concentration due to the amount effect as shown in Figure 3.6c.

4. Isotopic exchange - Molecular exchange processes with atmospheric water vapour will be dominant only when relative humidity is nearly 100% and big difference of isotopic composition between two vapours, vapour equilibrium with canopy water and vapour of the surrounding atmospheric moisture. This process can enrich or deplete heavy isotope concentration in throughfall. But the conditions are rarely observed in natural environments

(Rodhe, 1987) and this process may be significant especially in humid climate, e.g. (Kendall, 1993). Hourly (Tremoy *et al*., 2012) and daily (Deshpande *et al*., 2010) measurements of isotopic concentration of both vapour and rain water during individual event approaches to equilibrium as relative humidity increases. Nevertheless, high humidity with temporally varying isotopic composition could result in water stored in the canopy being isotopically different from the canopy air, creating potential conditions for exchange to take place. Without simultaneous water vapour isotopic data, this mechanism is difficult to quantify in the study.

5. Pre-event storage effect - Moisture retained between events can affect throughfall isotopic composition (Allen *et al*., 2013; Ikawa *et al*., 2011). This effect either increases or decreases $\delta^{18}O$ or *d*-excess respectively depending on the isotopic composition and residual amount of the previous event. Thus it is more likely to happen when time interval is short between events. On the one hand, this effect rarely happens in hot and dry summer in our study area. On the other hand, we lump several events as one batch throughfall collection, thus this effect is undetectable for this sampling method.

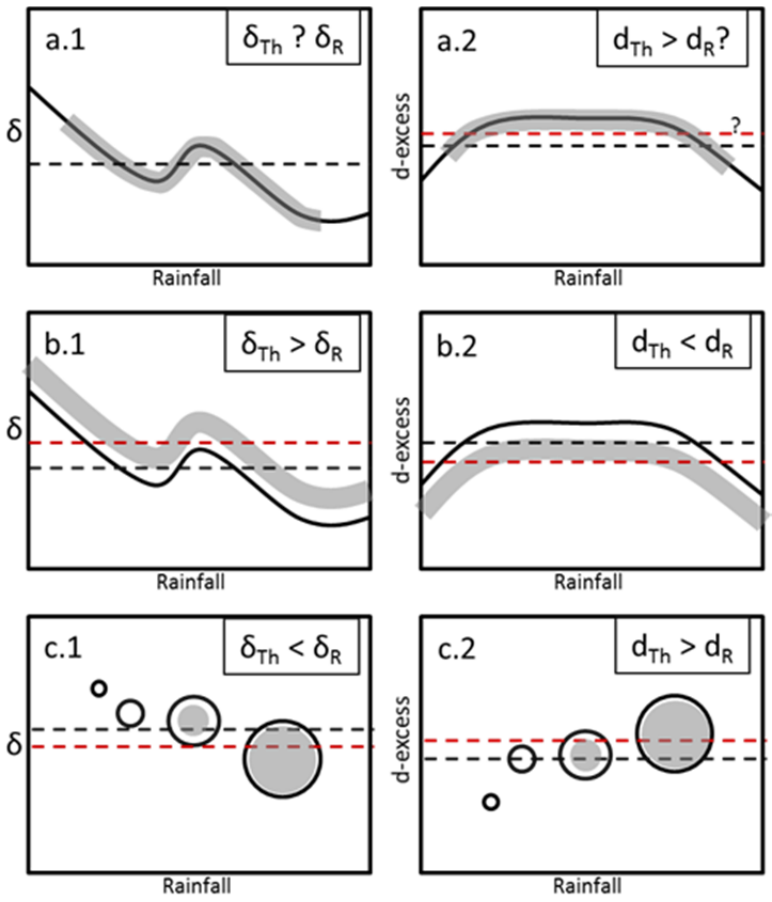

Figure 3.6 Conceptual framework for the isotopic composition of throughfall : a. Intra-event selection; b. Partial evaporation of interception; c. Inter-event selection (assumed amount effect especially in summer). δ for $\delta^{18}O$, δ_{Th} for $\delta^{18}O$ of throughfall, δ_R for $\delta^{18}O$ of rainfall; solid black line is for intra-event, grey bar is for throughfall collection of the corresponding rainfall; black dash line is weighted mean $\delta^{18}O$ of the event, red dash line is weighted mean $\delta^{18}O$ of the corresponding throughfall collection; in c.1 the black open circle is for $\delta^{18}O$ of each rain event, the grey filled circle is for $\delta^{18}O$ of each throughfall collection and the size of circles indicates the rainfall/throughfall amount. The same applies for *d*-excess.

Thus we classified the major effects or processes for P site and N site in summer and winter respectively by using both $\delta^{18}O$ and *d*-excess. The differences of $\delta^{18}O$ and *d*-excess between throughfall and open precipitation are calculated separately as shown in Table 3.1. The classification based on these differences (Table 3.1) and conceptual framework (Figure 3.6) gives the most likely control process. Only 3 batches at P site and 4 batches at N site are possibly controlled by partial evaporation thus it is not as important as the selection processes in the study area.

In summer, intra-event selection and inter-event selection cannot be completely

distinguished in our study when the changes $\delta^{18}O$ and *d*-excess in throughfall changes in the same direction between the two selection processes. One or both of these two processes is/are very likely to be the major control of the isotopic composition in throughfall at P site and N site. In winter, which is the raining season of South Australia, small events occur less frequently than that in summer as shown in Figure 3.7. The small events are potentially to evaporate totally in summer while they may be preserved in throughfall in winter. Thus intra-event selection is the most likely major control of the isotopic composition in throughfall at P site and N site in winter.

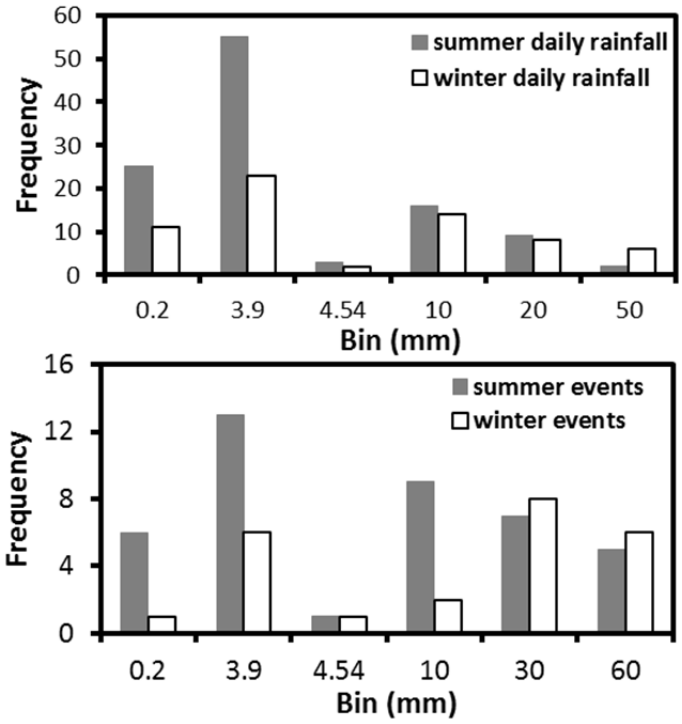

Figure 3.7 Histograms of daily rainfall and rain events in summer and winter, respectively from September 2009 to October 2010.

No matter how much enrichment or depletion, P site has more significant effects than N site on isotopic composition of throughfall due to its much denser vegetation cover. For $\delta^{18}O$, the range of the effect (difference between throughfall and open site) at P site is from -0.96‰ to 0.75‰ (±0.41‰, standard deviation), while at N site the range is from -0.64‰ to

0.39‰ (±0.22‰). In summer, the effect at P site ranges from -0.30‰ to 0.75‰ (±0.32‰), while at N site that ranges from -0.10‰ to 0.39‰ (±0.16‰). In winter, the effect ranges from -0.96‰ to 0.65‰ (±0.52‰), while N site that ranges from -0.64‰ to 0.1‰ (±0.27‰). The results indicate that denser vegetation can cause larger alteration of input isotopic composition of precipitation as generally expected. The alteration is larger in winter than in summer in our study area. Since major groundwater recharge happens in winter in South Australia, the vegetation effects on isotopic composition of throughfall should be considered when the catchment has a dense canopy cover.

3.4.5 Implications to groundwater recharge, hydrograph separation and paleoclimate

Canopy alterations of throughfall isotopes are observed in both vegetated surfaces in the study area, and can be attributed to three mechanisms. The question is whether this alteration is significant and should be considered in studies with isotopic applications. In studies about groundwater recharge sources, average isotopic values of seasonal or annual precipitation are often used to compare with groundwater. For example, in Guan *et al*. (2009), groundwater isotopic composition is compared with mean wet season rainfall to determine whether groundwater is recharged by local or upslope precipitation. A $\delta^{18}O$ difference of 0.5‰ is shown to be very sensitive in that examination. In this present study, input $\delta^{18}O$ of throughfall at P site and N site is -0.14‰ and -0.06‰, different from that of rainfall when calculated from weighted mean difference for the whole monitoring year. In wet season during which 70% rainfall happened from May to September, input $\delta^{18}O$ of throughfall at P site and N site is -0.17‰ and -0.10‰ different from that of rainfall. The difference is slightly larger than analytical uncertainty of liquid water sample which is 0.1‰ for $\delta^{18}O$. The difference is more obvious in wet season which is considered as the main recharge season in our study area. The effects of throughfall alteration on water stable isotope can be significant especially when the catchment has very dense vegetation cover.

In hydrograph separation studies, event sampling data of water stable isotope are usually used (Hooper and Shoemaker, 1986; Ladouche *et al*., 2001; Laudon and Slaymaker, 1997). Using $\delta^{18}O$ for an example, if baseflow isotope is -4.9‰, given a rain event -6‰, if we have a value of -5.5‰ in runoff water after the event, the calculated new water contribution for the runoff would be 54.5% from the event. If the rain event input in throughall is altered to -6.5‰, then the calculated new water contribution would be 37.5%. A 17 percentage point change happens with only 0.5‰ alteration of the isotopic input. This 0.5‰ alteration is likely in monthly throughfall (Table 3.1) and it is very likely larger at the event scale. Thus for hydrograph separation studies vegetation effects cannot be neglected.

Values of $\delta^{18}O$ in tree-ring cellulose closely reflect the $\delta^{18}O$ values in atmospheric precipitation and hence mean annual temperature (Burk and Stuiver, 1981). The annual mean of the cellulose $\delta^{18}O$ data can be used to reconstruct paleoclimate. But do effects of vegetation cover matter? In Liu *et al*. (2012), the standard deviation of tree-ring $\delta^{18}O$ is ±1.3‰ in south-western China. The alteration in throughfall isotopic composition at annual basis is quite small, similar to the analytical uncertainty of tree-ring cellulose which is commonly ±0.3‰ (Berkelhammer and Stott, 2008; Burk and Stuiver, 1981). As it mentioned that the input $\delta^{18}O$ of throughfall at P site and N site is -0.14‰ and -0.06‰ different from that of rainfall when it is calculated from weighted mean difference for the whole monitoring year. Thus vegetation effects of throughfall isotopic composition may be negligible for paleoclimate reconstruction.

It should be noted that the above discussion is based on the results of this study. Examination of these issues over other vegetation surfaces with different climate conditions is recommended.

3.5 Conclusions

Based on one year throughfall monitoring and using both ^{18}O and *d*-excess at two vegetated surfaces in Kuitpo Forest and previous studies we synthesized the conceptual framework for studying throughfall isotopic composition. The framework serves as a useful tool for studying effects of intra-event selection, partial evaporation and inter-event selection. The results indicate that in summer, one or both of intra-event selection and inter-event selection is/are very likely to be the major control of the isotopic composition in throughfall at P site and N site. In winter intra-event selection is possible the major control of the isotopic composition of throughfall at P site and N site. Partial evaporation is also observed at both sites, but not as important as intra-event selection or inter-event selection. P site has more significant effect on isotopic composition of throughfall than N site because of its much denser vegetation cover.

In vegetated catchments, the input isotopic information is altered from precipitation. The vegetation effects on isotopic input can be significant in densely vegetated catchments and is important for hydrograph separation studies but can be negligible for paleoclimate reconstruction and identification of groundwater recharge sources.

References

Ajami, H., Troch, P.A., Maddock, T., Meixner, T., Eastoe, C., 2011. Quantifying mountain block recharge by means of catchment-scale storage-discharge relationships. *Water Resour. Res.* 47.

Allen, S.T., Brooks, J.R., Keim, R.F., Bond, B.J., McDonnell, J.J., 2013. The role of pre-event canopy storage in throughfall and stemflow by using isotopic tracers. *Ecohydrology.*

Berkelhammer, M.B., Stott, L.D., 2008. Recent and dramatic changes in Pacific storm trajectories recorded inδ18O from Bristlecone Pine tree ring cellulose. *Geochem. Geophys.* 9(4).

Brodersen, C., Pohl, S., Lindenlaub, M., Leibundgut, C., von Wilpert, K., 2000. Influence of vegetation structure on isotope content of throughfall and soil water. *Hydrol. Process.* 14(8): 1439-1448.

Burk, R.L., Stuiver, M., 1981. Oxygen isotope ratios in trees refelect mean annual

temperature and humidity. *Science*. 211: 1417-1419.

Celle-Jeanton, H., Gonfiantini, R., Travi, Y., Sol, B., 2004. Oxygen-18 variations of rainwater during precipitation: application of the Rayleigh model to selected rainfalls in Southern France. *J. Hydrol.* 289(1-4): 165-177.

Chen, J.M., Black, T.A., Adams, R.S., 1991. Evaluation of hemispherical photograpgy for determing plant area index and geometry of a forest stand. *Agric. For. Meteorol.* 56(1-2): 129-143.

Clark, I.D., Fritz, P. (Eds.), 1997. Environmental isotopes in hydrogeology. CRC Press/Lewis Publishers, Boca Raton, FL.

Craig, H., Gordon, L., 1965. Deuterium and oxygen-18 in the ocean and the marine atmosphere, Spoleto.

Crockford, R.H., Richardson, D.P., 2000. Partitioning of rainfall into throughfall, stemflow and interception: effect of forest type, ground cover and climate. *Hydrol. Process.* 14: 2903-2920.

Dansgaard, W., 1964. Stable isotopes in precipitation. *Tellus*, 16: 436-468.

Darling, W.G., 2004. Hydrological factors in the interpretation of stable isotopic proxy data present and past: a European perspective. *Quaternary Sci. Rev*. 23(7-8): 743-770.

Deng, Z., Priestley, S.C., Guan, H., Love, A.J., Simmons, C.T., 2013. Canopy enhanced chloride deposition in coastal South Australia and its application for the chloride mass balance method. *J. Hydrol.* 497: 62-70.

Deshpande, R.D., Maurya, A.S., Kumar, B., Sarkar, A., Gupta, S.K., 2010. Rain-vapor interaction and vapor source identification using stable isotopes from semiarid western India. *J. Geophys. Res.* 115(D23).

Dewalle, D.R., Swistock, B.R., 1994. Differences in O-18 Content of Throughfall and Rainfall in Hardwood and Coniferous Forests. *Hydrol. Process*. 8(1): 75-82.

Frazer, G.W., Trofymow, J.A., Lertzman, K.P., 1997. A method for estimating canopy openness, effective leaf area index, and photosynthetically active photon flux density using hemispherical hotography and computerized image analysis techniques, Victoria, BC.

Frot, E., van Wesemael, B., Vandenschrick, G., Souchez, R., Solé Benet, A., 2007. Origin and type of rainfall for recharge of a karstic aquifer in the western Mediterranean: a case study from the Sierra de Gador–Campo de Dalias (southeast Spain). *Hydrol. Process.* 21(3): 359-368.

Gat, J.R., 1996. Oxygen and hydrogen isotopes in the hydrologic cycle. *Annu. Rev. Earth Planet. Sci.* 24: 225-262.

Gat, J.R. (Ed.), 2010. Isotope Hydrology: A Study of the Water Cycle. Series on Environmental Science and Management, 6. Imperial College Press, Weizmann Institute of Science, Israel, 75-77 pp.

Gat, J.R., Tzur, Y., 1967. Mofification of the isotopic composition of rain water by processes which occur before groundwater recharge, Isotopes in Hydrology: Proc. Symp.

IAEA, Vienna, pp. 49-60.

Gibson, J.J., Price, J.S., Aravena, R., Fitzgerald, D.F., Maloney, D., 2000. Runoff generation in a hypermaritime bog-forest upland. *Hydrol. Process.* 14: 2711-2730.

Goller, R., W. Wilcke, M.J. Leng, H.J. Tobschall, K. Wagner, C. Valarezo, W. Zech., 2005. Tracing water paths through small catchments under a tropical montane rain forest in south Ecuador by an oxygen isotope approach. *J. Hydrol.* 308(1-4): 67-80.

Guan, H., Simmons, C.T., Love, A.J., 2009. Orographic controls on rain water isotope distribution in the Mount Lofty Ranges of South Australia. *J. Hydrol.* 374(3-4): 255-264.

Guan, H., Zhang, X., Skrzypek, G., Sun, Z., Xu, X., 2013. Deuterium excess variations of rainfall events in a coastal area of South Australia and its relationship with synoptic weather systems and atmospheric moisture sources. *J. Geophys. Res.*: Atmospheres, 118(2): 1123-1138.

Hooper, R.P., Shoemaker, C.A., 1986. A Comparison of Chemical and Isotopic Hydrograph Separation. *Water Resour. Res.* 22(10): 1444-1454.

Ikawa, R., Yamamoto, T., Shimada, J., Shimizu, T., 2011. Temporal variations of isotopic compositions in gross rainfall, throughfall, and stemflow under a Japanese cedar forest during a typhoon event. *Hydrol. Res. Lett.* 5: 32-36.

Kato, H., Y. Onda, K. Nanko, T. Gomib, T. Yamanaka, S. Kawaguchi., 2013. Effect of canopy interception on spatial variability and isotopic composition of throughfall in Japanese cypress plantations. *J. Hydrol.* 504: 1-11.

Kendall, C., 1993. Impact of isotopic heterogeneity in shallow system on stormflow generation. (Ph.D. Dissertation). , University of Maryland, College Park, MD.

Kendall, C., McDonnell, J.J., 1993. Effect of intrastorm isotopic heterogeneities of rainfall, soil water, and groundwater on runoff modelling. In: Peters, N.E., Hoehn, E., Leibundgut, C., Tase, N., Walling, D.E. (Eds.). Tracers in Hydrology: Proceedings of an International Symposium. IAHS Press, Yokohama, Japan, pp. 41-48.

Kendall, C., McDonnell, J.J. (Eds.), 1998. Isotope tracers in catchment hydrology. Elsevier, Amsterdam, 100 pp.

Kubota, T., Tsuboyama, Y., 2004. Estimation of evaporation rate from the forest floor using oxygen-18 and deuterium compositions of throughfall and stream water during a non-storm runoff period. *J.For. Res.* 9(1): 51-59.

Ladouche, B. A. Probst, D. Viville, S. Idir, D. Baqué, M. Loubet, , J.-L. Probst, c, , T. Bariac., 2001. Hydrolograph separation using isotopic, chemical and hydrological approaches (Strengbach catchment, France). *J. Hydrol.* 242: 255-274.

Laudon, H., Slaymaker, O., 1997. Hydrograph separation using stable isotopes, silica and eclectrical conductivity: an alpine example. *J. Hydrol.* 201: 82-101.

Lee, J.-E., Fung, I., 2008. “Amount effect” of water isotopes and quantitative analysis of post-condensation processes. *Hydrol. Process.* 22(1): 1-8.

Liu, W.J., Liu, W.Y., Li, J.T., Wu, Z.W., Li, H.M., 2008. Isotope variations of throughfall,

stemflow and soil water in a tropical rain forest and a rubber plantation in Xishuangbanna, SW China. *Hydrol. Res.* 39: 437-449.

Liu, X., W. An, K. Treydteb, X. Shao, S. Leavitt, S. Hou, T. Chen, W. Sun, D. Qin., 2012. Tree-ring $\delta^{18}O$ in southwestern China linked to variations in regional cloud cover and tropical sea surface temperature. *Chem. Geol.* 291: 104-115.

Pichon, A., Travi, Y., Marc, V., 1996. Chemical and isotopic variations in throughfall in a Mediterranean Context. *Geophys. Res. Lett.* 23(5): 531-534.

Pionke, H.B., DeWalle, D.R., 1992. Intra- and inter-storm ^{18}O trends for selected rainstorms in Pennsylvania. *J. Hydrol.* 138: 131-143.

Rindsberger, M., Jaffe, S., Rahamim, S., Gat, J.R., 1990. Patterns of the isotopic composition of precipitation in time and space: data from the Israeli storm water collection program. *Tellus*, 42B: 263-271.

Risi, C., Bony, S., Vimeux, F., 2008a. Influence of convective processes on the isotopic composition ($\delta^{18}O$ andδD) of precipitation and water vapor in the tropics: 2. Physical interpretation of the amount effect. *J. Geophys. Res.* 113(D19).

Risi, C., S. Bony, F. Vimeux, L. Descroix, B. Ibrahim, E. Lebreton, I. Mamadou, B. Sultan., 2008b. What controls the isotopic composition of the African monsoon precipitation? Insights from event-based precipitation collected during the 2006 AMMA field campaign. *Geophys. Res. Lett.* 35(24).

Risi, C., S. Bony, F. Vimeux, C. Frankenberg, D. Noone, J. Worden., 2010. Understanding the Sahelian water budget through the isotopic composition of water vapor and precipitation. *J. Geophys. Res.* 115(D24).

Rodhe, A., 1987. The origin of streamwater traced by oxygen-18. Ph.D. Thesis, Uppsala University, 460, plus Appendix 73 pp.

Rozanski, K., Araguas-Araguas, L., Gonfiantini, R., 1992. Relation between long-term trends of oxygen-18 isotope composition of precipitation and climate. *Science*, 258: 981-985.

Rozanski, K., Araguas-Araguas, L., Gonflantini, R., 1993. Isotopic patterns in modern global precipitation. *Geophys. Monogr.* 78: 1-36.

Saxena, R.K., 1986. Estimation of canopy reservoir capacity and Oxygen-18 fractionation in throughfall in a pine forest. *Nord. Hydrol.* 17: 251-260.

Soderberg K., Good S. P., O'Connor M., Wang L., Kathleen R. and Caylor, K. K., 2013. Using atmospheric trajectories to model the isotopic composition of rainfall in central Kenya. Ecosphere 4, art 33.

Steinman, B.A., Abbott, M.B., Mann, M.E., Stansell, N.D., Finney, B.P., 2012. 1,500 year quantitative reconstruction of winter precipitation in the Pacific Northwest. *Proc. Natl. Acad. Sci.*109(29): 11619-11623.

Tremoy, G., F. Vimeux, S. Mayaki, I. Souley, O. Cattani, C. Risi, G. Favreau, M. Oi., 2012. A 1-year long $\delta^{18}O$ record of water vapor in Niamey (Niger) reveals insightful atmospheric processes at different timescales. *Geophys. Res. Lett.* 39(8).

Uemura, R., N. Yonezawa, K. Yoshimura, R. Asami, H. Kadena, K. Yamada, N. Yoshida., 2012. Factors controlling isotopic composition of precipitation on Okinawa Island, Japan: Implications for paleoclimate reconstruction in the East Asian Monsoon region. *J. Hydrol.* 475: 314-322.

Wels, C., Cornett, R.J., Lazerte, B.D., 1991. Hydrograph Separation - a Comparison of Geochemical and Isotopic Tracers. *J. Hydrol.* 122(1-4): 253-274.

Yoshimura, K., 2003. A quantitative analysis of short-term ^{18}O variability with a Rayleigh-type isotope circulation model. *J. Geophys. Res.* 108(D20).

Zhang, Y.Q., Chen, J.M., Miller, J.R., 2005. Determining digital hemispherical photograph exposure for leaf area index estimation. *Agric. For. Meteorol.* 133(1-4): 166-181.

CHAPTER 4 EXAMINATION OF ECOHYDROLOGICAL PROCESSES ON TWO CONTRASTING HILLSLOPES IN SOUTH AUSTRALIA USING $\delta^{18}O$ AND $\delta^{2}H$

4.1 Introduction

Water stable isotopes ($\delta^{18}O$ and $\delta^{2}H$) are commonly applied as tracers in ecohydrology studies such as the partitioning of evapotranspiration (e.g. Brunel *et al*., 1997; Good *et al*., 2014; Wang *et al*., 2010; Wang *et al*., 2013; Yepez *et al*., 2005) and the sources of plant water use (e.g. Dawson and Ehleringer, 1993; Ehleringer and Dawson, 1992) based on a simple assumption that no fractionation happens in $\delta^{18}O$ and $\delta^{2}H$ during root water uptake. In other words, $\delta^{18}O$ and $\delta^{2}H$ of twig (or stem) water reflect the mixed isotopic compositions from different water sources. This assumption, which has been verified in several laboratory and field experiments (Wershaw *et al*., 1966; White *et al*., 1985; Zimmermann *et al*., 1967), results in many interesting studies. For example, Dawson and Ehleringer (1991) reported a phenomenon that some streamside trees do not use stream water. The method becomes easier and more popular to use when Phillips and Gregg (2001; 2003; 2005) published the approach to deal with situations of multiple sources.

However, significant hydrogen isotope fractionation during root water uptake was observed by Lin and Sternberg (1993) in coastal wetland plants both in the field and greenhouse experiments. In their study, the depletion of $\delta^{2}H$ in stem water ranges from 2～13‰ compare to sources water. More shrub and tree species of arid and semi-arid regions have been examined by Ellsworth and Williams (2007) in greenhouse experiments. They reported that in 12 species, 3～9‰ depletion was observed in $\delta^{2}H$ of stem water in comparison to that of soil water. Unlike $\delta^{2}H$, the two studies above both showed that $\delta^{18}O$ of stem water can reflect that of soil water.

Although the mechanisms have not been fully resolved (Ellsworth and Williams, 2007), we can generalize two different patterns (A and B in Figure 4.1) of both $\delta^{18}O$ and $\delta^{2}H$ in soil water and twig water with known local meteoric water line (LMWL) if the tree absorbs soil moisture only. Because oxygen isotope has larger kinetic fractionation effect than hydrogen isotope during evaporation, soil water line has a smaller slope than LMWL. Given that soil moisture at different depths and different times has been experienced different degree of evaporation, it is expected that the soil water composition varies in a range constrained by two soil water line (upper bound SWL or lower bound SWL). Without any fractionation of hydrogen isotope from soil water to root water, the twig water line should lie in between the upper SWL and lower SWL. With depletion of hydrogen isotope in twig water, the twig water line very likely lies below the lower SWL. When a rain event happens resulting in sufficient infiltration, the twig water without hydrogen isotope fractionation will move toward and closely (A) to the event water line while the twig water with hydrogen isotope fractionation will move to the event as well but vertically further (B) from the event water line. Twig water of pattern B is also characterised with a very low slope of the twig water line beyond the range that can be interpreted by soil evaporation alone.

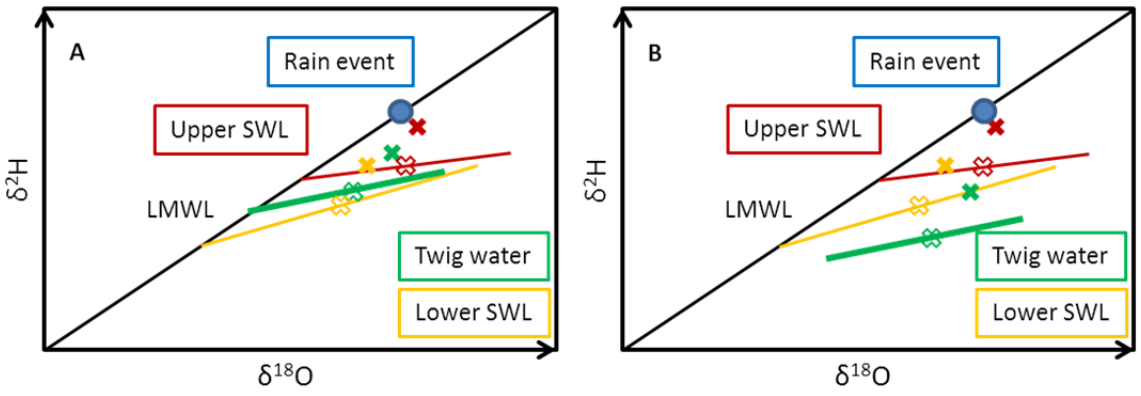

Figure 4.1 General performances of water stable isotopes of soil water line (SWL) and in twig water with known local meteoric water line (LMWL). The crosses (theoretical values) show the changes of isotopic compositions in soil water and twig water before (open crosses) and after (filled crosses) a rain event (the blue circle). Very often, twig water is considering as a simple mixture of different water sources, e.g. water

from different depths of soil (A). When hydrogen fractionation happens during root water uptake, twig water line will be likely to lie below the soil water line (B).

Both A and B patterns can be found in the previous studies. For example, Brunel *et al*. (1995) showed a typical A pattern to determine the water sources of plants in a semi-arid environment. In Wang *et al*. (2010), some isotopic data of stem water lie below the soil water line. But due to irrigation of deep groundwater, it is difficult to confirm that hydrogen isotopic fractionation during root water uptake occurred. However, results from Brooks *et al*. (2009) clearly follow a B pattern. Simple mixing is still able to be assumed for $\delta^{18}O$ of twig water, but for $\delta^{2}H$ it needs to be interpreted carefully.

Under the background of the two patterns above, in this study, we conducted observations on a native vegetation site on two contrasting hillslopes, the north facing slope (equator facing slope, exposed to more sun light in the southern hemisphere) and the south facing slope (pole facing slope) at a native vegetation catchment (Mount Wilson) in South Australia. The two slopes provide different environmental conditions to understand plant water use and infiltration processes. One-year twig sampling has been conducted for $\delta^{18}O$ and $\delta^{2}H$ analysis. From this investigation, we aim to evaluate twig water patterns in terms of $\delta^{18}O$ and $\delta^{2}H$ on the two hillslopes and examine how the root water uptake responds to precipitation seasonally and specific rain events.

4.2 Materials and methods

4.2.1 Study site

The study site is located in Mount Wilson (138.64˚ E, 35.21˚ S, 370 m a.s.l.) in the Mount Lofty Ranges of South Australia (Figure 4.2). This site is characterized with a Mediterranean type climate, being cold and humid in winter and hot and dry in summer. Long-term average annual precipitation (1982-2013) is 716 mm dominated by winter rain events (http://www.bom.gov.au/climate/data/stations/). In this native vegetation site, there

are four evergreen broad leaf tree species including *Eucalyptus leucoxylon, Acacia pycnantha, Acacia notabilis* and *Eucalyptus viminalis cygnetensis*. Especially, *Eucalyptus leucoxylon* and *Eucalyptus viminalis cygnetensis* are the dominant species. A transect including ten trees is selected across two contrasting hillslopes, the equator facing slope (hereafter referred to as NFS) and the pole facing slope (hereafter referred to as SFS) to conduct our monitoring work with five trees on each slope.

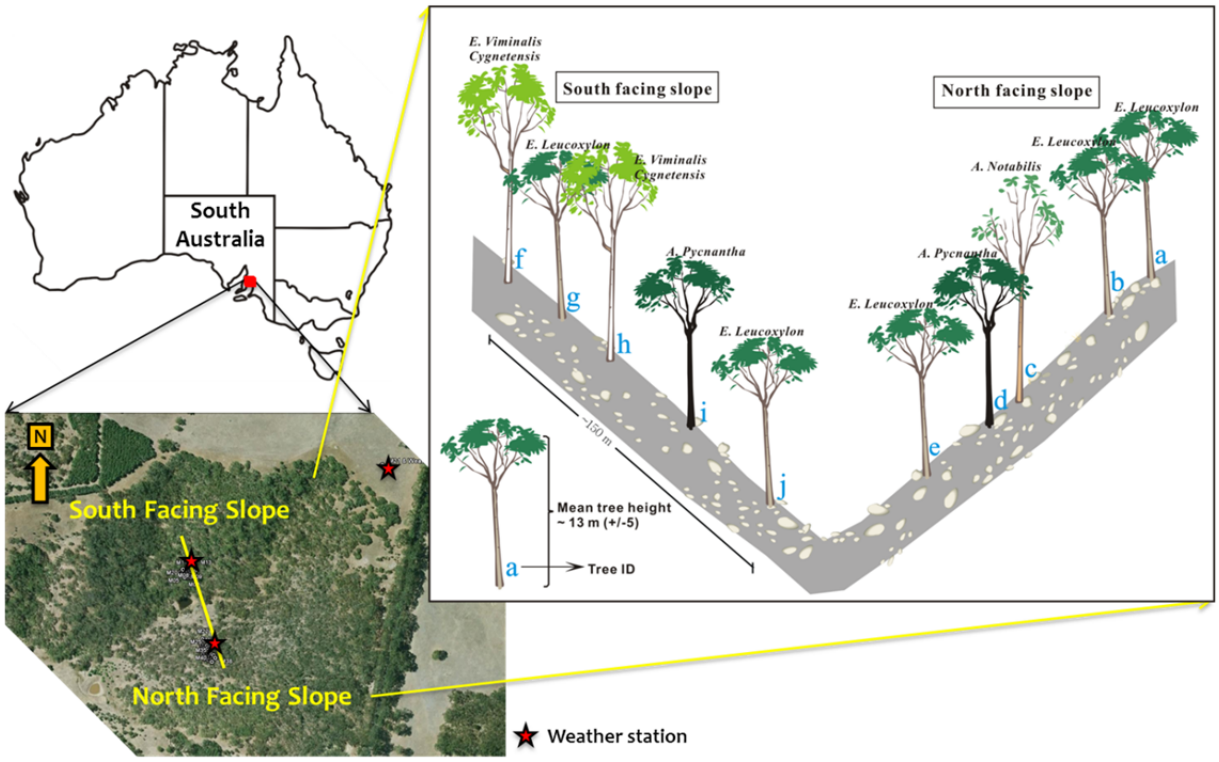

Figure 4.2 The study site and locations of 10 sampling trees on two contrasting hillslopes, the pole facing slope (SFS) and equator facing slope (NFS).

4.2.2 Field work and sample storage

From August 31st, 2012 to September 2nd, 2013, 16 batches of twig samples have been collected. In every batch, samples were collected in four directions (east, south, west and north) for each tree except that the tree did not have a twig in a direction. The first order twigs, 8 to 10 cm in length and 0.5 to 1.0 cm in diameter, were chosen to avoid back diffusions of water stable isotopes from neighbour branch. Once cut down, the twig was

sealed by wrap and tapes with care. Then the wrapped twig was stored in 120 mL vials which were sealed with parafilm. The vial was placed into a container to prevent contamination before going to a cold ice chest box. The samples were all frozen until we extract the water for water stable isotope analysis.

To characterize the input isotopic signal, 22 batches of bulk precipitation and throughfall samples were also collected from March 12, 2012 to August 27, 2013. In an open field, one funnel collector was placed to sample bulk precipitation. On each hillslope, twenty collectors were placed randomly in a plot of 10 × 10 m^2. Each collector was made of 15 cm diameter funnel connected to a bottle of 1.5 L capacity. The funnel had coarse filters to stop leaf litter from falling into the bottle. The collector was held up in a plastic tube 55 cm above the ground to avoid dirt splashing into the funnels. To prevent water evaporation, each sampling bottle was filled with around 1 cm thick of liquid paraffin (Ajax Finechem Pty. Ltd., Adelaide) before being placed in the field.

To check how plant water use responds to precipitation, intra-event samples of 3 rain events were collected at the open site in the study area. Each sample was prescribed to collect a maximum of 2 mm rain water using an automatic rain water collector. To prevent water evaporation, each sampling vial was also filled with around 1 cm thick of liquid paraffin. Groundwater samples were collected from two boreholes which are 2 km and 4 km away from the study catchment. Water surface of these two boreholes are both 35 m below the ground surface. Soil water samples were collected daily at depths of 20 cm and 50 cm on NFS and 30 cm and 50 cm on SFS, respectively. Detailed data information of soil water can be found in Appendix I, Table A.2.

Capacitance probes (Sentek Pty. Ltd., Adelaide) were installed on SFS and NFS to monitor volumetric soil moisture. To measure the transpiration rate (Tr), twenty four sets of compensation heat pulse sap flow meters (Tranzflo NZ Ltd., New Zealand) (Green *et al*.,

2003) were installed of the trees on two hillslopes. Leaf area index (LAI) on the two hillslopes were obtained from digital photos using digital camera (DSC-F717 Cyber-shot, Sony) with lens (Carl Zeiss Vario-Sonnar). The method based on which we calculate LAI follows Macfarlane *et al*. (2007). Potential evapotranspiration are calculated from the weather station data on each hillslope using Priestly-Taylor method (1972, section 2.2.4 of Chapter 2).

4.2.3 Isotopic analysis

Cryogenic vacuum distillation method was used to extract twig water in West Australian Biogeochemistry Centre (WABC, University of Western Australia, Perth). In this method, two glass tubes were attached to a vacuum pump. The sample was placed in one tube (sample tube) and frozen by submerging the tube in liquid nitrogen. A high evacuation was conducted by the vacuum pump to suck the air out. The sample tube was then submerged in boiling water and another tube (collection tube) was submerged in liquid nitrogen for water collection. This distillation needs one hour for each sample. Four standard samples, which need one hour and a half for distillation, went through the whole processes with samples as quality control.

Precipitation and throughfall water samples were filtered with 0.45 μm filter paper (GN-6 Metrice Grid, Pall 186 Corporation) and kept in a cold room (4 ºC) before isotope analysis. Both ^{18}O and deuterium analysis of all samples were performed at WABC using L1102-*i* Cavity Ring-Down Spectroscopy (CRDS) Isotopic Water Analyzer (Picarro Inc., Santa Clara, CA, USA). Delta notation is used to express the stable isotope ratios of hydrogen and oxygen in samples:

$$\delta(‰) = \left(\frac{R_{sample}}{R_{s\tan dard}} - 1 \right) \times 1000 \quad (4.1)$$

where R_{sample} and $R_{standard}$ represent the $^{2}H/H$ or $^{18}O/^{16}O$ abundance ratios in sample and

standard, respectively, and the standard refers to the Vienna Standard Mean Ocean Water (VSMOW). Given by Gonfiantini (1978), $R_{standard}$ = 155.76×10^{-6} for H^{2}HO and $R_{standard}$ = 2005.2×10^{-6} for $H_2{}^{18}O$. Precision (1σ) was reported to be 0.1‰ for $\delta^{18}O$ and 1.0 ‰ for δ^2H of our analysis results. The secondary parameter, *d*-excess, is calculated as $d = \delta^2H - 8\times\delta^{18}O$ (Dansgaard, 1964).

4.2.4 The slope of water line

To better understand the evaporation process effects on $\delta^{18}O$ and δ^2H of soil water, we introduce the evaporation of a water column first. For an evaporated water column, the total fractionation between the water column and the open air is the sum of the fractionation for equilibrium water-vapour exchange (ε_e) and the kinetic factor (ε_k) (Clark and Fritz, 1997). Under equilibrium conditions, the fractionation of ^{18}O and ^2H can be determined by temperature (Horita and Wesolowski, 1994) with the current formulations given as

$$10^3 \ln \alpha_e(^{18}\mathrm{O}) = -7.685 + 6.7123(\frac{10^3}{T}) - 1.6664(\frac{10^6}{T^2}) + 0.35041(\frac{10^9}{T^3}) \quad (4.2)$$

$$10^3 \ln \alpha_e(^{2}\mathrm{H}) = 1158.8(\frac{T^3}{10^9}) - 1602.1(\frac{T^2}{10^6}) + 794.84(\frac{T}{10^3}) - 161.04 + 2.9992(\frac{10^9}{T^3}) \quad (4.3)$$

where α_e is equilibrium fractionation factor for ^{18}O (^2H) in liquid water compared to that in vapour water and *T* is the water temperature in K.

The liquid water would be enriched in ^{18}O and ^2H from the water vapour as large as

$$\varepsilon_e(‰) = (\alpha_e - 1)\times 10^3 \quad (4.4)$$

Under different humidity conditions, Gonfiantini (1986) described the kinetic factors as

$$\varepsilon_k(^{18}O) = 14.2\times(1 - RH)‰ \quad (4.5)$$

$$\varepsilon_k(^2H) = 12.5 \times (1 - RH)‰ \quad (4.6)$$

If we assume that evaporating water follows a Rayleigh process for both ^{18}O and ^{2}H:

$$\delta = \delta_0 + (\varepsilon_e + \varepsilon_k) \times \ln f \quad (4.7)$$

where δ is $\delta^{18}O$ or $\delta^{2}H$ of the evaporating water and δ_0 is the initial value, f is the fraction of the residual water. The slope of evaporating water in terms of $\delta^{18}O$ or $\delta^{2}H$ can be estimated by

$$S = \frac{(\delta - \delta_0)(^2\mathrm{H})}{(\delta - \delta_0)(^{18}\mathrm{O})} = \frac{(\varepsilon_e + \varepsilon_k)(^2\mathrm{H})}{(\varepsilon_e + \varepsilon_k)(^{18}\mathrm{O})} \quad (4.8)$$

Thus the theoretical slope of evaporation water line can be determined by temperature and humidity.

However, evaporation can cause different enrichment of $\delta^{18}O$ and $\delta^{2}H$ in soil profile than those in water column since the kinetic factor (ε_k) has been modified because of soil layers (Allison *et al*., 1983). There are several choices for this value (Cappa *et al*., 2003; Horita *et al*., 2008; Luz *et al*., 2009; Merlivat, 1978) but no agreement exists on which kinetic factor performs better under which conditions (Braud *et al*., 2005; Soderberg *et al*., 2012). Results in Allison *et al*. (1983) show that soil water line can have a slope of 2.64 after one year evaporation. Nevertheless, the theoretical slope of evaporation water line based on Eq. 4.8 can be seen as a reference for that of twig water line and it is certain that stronger evaporation can cause a lower slope of the soil water line.

4.3 Results and discussion

4.3.1 Seasonal plant water use

The isotopic composition of input water may have been altered by vegetation compared to

precipitation (Xu *et al*., 2014). In all the throughfall batches we collected, the $\delta^{18}O$ and *d*-excess on the two hillslopes are very similar to that of precipitation except batch 1, 19, 21 and 22 (Table 4.1). The higher $\delta^{18}O$ and lower *d*-excess of throughfall on the two hillslopes in batch 1 is very likely due to partial evaporation while the other three batches, which characterized by the lower $\delta^{18}O$ and higher *d*-excess of throughfall, are more likely controlled by selection process. The $\delta^{18}O$ and *d*-excess on NFS and SFS are so close to each other that makes the comparison between the two hillslopes much easier.

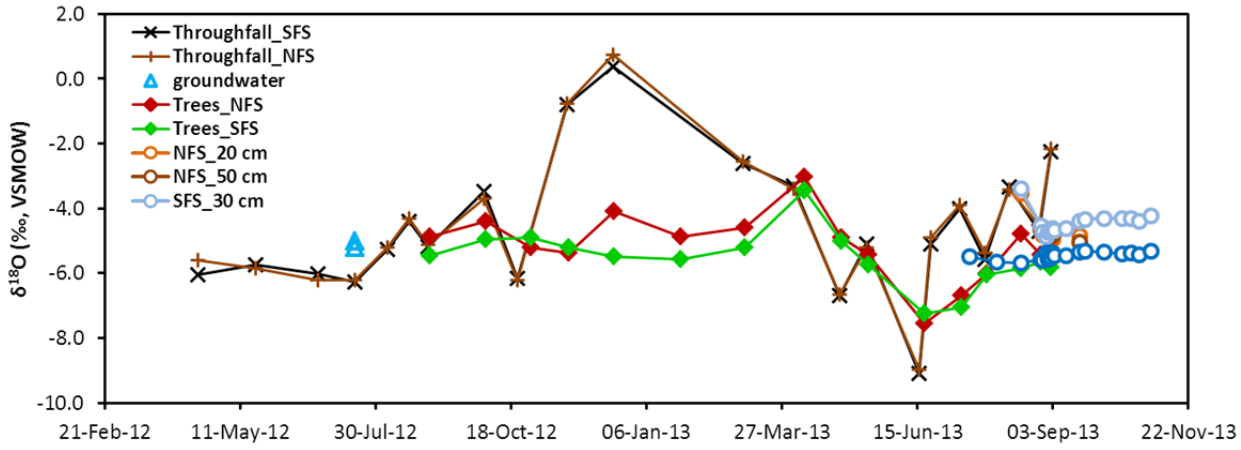

Figure 4.3 Time series data of $\delta^{18}O$ in throughfall (crosses), groundwater (triangles) soil water at different depths (circles) and twigs (diamonds) which are averaged for each hillslope, respectively.

Results of $\delta^{18}O$ of groundwater and one-year observations for throughfall and twig water are shown in Figure 4.3. It is evident that $\delta^{18}O$ values of throughfall in the dry season (November to March) are much higher than that in the wet season (June to October). $\delta^{18}O$ values of throughfall in the wet season are close to that of groundwater. These suggest that the main groundwater recharge season of the study area is very likely in the wet season. $\delta^{18}O$ values of twig water are much more stable than that of throughfall, especially in the dry season. This result suggests that plant water use in the dry season may not be sourced from throughfall in the same period.

Table 4.1 Volume weighted mean of $\delta^{18}O$ and *d*-excess of throughfall samples on north facing slope (NFS), south facing slope (SFS) and that of precipitation at the open site.

Batch No.	Sampling period		$\delta^{18}O$			*d*-excess		
	Start	End	NFS	SFS	Open	NFS	SFS	Open
1	03-Mar-12	16-Apr-12	-5.60	-6.04	-7.07	14.9	17.2	23.0
2	17-Apr-12	20-May-12	-5.87	-5.73	-5.89	14.6	14.2	14.4
3	21-May-12	26-Jun-12	-6.21	-6.03	-6.50	12.2	12.2	14.3
4	27-Jun-12	18-Jul-12	-6.21	-6.28	-6.31	18.9	18.9	19.2
5	19-Jul-12	06-Aug-12	-5.22	-5.28	-5.50	14.7	14.8	15.1
6	07-Aug-12	19-Aug-12	-4.32	-4.40	-4.74	15.5	15.2	15.9
7	20-Aug-12	30-Aug-12	-5.12	-5.18	-5.31	19.5	19.8	20.2
8	31-Aug-12	02-Oct-12	-3.71	-3.49	-4.09	18.9	17.5	20.1
9	03-Oct-12	22-Oct-12	-6.23	-6.15	-6.50	22.6	22.4	22.7
10	23-Oct-12	20-Nov-12	-0.78	-0.79	-1.08	10.7	10.8	11.6
11	21-Nov-12	17-Dec-12	0.74	0.36	0.07	8.1	9.7	10.3
12	18-Dec-12	04-Mar-13	-2.55	-2.63	-2.75	9.5	9.5	9.9
13	05-Mar-13	03-Apr-13	-3.38	-3.33	-3.28	15.9	15.5	15.8
14	04-Apr-13	30-Apr-13	-6.66	-6.69	-6.59	18.1	17.5	18.0
15	01-May-13	16-May-13	-5.21	-5.11	-5.28	19.5	18.8	19.4
16	17-May-13	16-Jun-13	-8.99	-9.10	-9.21	14.8	14.7	14.5
17	17-Jun-13	23-Jun-13	-4.90	-5.09	-5.33	19.3	19.2	20.2
18	24-Jun-13	10-Jul-13	-3.90	-4.00	-4.21	20.7	21.1	21.1
19	11-Jul-13	25-Jul-13	-5.38	-5.57	-3.87	17.1	17.2	12.2
20	26-Jul-13	08-Aug-13	-3.43	-3.34	-3.27	17.3	16.7	16.2
21	09-Aug-13	26-Aug-13	-4.54	-4.71	-1.86	18.1	18.4	11.9
22	27-Aug-13	02-Sep-13	-2.17	-2.25	-0.17	11.3	11.3	8.1

In the dry season, stronger soil evaporation (evaporation amount versus water availability) was expected on both hillslopes due to dryer conditions than that in the wet season (Table 4.2), which is the reason that twig water has heavier ^{18}O in the dry season than that in the wet season. Compare $\delta^{18}O$ and $\delta^{2}H$ of twig to that of throughfall (Figure 4.3), tree water use mainly relies on the wet season precipitation.

Table 4.2 Climate conditions including mean daily temperature (T) and mean daily relative humidity (RH) obtained from sensors on the masts on each slope, and mean daily potential evapotranspiration (PET) calculated by Priestley-Taylor equation in the dry season and the wet season of equator facing slope and pole facing slope, respectively. Leaf area index (LAI) and mean daily transpiration rate (Tr) on each hillslope are also given in this table.

	Total	**NFS (LAI =1.43)**				**SFS (LAI=1.43)**			
	P (mm)	**T (˚C)**	**RH (%)**	**PET (mm/day)**	**Tr (mm/day)**	**T (˚C)**	**RH (%)**	**PET (mm/day)**	**Tr (mm/day)**
Dry season	80.2	18.7	61.3	10.5	1.5	18.5	63.9	8.5	1.5
Wet season	471.4	11.3	76.7	4.8	1.4	11.2	79.3	3.4	1.6

Generally, both throughfall and twig water lines have smaller slopes in the dry season than in the wet season (Figure 4.4), respectively. The twig water line on NFS has larger slopes than that on SFS in both seasons. During the dry season, the slope of twig water line on SFS is as low as 2.72 (beyond the range of the slope values of theoretical evaporation line as shown in Table 4.3) with a weak correlation (R^2=0.30) between ^{18}O and ^{2}H, while the slope is 5.03 on NFS and a R^2=0.72.

Table 4.3 Theoretical slopes (*S*) of evaporated water line are calculated from the temperature (T) and relative humidity (RH) for north facing slope and south facing slope. Minimum T and maximum RH can give largest *S* while maximum T and minimum RH will have smallest *S.*

Location	T (˚C)	RH (%)	$\varepsilon^{18}O$	$\varepsilon^{2}H$	$\varepsilon_k{}^{18}O$	$\varepsilon_k{}^{2}H$	*S*
NFS	5.3 (min)	97.2 (max)	11.2	103.6	0.4	0.35	8.9
	34.6 (max)	18.6 (min)	8.6	69.1	11.6	10.175	3.9
SFS	5.3 (min)	97.3 (max)	11.2	103.63	0.4	0.3	9.0
	34.8 (max)	16.4 (min)	8.6	68.90	11.9	10.5	3.9

Evaporation associated with larger kinetic fractionation can result in lower slope of the water line, because $\varepsilon_k(^{18}O)$ is larger than $\varepsilon_k(^{2}H)$. Smaller slopes in the dry season than that in the wet season are consistent with our expectation. However, twig water line on NFS has larger slopes than SFS in both seasons is opposite to what we thought even without isotopic information of any soil profile. First, isotopic input information and amount of throughfall is almost the same. Second, similar soil texture conditions (Table 4.4) should have similar infiltration process on the two hillslopes. Third, tree species are the same and canopy cover (LAI is the same) is similar on the two hillslopes. A larger potential evapotranspiration on NFS than SFS (Table 4.2) would lead to smaller slopes of twig water line on NFS than on SFS. Thus evaporation alone cannot be used to interpret the small slopes of twig water line on SFS.

Table 4.4 Soil texture for equator facing slope and pole facing slope using sedimentation method based on Stoke's law. Data for each depth are averaged from 5 soil columns on each slope at the same depth.

Depth (cm)	NFS			SFS		
	Clay (%)	Silt (%)	Sand (%)	Clay (%)	Silt (%)	Sand (%)
0-20	13.3	40.1	46.6	14.9	36.9	48.1
20-40	25.7	35.8	46.3	15.7	31.4	52.8
40-60	19.3	34.4	46.2	15.4	31.2	53.3
60-80	10.6	32.2	57.1	9.5	28.9	61.5
80-100	13.8	29.7	56.5	11.0	28.5	60.5
100-120	19.5	33.1	47.4	11.0	33.5	55.5

In detail, the difference in δ^2H in twig water of the two seasons on SFS is much smaller than that on NFS. Correlation (square root of R^2) between ^{18}O and ^2H are both smaller in two seasons on SFS than that on NFS (Figure 4.4). It means that a possible process 'prevents' the ^2H to become enriched in twig water and behaves differently from ^{18}O. This process is very likely to be hydrogen fractionation during root water uptake (Ellsworth and Williams, 2007). Hydrogen fractionation during root water uptake can deplete ^2H in the twig water compared to source water. But no significant fractionation in this process has been reported for ^{18}O (Lin *et al*., 1993; Ellsworth and Williams, 2007). Thus $\delta^{18}O$ and δ^2H of the twig water is possible to follow the B pattern as we hypothesized in Figure 4.1.

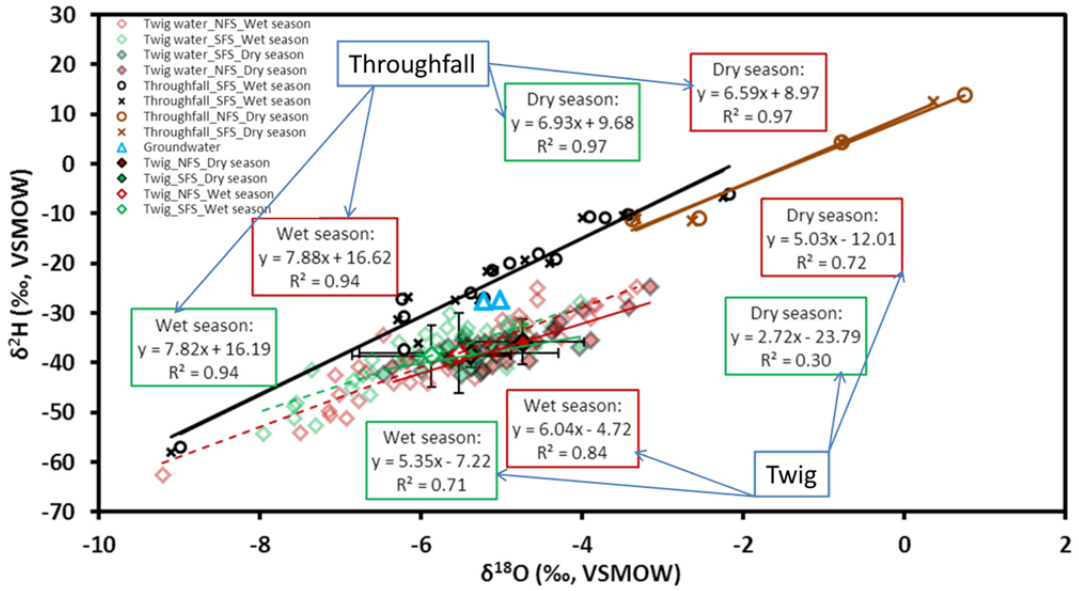

Figure 4.4 Isotopic compositions of throughfall, groundwater at the study site and twig water of the 10 sampling trees from 31/Aug/2012 to 02/Sep/2013. More specifically, isotopic compositions of twig water are shown in mean values (open diamonds) with error bars based on data clouds in light colours. Linear relationships between $\delta^{18}O$ and $\delta^{2}H$ of throughfall (upper part) and twig water (lower part) in wet season and dry season for pole facing slope and equator facing slope are also given separately. Wet season is from November to March and dry season is from June to October.

As shown in Figure 4.4, all the data points of the dry season tend to locate on the upper-right corner while those of the wet season distribute in the lower-left of the plot. $\delta^{18}O$ and $\delta^{2}H$ of throughfall in the dry season are much larger than that in the wet season. $\delta^{18}O$ and $\delta^{2}H$ of twig water in dry season are also more enriched than that in the wet season for both hillslopes. As seen from the mean values, the differences of $\delta^{18}O$ and $\delta^{2}H$ of twig water between the two seasons are much larger on NFS than those on SFS (Table 2.1).

The depletion caused by root water uptake is positively correlated with transpiration rate (Lin *et al*., 1993). In the wet season, mean transpiration rate is 1.5 mm/day on NFS and 1.4 mm/day on SFS while in the dry season mean transpiration rate is still 1.5 mm/day on NFS but 1.6 mm/day on SFS (Table 4.2). The difference between the two hillslopes, which is only 0.1 mm/day, has different effects in the two seasons in terms of $\delta^{18}O$ and $\delta^{2}H$ in twig water for the two hillslopes, especially in the dry season. The dry season has more

than double potential evapotranspiration and almost only 1/5 amount of precipitation than the wet season resulting in very different soil water availability in the two seasons. Soil moisture should be much lower in the dry season than in the wet season. Under such conditions, the difference of transpiration rate which is 0.1 mm/day is more important in the dry season when we normalize it by soil moisture.

4.3.2 Rain event and plant water use

If we know the $\delta^{18}O$ and $\delta^{2}H$ of twig water before and after a rain event, we may be able to track how plant water uses response to the event. Three intra-events and the $\delta^{18}O$ and $\delta^{2}H$ of twig water are shown in Fig. 4.5. Generally, the change of the $\delta^{18}O$ and $\delta^{2}H$ of twig water after the three rain events is similar between the two hillslopes. Similar isotopic input information (Table 4.1), similar soil texture and similar fractional vegetation cover, it is reasonable that the plant water use respond similarly to the same rain event from the $\delta^{18}O$ and $\delta^{2}H$ of twig water on the two hillslopes. However, the situation is different from event to event in terms of how precipitation is used by the plant.

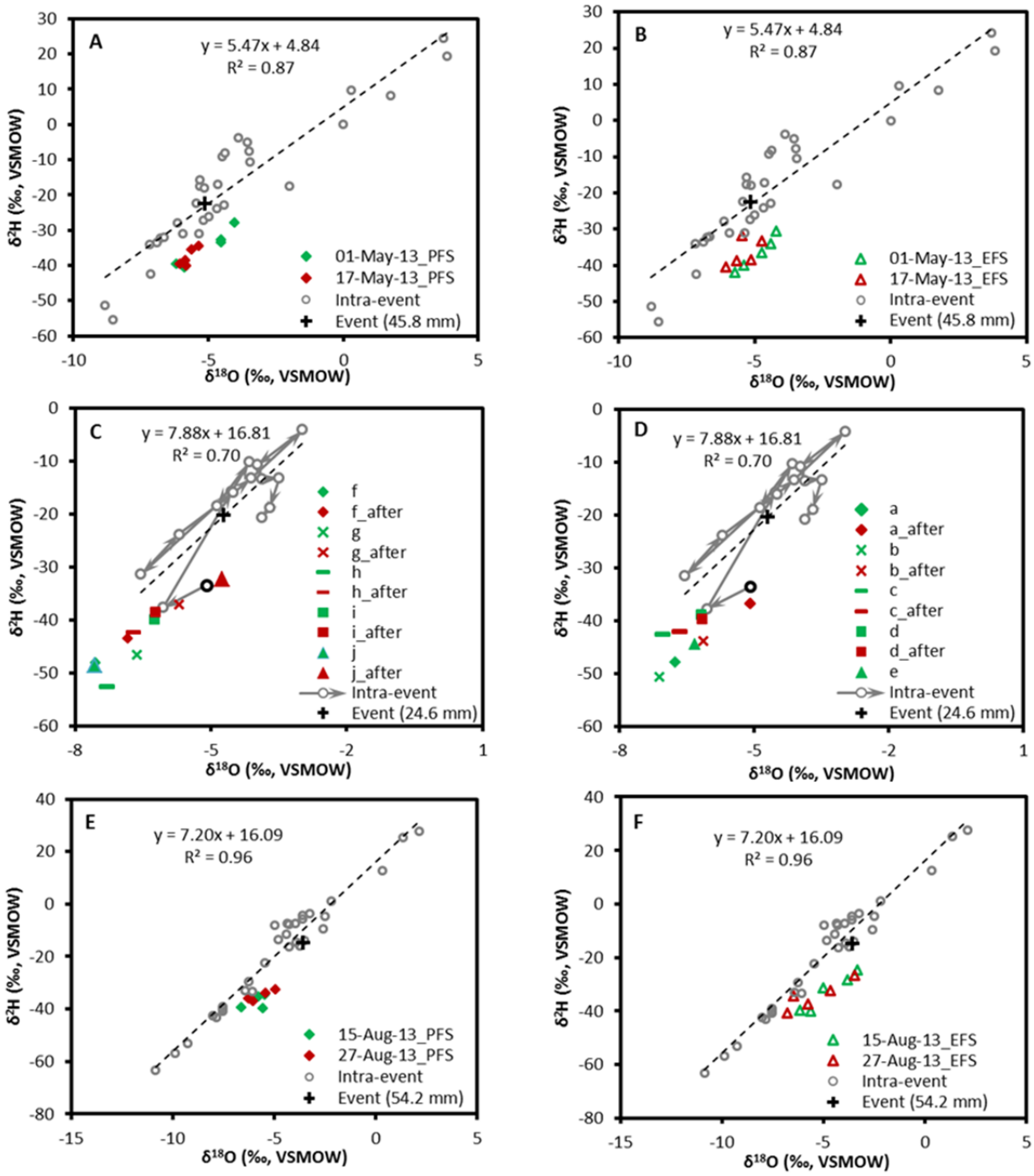

Figure 4.5 Isotopic compositions of twig water before (in green) and after rain events (in red) for SFS (left panel A, C and E) and NFS (right panel B, D and F), respectively. Rain events were collected in 2 mm (maximum) increment thus named as intra-event. Three events (A and B, C and D, E and F), 2/May-16/May, 12/Jul-15/Jul and 16/Aug-26/Aug of 2013, are given here respectively. Different trees are shown in details in panels C and D when event from 12/Jul/2013 to 15/Jul/2013 has very different values of isotopic composition from those of twig water before the event. Tree ID (e.g. *f*) is the twig water before while Tree ID_after (*f*_after) is the twig water after the event.

The event in May happened in the very end of the dry season. It can be traced from the

$\delta^{18}O$ and $\delta^{2}H$ of twig water (A and B in Figure 4.5), even the weighted mean isotopic composition of the event ($\delta^{18}O$ is -5.13‰ and $\delta^{2}H$ is -22.6‰) is very close to that of the twig before the rain event makes it hard to identify the water plant water sources. The distribution of data points of $\delta^{18}O$ and $\delta^{2}H$ of twig water become closer to each other after the event. We also notice that it follows sort of the B pattern as $\delta^{2}H$ are horizontally moving to the intra-event but not vertically closer to the event especially on SFS.

The event in July (C and D in Figure 4.5) occurred in the early stage of the wet season. This event is plotted in detail as it has much higher content of ^{18}O and ^{2}H than the pre-event twig water. This event, which is 24.6 mm, has been used by the plant as the data points of twig water all move to the direction but parallel to the rain event. The change follows the B pattern.

The event in late August (E and F in Figure 4.5) took place near the end of the wet season. This event has little effect on the $\delta^{18}O$ and $\delta^{2}H$ of twig water. Even the weighted mean isotopic composition of the event is very different from that of the pre-event twig water. No significant alteration in isotopic composition of twig water has been observed after the event. In other words, this large rain event (54.2 mm) does not contribute to the plant water use.

In summary, the $\delta^{18}O$ and $\delta^{2}H$ of twig water are significantly affected by the rain events following the dry season. But the response of $\delta^{18}O$ and $\delta^{2}H$ of twig water to the precipitation indicates that not all events contribute to immediate plant water use even it is quite large.

4.3.3 Root zone moisture replenishment

The understanding of $\delta^{18}O$ and $\delta^{2}H$ of twig water can help us to study the root zone moisture replenishment on the two hillslopes. As we discussed above that the large event

in late August has not contributed to the soil moisture of the root zone. During the same event, soil moisture (Figure 4.6) at depths of 30 cm and 50 cm does not show much change on August 15th, 2013 on the two hillslopes. However, at the depth of 100 cm on the same day on SFS, the soil moisture shows a significant increase. This response of soil moisture change to the rain event suggests that, if a rain event occurs when the soil is already very wet the rain water infiltrates as preferential flow into the deep soil in the study area with not too much contribution to the root zone soil moisture. Such wet soil may be close to the field capacity and the timing when the event occurs determines its efficiency as the sources of soil moisture. This regime of infiltration is very similar as the thorough investigation in a Mediterranean climate upland humid watershed in Brooks *et al*. (2009) and the study using $\delta^{18}O$ of soil water in Gazis and Feng (2004).

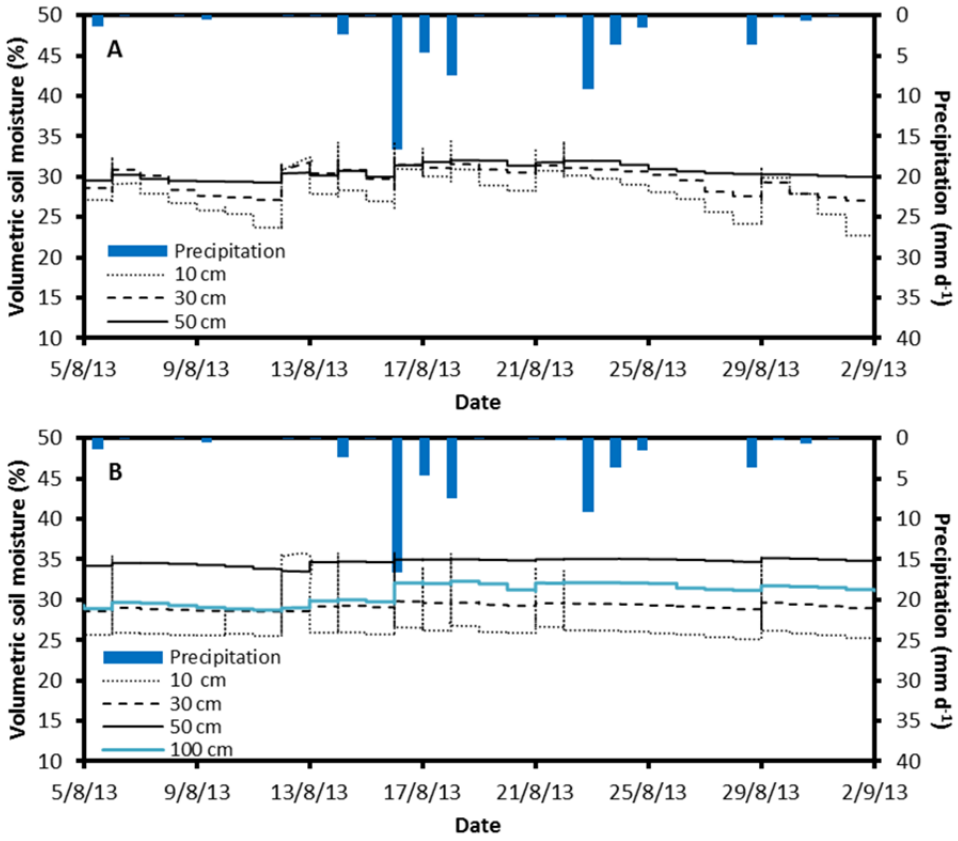

Figure 4.6 Daily precipitation from and soil moisture data at different depths for NFS (A) and SFS (B) from 05/Aug/2013 to 02/Sep/2013.

Some isotopic signals of throughfall are rare found in twig water, especially in the dry season (Figure 4.3 and Figure 4.4). It indicates that the main season for root zone moisture replenishment is the wet season and so as the possible groundwater recharge. More specifically, from the results of the three events (Figure 4.5) at the different stages of the wet season shows that the root zone moisture replenishment mainly reflects the isotopic signal before mid-period of the wet season. Toward the later-period of the wet season, isotopic signals are also rare can be found in the twig water either. The results from isotopic signal and soil moisture data suggest that piston flow is not dominant but preferential flow may play a significant role for the root zone moisture replenishment. This mechanism may also important for groundwater recharge when we compare the isotopic composition of groundwater and throughfall.

4.4 Conclusions and implications

We have generalized two typical patterns of $\delta^{18}O$ and $\delta^{2}H$ of tree water use with or without hydrogen fractionation by root water uptake. The slope of twig water line on pole facing slope is much lower than that on the equator facing slope in the wet season (5.4 to 6.0) and particularly in the dry season (2.7 to 5.0) suggests that hydrogen isotopic fractionation may take place during root water uptake. This information re-emphasizes the problem of using water isotope (particularly $\delta^{2}H$) to study the sources of plant water use. We should also keep in mind that the low slope of twig water line for different tree species may not necessarily resulted from soil evaporation. This also calls for attention in using both $\delta^{18}O$ and $\delta^{2}H$ for evaporation and transpiration partitioning over vegetated surfaces.

The response of $\delta^{18}O$ and $\delta^{2}H$ of twig water to the rain events indicates landscape water storage capacity of winter rain is important for plant growth and survival during dry summer. The timing that the events occurs when the soil is dry or wet, determines its efficiency as the sources of soil moisture. By comparing the results of the $\delta^{18}O$ and $\delta^{2}H$ of groundwater

with a mean value -5.1‰ and -27.5‰ respectively and that of throughfall in the wet season with a mean value -5.1(±1.7)‰ and -23.4(±13.3)‰ correspondingly, groundwater recharge is dominated by events in the wet season.

References

Allison, G.B., C.J. Barnes, M.W. Hughes., 1983. The distribution of deuterium and ^{18}O in dry soils 2. Experimental. *J. Hydrol.* 64: 377-397.

Braud, I., T. Bariac, J.-P. Gaudet, and M. Vauclin., 2005. SiSPAT-Isotope, a coupled heat, water and stable isotope (HDO and $H_2{}^{18}O$) transport model for bare soil: I. Model description and first verifications. *J. Hydrol*. 309: 277-300.

Brooks, J.R., H.R. Barnard, R. Coulombe, J.J. McDonnell., 2009. Ecohydrologic separation of water between trees and streams in a Mediterranean climate. *Nat. Geosci*. 3: 100-104.

Brunel, J-P., G.R. Walker, A.K. Kennett-Smith., 1995. Field validation of isotopic procedures for determining sources of water used by plants in a semi-arid environment. *J.Hydrol.* 167: 351-368.

Brunel, J-P., G.R. Walker, J.C. Dighton, B. Monteny., 1997. Use of stable isotopes of water to determine the origin of water used by the vegetation and to partition evaporatranspiration. A case study from HAPEX-Sahel. *J.Hydrol*. 188-189: 466-481.

Cappa, C.D., M.B. Hendricks, D.J. DePaolo, R.C. Cohen., 2003. Isotopic fractionation of water during evaporation. *J. Geophys. Res.* 108:4525.

Clark, I.D., P. Fritz., 1997. Environmental Isotopes in Hydrogeology. CRC Press/Lewis Publishers, pp 35-60.

Dansgaard, W., 1964. Stable isotopes in precipitation. *Tellus*, 16: 436-468.

Dawson, T.E., J.R. Ehleringer., 1991. Streamside trees that do not use stream water. *Nature*. 350: 335-337.

Dawson, T.E., J.R. Ehleringer., 1993. Isotopic enrichment of water in the 'woody' tissues: Implications for plant water source, water uptake, and other studies which use the stable isotopic composition of cellulose. *Geochim. Cosmochim. Acta.* 57: 3487-3492.

Ellsworth, P.Z., D.G. Williams., 2007. Hydrogen isotope fractionation during water uptake by woody xerophytes. *Plant Soil.* 291: 93-107.

Ehleringer, J.R., Dawson, T.E., 1992. Water uptake by plants: pespectives from stable isotope composition. *Plant Cell Environ*. 15: 1073-1082.

Gazisa, C., X. Feng., 2004. A stable isotope study of soil water: evidence for mixing and preferential flow paths. *Geoderma.* 119: 97-111.

Gonfiantini, R., 1978. Standards of stable isotope measurement in natural compounds.

Nature. 271: 534–536.

Gonfiantini, R., 1986. Environmental isotopes in lake studies. In: P. Fritz and J.Ch. Fontes (Eds), Handbook of Environmental Isotope Geochemistry. The Terrestrial Environment B, Vol. II. *Elsevier*, Amsterdam, pp. 113-168.

Good, S. P., K. Soderberg, K. Guan, E. G. King, T. M. Scanlon, and K. K. Caylor., 2014. δ^2H isotopic flux partitioning of evapotranspiration over a grass field following a water pulse and subsequent dry down. *Water Resour. Res.* 50: 1410–1432.

Green, S., B. Clothier, B. Jardine., 2003. Theory and practical application of heat pulse to measure sap flow. *Agron. J*. 95(6): 1371-1379.

Horita, J., D.J. Wesolowski., 1994. Liquid-vapour fractionation of oxygen and hydrogen isotopes of water from the freezing to the critical temperature. *Geochim. Cosmochim. Acta* 58: 3425-3437.

Horita, J., K. Rozanski, S. Cohen., 2008. Isotope effects in the evaporation of water: A status report of the Craig-Gordon model. *Isot. Environ. Health Stud.* 44:23–49.

Lin, G., L. da S. L. Sterngerg., 1992. Comparative study of water uptake and photosynthetic gas exchange between scrub and fringe red mangroves, *Rhizophora mangle* L. *Oecologia* (Ber.). 90: 399-403.

Lin, G., L. da S. L. Sterngerg., 1993. Hydrogen isotopic fractionation by plant roots during water uptake in coastal wetland plants. In: Ehleringer, J.R., Hall, A.E., Farquhar, G.D. (eds), Stable isotopes and plant carbon-water relations. Academic Press Inc., New York, pp 497-510.

Luz, B., E. Barkan, R. Yam, A. Shemesh., 2009. Fractionation of oxygen and hydrogen isotopes in evaporating water. *Geochim. Cosmochim. Acta.* 73:6697–6703.

Macfarlane, C., M. Hoffman, D. Eamus, N. Kerp, S. Higginson, R. McMurtrie, M. Adams., 2007. Estimation of leaf area index in eucalypt forest using digital photography. *Agric. For. Meteorol.*143: 176-188.

Merlivat, L. 1978. Molecular diffusivities of $H_2{}^{16}O$, $HD^{16}O$, and $H_2{}^{18}O$ in gases. *J. Chem. Phys.* 69: 2864-2871.

Phillips, D.L., J.W. Gregg., 2001. Uncertainty in source partitioning using stable isotopes. *Oecologia.* 127: 171-179.

Phillips, D.L., J.W. Gregg, J.W. 2003. Source partitioning using stable isotopes: coping with too many sources. *Oecologia.* 136: 261–269.

Phillips, D.L., S.D. Newsome, J.W. Gregg, J.W. 2005. Combining sources in stable isotope mixing models: alternative methods. *Oecologia.* 144: 520–527.

Priestley, C.H.B., R.J. Taylor., 1972. On the assessment of surface heat flux and evaporation using large-scale parameters. *Mon. Weather Rev.* 100 (2), 81-92.

Soderberg, K., S. P. Good, L. Wang, K. Caylor., 2012. Stable Isotopes of Water Vapor in the Vadose Zone: A Review of Measurement and Modeling Techniques. *Vadose Zone J*.

Wang, L., K. K. Caylor, J. C. Villegas, G. A. Barron-Gafford, D. D. Breshears, T.E. Huxman, 2010. Partitioning evapotranspiration across gradients of woody plant cover: assessment of a stable isotope technique. *Geophys.Res. Lett.* 37, L09401.

Wang, L., S. Niu, S. Good, K. Soderberg, X. Zhou, J. Xia, R. Sherry, Y. Luo, K. Caylor, M. McCabe, 2013. The effect of warming on grassland evapotranspiration partitioning using laser-based isotope monitoring techniques. *Geochim. Cosmochim. Ac*.111, 28-38.

Wang, P., X. Song, D. Han, Y. Zhang, X., Liu., 2010. A study of root water uptake of crops indicated by hydrogen and oxygen stable isotopes: A case in Shanxi Province, China. *Agric. Water Manag.* 97: 475–482.

Wershaw R.L, I. Friedman, S.J. Heller., 1966. Hydrogen isotopic fractionation of water passing through trees. In Advances in Organic Geochemistry. Pergamon, New York, pp 55-67.

White, J.W.C., E.R. Cook, J.R. Lawrence, W.S. Broecker., 1985. The D/H ratios of sap in trees: Implications for tree water sources and tree ring D/D ratios. *Geochim. Cosmochim. Acta.* 49: 237-246.

Xu, X., H. Guan, Z. Deng., 2014. Isotopic composition of throughfall in pine plantation and native eucalyptus forest in South Australia. *J. Hydrol*. 514: 150-157.

Yepez, E. A., T.E. Huxman, D.D. Ignace, N.B. English, J.F. Weltzin, A.E. Castellanos, D.G. Williams., 2005. Dynamics of transpiration and evaporation following a moisture pulse in semiarid grassland: A chamber-based isotope method for partitioning flux components. *Agric. For.t Meteoro.* 132: 359–376.

Zimmermann, U., E. Ehhalt, K.O. Munnich., 1967. Soil-water movement and evapotranspiration: changes in the isotopic composition of the water. In: Proceedings of the symposium on isotopes in hydrology. International Atomic Energy Agency, Vienna, pp 567-585.

CHAPTER 5 DYNAMIC GROUNDWATER RECHARGE ESTIMATION USING STORAGE-DISCHARGE RELATIONSHIPS[3]

5.1 Introduction

Groundwater recharge estimation is a challenge for groundwater resources management (Scanlon *et al.*, 2006). Recharge estimation in mountainous catchments is quite difficult due to hydrogeological and hydrometeorological complexities and limited observational data (Green *et al.*, 2011; Manning and Solomon, 2005; Taylor *et al.*, 2012; Wilson and Guan, 2004). However, reliable recharge estimates are essential in mountainous catchments. Mountainous areas provide significant sources of fresh water for adjacent lowlands (Manning and Solomon, 2005; Viviroli *et al.*, 2007; Wilson and Guan, 2004), particularly for regions where water supply is vulnerable from seasonal water shortage.

Various approaches based on groundwater models and tracer techniques such as the chloride mass balance (CMB) method, have been widely utilized to estimate groundwater recharge in mountainous catchments (e.g. Bazuhair and Wood, 1996; Gee *et al.*, 2005; Somaratne and Smettem, 2014). However, scarcity of observation wells and hydrogeological complexity of bedrock aquifers have caused practical difficulties in using groundwater models for mountainous catchments. Studies have shown that performance of groundwater models is greatly degraded if hydraulic conductivity cannot be well characterized for the catchment (Cook, 2003; Scanlon *et al.*, 2006). Manning and Solomon (2005) improved recharge estimation from groundwater modelling by incorporating environmental tracers , as shown in a study based on the Salt Lake Valley in northern Utah. Due to a lack of data, common for many mountainous areas, they had to assume a relatively uniform hydraulic conductivity and circulation depth, which inevitably caused uncertainties in recharge estimation.

[3] A revised version of this chapter is under review in *Water Resources Research*, with co-authors Huade Guan, Hoori Ajami and Craig T. Simmons.

Inter-annual variability of mountain recharge in response to climate variability and changes is important for water resources management particularly in regions where mountain system recharge constitutes a major component of the water budget. Application of tracer based techniques (e. g. CMB) to estimate inter-annual variability of recharge is limited as these methods usually give long-term average recharge estimates at a temporal resolution from years to decades. For example, Aishlin and McNamara (2011) estimated net groundwater recharge of Dry Creek Experimental Watershed on the Boise Front in south-western Idaho using the CMB method, which was thought to have an integration period of at least 5 years. However, to understand how groundwater recharge responds to input (precipitation) or is affected by drought spells, this long-term average value provides limited information. In addition to the time-scale related limitation, spatial variability of the groundwater recharge which can occur in a small area causes another difficulty in using tracer-based method for areal estimation. Cook *et al.* (1989) estimated ground recharge in an area of about 14 ha near the town of Borrika in the southern Australia, having a range from 0.04 to over 33 mm/year using 13 chloride profiles. In such a case, it is difficult to obtain an areal average recharge based on just a few point data. Considering the above limitations to estimate catchment groundwater recharge in mountainous regions, it is necessary to develop an alternative method which is relatively easy to apply and provides representative estimation over the whole catchment.

Among different components of catchment water balance, stream discharge is the only aggregated measurement of the catchment response to changes in atmospheric and land cover conditions (Brutseart and Nieber, 1977; Kirchner, 2009). In catchments with gaining streams, stream discharge has been found to be a good indicator of changes in catchment water storage (e.g. Creutzfeldt *et al.*, 2014; Gan and Luo, 2013; Hassan, 2012). Given this relationship, the storage-discharge (S-Q) functions have been developed in many catchment hydrology studies for long-term basin scale evapotranspiration (*ET*) (Palmroth

et al., 2010) and precipitation estimation (Kirchner, 2009), and characterizing variability of catchment storage for water resources management (e.g. Krakauer and Temimi, 2011; Peña-Arancibia *et al.*, 2010; van Dijk, 2010). In addition, the storage-discharge relationships have been applied to quantify the lower-bound of mountain block recharge in areas with distinct precipitation seasonality (Ajami *et al.*, 2011). Using the S-Q functions developed from daily streamflow during dry seasons, the method estimates dynamic mountain block recharge without requiring other field observations than streamflow and precipitation data. However, in Ajami *et al.*, (2011), baseflow and net subsurface lateral outflow during dry seasons are not considered in the recharge estimation. Without considering net subsurface lateral outflow, it is very likely to underestimate catchment recharge, and neglecting baseflow in dry season would potentially result in overestimation of catchment recharge. Therefore, the wet season recharge rate estimated from the storage-discharge relationship during the dry season does not necessarily give the lower bound of annual groundwater recharge. Further improvement to the storage-discharge relationship method is needed to better quantify groundwater recharge.

Before introducing the improved recharge estimation method, we firstly need to clarify the different terms of recharge in mountainous regions. For a mountainous catchment, mountain block includes all the mass composing the mountains, including vegetation, soil, bedrock and water (Wilson and Guan, 2004). Instead of using mountain front recharge, mountain block recharge (e.g. Ajami *et al.*, 2011; Kao *et al.*, 2012) or mountain system recharge (e.g. Ajami *et al.*, 2012) which is sometimes incomparable between studies, we focus on the catchment itself. Simply we use direct water-table recharge to describe the part of infiltrated water that has reached the fractured bedrock storage and refer net recharge, which equals to net subsurface lateral outflow, to the water amount that left from direct water-table recharge after the baseflow discharge.

In this study, an improved method based on the storage-discharge relationship (hereafter referred to as SQR) is proposed for groundwater recharge estimation in mountainous catchments. The improvement from the original model includes that groundwater discharge in dry seasons is considered in the SQR to estimate net catchment recharge, and net subsurface lateral outflow from the catchment is considered in the water balance equation. The research questions are: (i) How does the improved SQR method work for mountainous catchments in the Mount Lofty Ranges in South Australia? (ii) Is the recharge estimated from the SQR method comparable with that from the CMB method? (iii) How does the recharge respond to the variability in climate conditions? The paper is structured as follows to answer these questions. The conceptual model theory is given in Section 5.2, followed by descriptions of study catchments and data collection in Section 5.3. The results and discussion are presented in Section 5.4, and the limitations of the improved SQR method are summarized in Section 5.5. Conclusions are given in Section 5.6.

5.2 Theory

5.2.1 Conceptual model

In order to understand groundwater recharge in mountainous catchments, we need to understand precipitation seasonality (input characterization), the dynamic storage changes of the catchments, and streamflow patterns (output characterization). In a typical mountainous catchment with semi-arid climate, groundwater recharge is dominant during the wet season while there is little recharge in the dry season. Groundwater recharge in a wet season replenishes groundwater storage of the catchment, leading to an increase in the baseflow component of the streamflow. In a dry season, when the recharge rarely happens, groundwater storage of the catchment is depleted by continuous loss of water via baseflow (Figure 5.1, left), net subsurface lateral outflow and potential loss due to *ET* in areas of shallow subsurface. The response of streamflow (mainly composed of baseflow)

to catchment storage changes as shown in the hydrograph (Figure 5.1, right) in turn can be utilized as an indicator of catchment storage status. If the storage changes before and after a wet season can be quantified from the storage-discharge relationship, and groundwater discharge through baseflow in the dry season can be estimated, the annual net groundwater recharge rate of the mountainous catchment can be quantified.

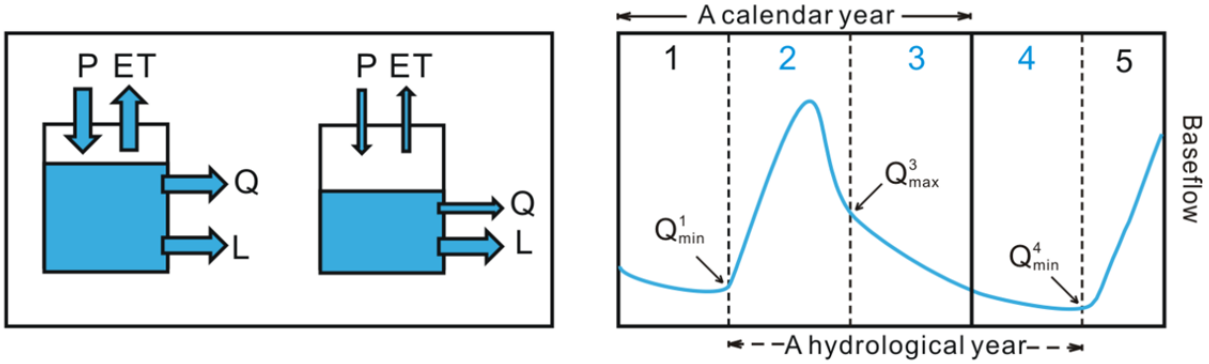

Figure 5.1 Conceptual diagram to illustrate groundwater recharge processes for areas of distinctive dry and wet seasons. On the left panel: two conditions (one in wet season and the other in dry season) are demonstrated, where *P* is precipitation, *ET* is evapotranspiration, *Q* is streamflow, and *L* is net subsurface lateral outflow. The magnitude of *Q* is controlled by groundwater storage *S* through baseflow. The detail of change in streamflow is shown in the right panel for a typical year. Period 1 refers to the dry condition of the catchment before the recharge season (wet season), period 2 refers to the recharge season, period 3 refers to the beginning of dry season (drying period) after the recharge of the year, and period 4 refers to the dry period of the next year in which catchment storage releases water recharged in the previous year. Thus period 3 and 4 constitute the dry season of the year and period 5 refers to the beginning of the next recharge season. Simply, periods 2, 3 and 4 is considered as a hydrological year in this study.

We will demonstrate this conceptual framework based on several catchments in the Mount Lofty Ranges, South Australia. This study area has one distinct raining season from April to October (corresponding to period 2 in Figure 5.1, right) dominated by winter frontal storms. Groundwater recharge occurs in this wet season and dynamic storage changes of the catchment during this season will be estimated by measuring changes in streamflow (mainly baseflow) before and after the recharge season using a hydrographic recession analysis outlined by Brutsaert and Nieber (1977) and Kirchner (2009). To explain the dynamics of catchment storage in response to precipitation, we define different periods of a calendar year according to precipitation and streamflow rather than the subsurface

moisture conditions because continuous and representative observations of the catchment storage are not available. We have identified three periods to present a hydrologic year in our catchments (periods 2, 3 and 4 in Figure 5.1). The hydrologic year starts from a dry catchment state where baseflow is minimum ($Q^1_{\min}$, in period 1). As a result of precipitation and recharge in period 2, baseflow reaches its maximum value ($Q^3_{\max}$, in period 3). Therefore, changes in catchment storage between $Q^1_{\min}$ and $Q^3_{\max}$ can be used to estimate changes in groundwater storage of the catchment after recharge. Similarly, dynamic storage changes of the catchment from the wet period (period 2) to the dry period (period 4) can be estimated by using $Q^3_{\max}$ and minimum baseflow before the next recharge season ($Q^4_{\min}$, period 4) based on the same S-Q function of the given catchment.

5.2.2 Recharge estimation

5.2.2.1 Derivation of the storage-discharge (S-Q) function

Changes of the water storage in a catchment over a given period can be described by the mass conservation:

$$\frac{dS}{dt} = P - ET - Q - L \quad (5.1)$$

where *S* is catchment storage, *P* is precipitation, *ET* is evapotranspiration, *Q* is streamflow, and *L* is the net subsurface lateral outflow to the regional aquifer. When streamflow is a function of catchment storage, the catchment sensitivity function can be obtained from the streamflow time series data in the condition that $P \ll Q$, $ET \ll Q$, $L \ll Q$, according to

$$g(Q) = \frac{dQ}{dS} \approx \frac{-dQ/dt}{Q} \quad (5.2)$$

where $g(Q)$ (T^{-1}) is the catchment sensitivity function following Kirchner (2009). This relationship only applies when *Q* is primarily composed of baseflow.

To derive the catchment sensitivity function $g(Q)$, the hydrograph recession analysis of Brutsaert and Nieber (1977) is applied by using daily streamflow data for the periods when precipitation and *ET* are much smaller than streamflow. Thus, data in rainy days and wet season should be excluded from this analysis. *ET* may still be important in the remaining days (dry season) but its effect on dry season baseflow is very limited. This is because soil moisture storage during dry season does not contribute to groundwater recharge and therefore is disconnected from the groundwater storage.

The recession plot ($-dQ/dt$ *vs* dQ) is used to obtain the catchment sensitivity function. In Brutsaert and Nieber (1977), the recession plot is constructed with streamflow measurements of two consecutive days, which is $-dQ/dt = (Q_{i-j} - Q_i)/(t_i - t_{i-j})$ where j=1 day. However, the use of a constant (t_i-t_{i-j}) can lead to situations that both upper and lower boundaries are purely numerical artifacts in the recession plot (Rupp and Selker, 2006). Especially the lower envelope, which is used to determine $g(Q)$ in Brutsaert and Nieber (1977), is heavily affected by the precision level of the measurements, including the precision at which Q is recorded and the precision of stage height records (Rupp and Selker, 2006). In order to minimize the effects of streamflow measurement errors in recession plot, we use the scaled-Δt method of Rupp and Selker (2006) to estimate recession slopes for each Q_i when the difference between two measured streamflow values is larger than a threshold value:

$$Q_{i-j} - Q_i \geq C(Q_{\max} - Q_{\min}) \quad (5.3)$$

where i is the data point taken at time step i, j is the number of time increments depending on the magnitude of measurement error in streamflow, and C is a constant equal to or larger than one which is determined empirically. Q_{max} and Q_{min} are the maximum and minimum Q respectively for a given stage value in the time series of streamflow data.

After correction for the stream flow measurement error, the recession plot presents $-dQ/dt = (Q_{i-j} - Q_i)/(t_i - t_{i-j})$ as a function of $(\sum_{k=i-j}^{i} Q_k)/(j+1)$ and mean value is applied for the estimation of g(*Q*) (Kirchner, 2009). Brutsaert and Nieber (1977) suggested to obtain the S-Q function from the lower envelope as they stated that the lowest (-d*Q*/dt) data points were solely determined by the change of groundwater at a given *Q*. However, in practice this lower envelope is more likely influenced by the resolution-induced measurement errors mentioned above. More importantly, g(*Q*) should representatively capture the catchment behaviour in terms of catchment storage change and streamflow. The scatter of data points in a recession plot often shows randomly in different directions around an average recession trend to a certain degree (Kirchner, 2009). The lower envelope may lead to biased estimation of g(*Q*). Therefore, the recession flow data are binned using the quantile method (Ajami *et al.*, 2011; Kirchner, 2009), and only the data where the standard error of $-dQ/dt = (Q_{i-j} - Q_i)/(t_i - t_{i-j})$ is less than half of the mean for each bin are selected for the scatter plot of $\ln(-dQ/dt)$ *vs* $\ln Q$ (Kirchner, 2009). Depending on the pattern of this scatter plot, linear or quadratic fitting is performed to derive the S-Q function. In this study, linear fitting is used according to the data pattern in the study area. The following formulation is derived based on this linear regression. Formulation for nonlinear fitting functions can be found in Kirchner (2009).

If this fitting results in a slope and intercept of a linear function, they can then be used to produce the catchment sensitivity function *g*(*Q*):

$$-\frac{dQ}{dt} = aQ^b \quad (5.4)$$

where *b* is the slope of the linear fitting based on the scatter plot of $\ln(-dQ/dt)$ *vs* $\ln Q$.

Equation (5.2) can be re-organized and transformed into,

$$\int dS = \int \frac{dQ}{g(Q)} = \int \frac{1}{a} * Q^{1-b} dQ \quad (5.5)$$

which leads to

$$S - S_0 = \frac{1}{a(2-b)} Q^{(2-b)} \quad (5.6)$$

where S_0 is the initial water storage in the catchment.

Catchment properties, e.g. characteristic recession time (CRT) and storage depletion response, can be reflected in the sensitivity function (Kirchner *et al.,* 2009). Reciprocal of the sensitivity function ($1/g(Q) = 1/a * Q^{(1-b)}$) is the *CRT* ($\tau = \frac{dS}{dQ}$) of the catchment. The parameter *b* reflects the steepness of the CRT function. For a given streamflow value which is commonly less than 1 mm/day, a larger *a* is corresponding to a lower value of CRT, and a larger *b* is corresponding to a higher value of CRT.

5.2.2.2 Groundwater recharge estimation from the S-Q function

Based on the S-Q function (equation (5.6)), storage change of the catchment in the wet season (ΔS_w) is obtained by using measured streamflow values before ($Q^1_{\min}$, minimum streamflow in period 1, Figure 5.1) and after ($Q^3_{\max}$, maximum streamflow in period 3, Figure 5.1) wet season. Similarly, to estimate storage change in the dry season (ΔS_d) stream flow values corresponding to period 4, $Q^3_{\max}$ and $Q^4_{\min}$ as shown in Figure 5.1 are used:

$$\Delta S_w = \left(\frac{1}{a(2-b)}(Q^3_{\max})^{(2-b)} - \frac{1}{a(2-b)}(Q^1_{\min})^{(2-b)}\right) \quad (5.7\text{-}1)$$

$$\Delta S_d = \frac{1}{a(2-b)}(Q^4_{\min})^{(2-b)} - \frac{1}{a(2-b)}(Q^3_{\max})^{(2-b)} \quad (5.7\text{-}2)$$

Mountain catchments are very often composed of fracture rocks with thin root zone soil layers overlying thick vadose zone. Catchment water storage changes inferred from equation (5.7) is disconnected from evapotranspiration, and changes in storage can be regarded as potential direct groundwater recharge or discharge. Considering potential groundwater recharge will eventually join the aquifer by direct water-table recharge, we assume that the result from equation (5.7) approximates groundwater storage change of the catchment. Changes in groundwater storage which is replenished by direct water-table recharge and depleted by baseflow and net subsurface lateral outflow from the catchment can be expressed for wet and dry seasons as follows:

$$\Delta S_w = R_w - B_w - L_w \quad (5.8\text{-}1)$$

$$\Delta S_d = R_d - B_d - L_d \quad (5.8\text{-}2)$$

where ΔS is catchment storage change, *R* is direct water-table recharge, *B* is baseflow and *L* is net lateral subsurface outflow of the catchment. The subscript *w* and *d* refers to wet and dry season respectively.

Lateral subsurface outflow is determined by across catchment hydraulic gradient and transmissivity. Generally speaking, the hydraulic head in the aquifer changes symmetrically in wet and dry seasons. Without better knowledge, we assume that the net subsurface lateral outflow does not differ too much between the two seasons.

$$L_w \approx L_d \quad (5.9)$$

Little is known about the quantitative role of net subsurface lateral outflow in the mass balance equation in complex mountainous catchment. The net subsurface lateral outflow is also termed as mountain block recharge (Manning, 2002) which is difficult to be quantified. Following the above assumption (equation 5.9) and based on the mass balance equations

described above, it is possible to quantify the amount of net subsurface lateral outflow of a mountainous catchment, as shown below.

From equation (5.8-1), (5.8-2), and (5.9), we eliminate net subsurface lateral outflow:

$$\Delta S_w - \Delta S_d = R_w - B_w + B_d \quad (5.10)$$

The net catchment recharge defined as the difference between direct water-table recharge and baseflow is:

$$R_n = R_w - B_w + R_d - B_d \quad (5.11)$$

Direct water-table recharge in dry season is often very limited. By assuming $R_d \approx 0$ and combining with rearranging equation (5.10) and (5.11), net recharge can be expressed as:

$$R_n = \Delta S_w - \Delta S_d - 2B_d \quad (5.12)$$

Based on calculated net groundwater recharge (R_n) from equation (5.12), we are able to back estimate direct groundwater recharge (R_w) from equation (5.11) and the net subsurface lateral outflow (L_w or L_d) from equation (5.8-1) or (5.8-2).

5.3 The study area and methods

5.3.1 Study site and hydrogeology

Six catchments examined in this study are located in the Mount Lofty Ranges (MLR) of South Australia as shown in Figure 5.2. They include streamflow and precipitation data for all six catchments over various periods as shown in Table 1. Isotopic and major ions data are only available for catchment 3. Catchment 1 and 2 are located in the eastern flank of the MLR and catchment 3, 4, 5 and 6 are situated at the western MLR. More details of the catchments can be found in Table 1. The catchment areas range from 5 km^2 to 227.3 km^2, with annual precipitation from 725 mm to 973 mm. The climate is Mediterranean with dry

summers and wet winters. The types of dominant land use are grazing modified pastures along with irrigated sown grasses and native vegetation (according to the landuse map supplied by Department of Environment, Water and Natural Resources of Government of South Australia).

Table 5.1. The area, gauge elevation, and annual precipitation of 6 catchments in the study area.

No.	Catchment site	Gauge ID	Area (km^2)	Elevation (m)	Precipitation (mm/year)
1	Finniss River near Yundi	A4260504	192.2	203.3	832.5
2	Hindmarsh River at Hindmarsh Valley	A5010500	55.8	90.0	870.9
3	Onkaparinga River at Hahndorf	A5031001	227.3	312.0	921.4
4	First Creek at Waterfall Gully	A5040517	5.0	283.4	973.0
5	Chambers Creek at Coromandel Valley	A5040521	9.8	194.0	724.7
6	Sturt River upstream catchment	A5040530	60.0	152.0	762.2

The six catchments are mainly composed of fractured rocks. Bedrock is primarily late Precambrian metamorphic sedimentary rock composed of shale and sandstone, and some limestone (Preiss, 1987). In the MLR, the sedimentary aquifers of lower catchments are recharged by the fractured rock aquifer system of mountainous catchments according to the potentiometric observations and catchment topography (Banks *et al.*, 2007; Green *et al.*, 2007; Radke *et al.*, 2000).

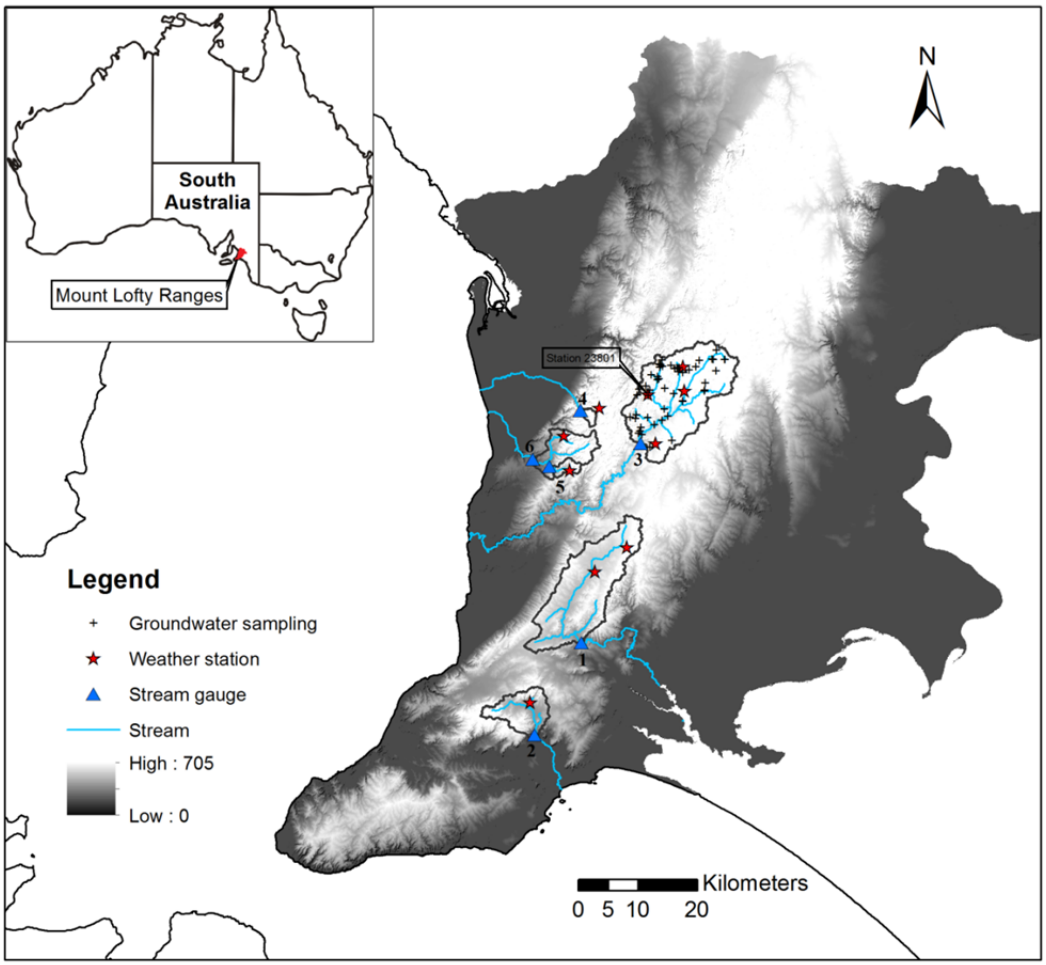

Figure 5.2 The study area showing six catchments chosen for storage-discharge relationship analysis because of data availability.

5.3.2 Data

Time series of daily streamflow and precipitation for the six catchments are downloaded from the Surface Water Data of Government of South Australia (https://www.waterconnect.sa.gov.au) and Bureau of Meteorology of Australian Government (https://www.bom.gov.au) covering the periods which vary with catchments as shown in Table 1. In order to understand how climate conditions affect recharge processes, we obtain the reference *ET* values from the SILO climate database calculated using the Food and Agriculture Organization (FAO) method which is Penman-Monteith equation for the reference grass surface (http://www.longpaddock.qld.gov.au/silo/).

In order to verify our assumption that groundwater recharge predominantly occurs in the wet season, stable isotopic signature of groundwater and precipitation are examined in catchment 3, for which data are available. Isotopic data of catchment 3 include data from 42 out of 51 groundwater samples collected from 1994 to 1995 by Radke *et al.* (2000), and multi-month precipitation samples (11 collections) from 2004 to 2006 in summer and winter by the Department of Land Water and Biodiversity Conservation of South Australia (DWLBC, which is now merged into the Department of Environment, Water and Natural Resources).

The recharge estimate from the S-Q method is compared to the independent chloride mass balance method. In the Mount Lofty Ranges, historical forest clearance has made it difficult to apply the CMB method. A recent development using principal component analysis of major ions in groundwater provides a tool to identify groundwater samples resulting from post-clearance chloride equilibrium conditions (Guan *et al.*, 2013). Of the six studied catchments, only catchment 3 has available hydrochemical data for this analysis. Groundwater hydrochemical data in this catchment collected from 51 locations between 1994 and 1995 are obtained from the Australian Geological Survey Organization database (Radke *et al.*, 2000). Standard major ionic species Ca^{2+}, Mg^{2+}, Na^{+}, K^{+}, HCO_3^{-}, Cl^{-}, SO_4^{2-} and NO_3^{-} are used for principle component analysis.

5.3.3 Recharge estimation

To estimate net recharge in the Mount Lofty Ranges, storage change and baseflow (equation (5.12)) are the two components that need to be estimated. We firstly separated different periods for the study area corresponding to our conceptual model. According to long term averaged hydrograph, April 15th was used to separate period 1 and period 2 while a day roughly around October 15th was to separate period 2 and period 3. The month followed the peak monthly streamflow was selected to determine $Q^3_{\max}$. The duration of

time after a peak in daily streamflow during which the components of streamflow due to surface runoff and interflow are significant can be estimated from the empirical relation by Linsley *et al.* (1982) as follows:

$$N = (0.386 * A)^{0.2} \qquad (5.13)$$

where *N* is the number of the days after the peak in the selected month and *A* is the catchment area in km^2. Then $Q^3_{\max}$ is the streamflow value of the day *N*+1after the peak.

Streamflow values which are the indicators of water storage change of the catchments: minimum streamflow in period 1 ($Q^1_{\min}$), maximum streamflow after wet season in period 3 ($Q^3_{\max}$), and minimum streamflow in period 4 ($Q^4_{\min}$, as $Q^1_{\min}$ for the following year) are summarized in Table 5.3. Then, the catchment sensitivity function is obtained for every catchment using the mean value of the recession flow data from the recession plot (e.g. Figure 5.3). Storage-discharge relationships are derived from the catchment sensitivity functions. Finally, dynamical storages of both wet and dry seasons are estimated (e.g. Table 5.3) from our summarized streamflow values and the storage-discharge relationships.

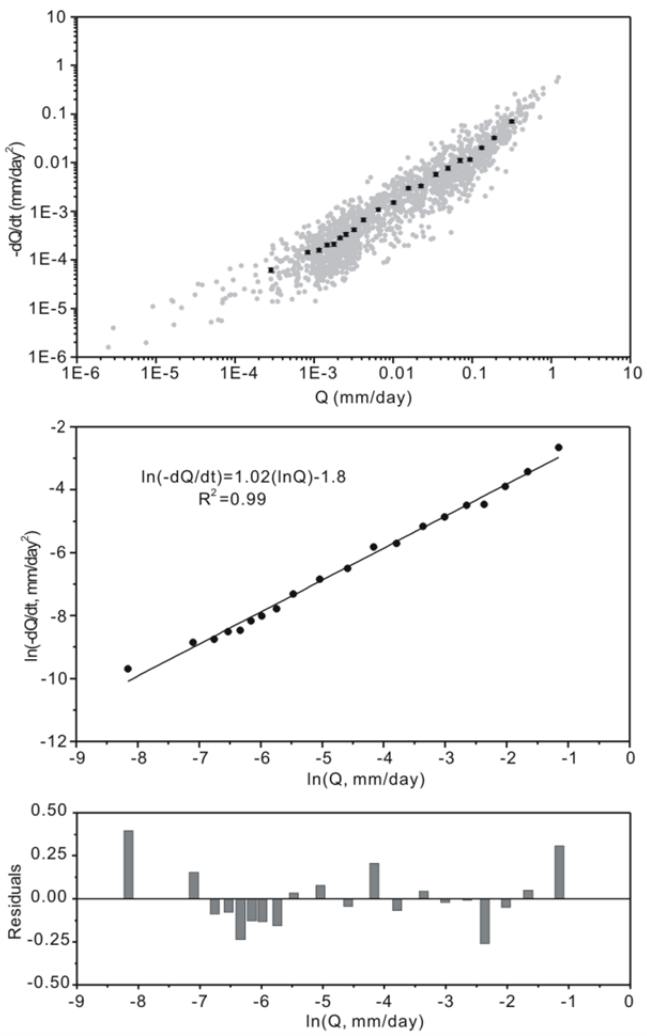

Figure 5.3 A recession plot for the catchment of Onkaparinga River at Hahndorf (catchment 3) based on daily streamflow data of January to mid-April and mid-October to December from 2002 to 2013 excluding rainy days. Black dots represent binned values obtained using the quantile method, and error bars represent bin standard errors. Standard error of (-d*Q*/d*t*) for each bin is less than a half of its mean (d*Q*/d*t*). Residuals are shown for linear fits of *ln*(-d*Q*/d*t*) and *Q*. Recession plots for other catchments are provided in the Appendix.

In recession analysis, both the extraction procedure to select data points and fitting model for the S-Q function can have certain effects on estimating catchment recession characteristics (Stoelzle *et al.*, 2013). Stoelzle (2013) pointed out that Kirchner's extraction procedure (mean value of the recession) considers early stages of recession period and binning of the recession flows for the regression leads to a higher *a* and lower *b* than those from the Vogel method (Vogel and Kroll, 1992) and the Brutsaert method (Brutsaert, 2008). However, we excluded streamflow in wet season and all rainy days during our analysis

and the problem of early stages of recession which may not reflect the real storage-discharge relationship should not be significant in our analysis. Before binning the data, we applied scaled-*Δt* method of Rupp and Selker (2006) to reduce the effect of measurement error on derivation of the sensitivity function. Thus the binning method, which may cause a problem that lower $-dQ/dt$ with lower *Q* gains more weight in the regression model, should not be significant for our recharge estimation. More importantly, this scaled-*Δt* method has greatly improved the model performance in Ajami *et al*. (2011).

Baseflow of wet season or dry season is estimated by the recursive digital filtering of hydrographs (Eckhardt, 2005; 2012):

$$B_i = \frac{[(1-BFI_{\max})*c*B_{i-1} + (1-c)*BFI*y_i]}{(1-c*BFI_{\max})} \quad (5.14)$$

where B_i is baseflow at day *i*, B_{i-1} is baseflow at day *i*-1, y_i is total streamflow at day *i*, *BFI* is baseflow index (ratio of baseflow to the total flow), $BFI_{\max}$ is assumed to be 0.25 as suggested by Eckhardt (2005; 2012) for hard rock aquifers, and *c* is the filter parameter which is estimated to be 0.98. Based on this method, we are able to obtain daily baseflow estimation. Total baseflow after the recharge season can be obtained by summing the daily baseflow from November 15th to March 15th of the next year. This estimation window is one month after the wet season to avoid the disturbance from perched aquifer water release to the streamflow, and one month before the next wet season to avoid the variation in the beginning of wet season for certain years. The error (an error Δc and an error $\Delta BFI_{\max}$) propagation into the calculated baseflow index *BFI* is estimated by the partial derivatives of *BFI* with respect to *c* and $BFI_{\max}$ (Eckhardt, 2012). Instead of detailed derivatives (see Eckhardt, 2012) we simply present the equations here:

$$S(BFI|c) = \frac{\Delta_c BFI}{BFI} \Big/ \frac{\Delta c}{c} = \frac{(1 - BFI_{\max})(BFI - BFI_{\max})}{(1 - cBFI_{\max})^2} \frac{c}{BFI} \quad (5.15\text{-}1)$$

$$S(BFI|BFI_{\max}) = \frac{\Delta_{BFI_{\max}} BFI}{BFI} \Big/ \frac{\Delta BFI_{\max}}{BFI_{\max}} = \frac{(c-1)(cBFI-1)}{(1 - cBFI_{\max})^2} \frac{BFI_{\max}}{BFI} \quad (5.15\text{-}2)$$

S|(BFI|c) is the sensitivity index for the parameter *c*. In this notation, *S* stands for "sensitivity index", the first symbol in the parentheses (here *BFI*) indicates the output that is assessed, and the second symbol (here *c*) the uncertain input. Similarly the sensitivity index *S* (BFI|BFI_{max}) is for parameter BFI_{max}. The value of $S(BFI|c)$, for example -0.75, means that a relative error of *X* percent in parameter *c* causes a relative error of -0.75 times *X* percent in *BFI*. By means of equation 5.14, the additional information of uncertainties for this baseflow separation technique can be provided.

5.3.4 Recharge estimation using the CMB

The independent CMB method provides a good reference to evaluate the SQR method. With the assumption that the whole catchment is under chloride steady state condition, the net catchment recharge is equal to direct water table recharge with losing stream while the net catchment recharge is less than direct water table recharge with gaining stream. The detailed CMB equations using catchment 3 as an example should be:

$$P * C_p = R * C_R + Q * C_Q \quad (5.16)$$

$$Q * C_Q = Q_e * C_e + B * C_B \quad (5.17)$$

where *P* is precipitation, *R* is direct water-table recharge, Q_e is event quickflow, *B* is baseflow and *Q* is total streamflow. C_P, C_R, C_e, C_B and C_Q are chloride concentration for the corresponding component. In practice, we usually have the observation data of total streamflow and combine the two equations without separating the event quickflow and baseflow as follows:

$$P * C_p = (R * C_R - B * C_B) + Q * C_Q \quad (5.18)$$

Thus net catchment recharge by CMB is $R_n = R - B$ which is consistent as what we calculated from *SQR* method.

The atmospheric chloride input for the study area is estimated by a de-trended residual kriging model (Guan *et al.*, 2010b). Chloride concentration of groundwater recharged at the steady state condition is identified by principal component analysis (PCA) of the major ions in groundwater samples (Guan *et al.*, 2013). The PCA analysis provides a good solution to check the steady state of the chloride concentration in groundwater rather than simply using an averaged chloride concentration value from all observation wells. To perform the PCA analysis, standard major ionic data (Ca^{2+}, Mg^{2+}, Na^{+}, K^{+}, HCO_3^{-}, Cl^{-}, SO_4^{2-} and NO_3^{-}) for each observation well are required. Therefore, this analysis can be only applied in catchment 3 which has available data.

PCA can be applied to distinguish different physical processes that affect hydrochemical signals (Likens and Buso, 2006; Price *et al.*, 2012; Ouimet and Duchesne, 2005). By examining the correlation coefficients between principal component scores and original variables, certain specific process(es) can be connected with each principal component (PC). For instance, if a PC score, such as PC1 in Table 5.4, has similar correlation with all ion concentrations, the PC should correspond to the effect of *ET* concentrating process. More detailed application of PCA can be found in Guan *et al*. (2013).

5.4 Results and discussion

5.4.1 Hydrological seasonality of the study area

Characterizing seasonality of recharge and discharge of a catchment is the first step for recharge estimation. Isotopic composition of precipitation usually has a seasonal pattern (Dansgaard, 1964; Kendall and McDonnell, 1998) in mid-latitude area. This seasonal

pattern has been used to characterize the seasonality of groundwater recharge (Craig and Gordon, 1965; Kendall and McDonnell, 1998). In the study area, winter precipitation tends to have more negative delta values of oxygen-18 and deuterium while summer precipitation tends to have less negative delta values (Xu *et al.*, 2014). For example in catchment 3 (Figure 5.4), water stable isotope ratios of groundwater and winter precipitation, are very close to each other and they are more negative than that of summer precipitation. This result indicates that groundwater recharge in the study area is dominated from winter precipitation. The hydrological seasonality can also be identified by long term average of monthly precipitation and pan evaporation as shown in Figure 5.5. As can be seen in Figure 5.5, the raining season from April to October corresponds to low pan evaporation while the period from November to March is the dry season.

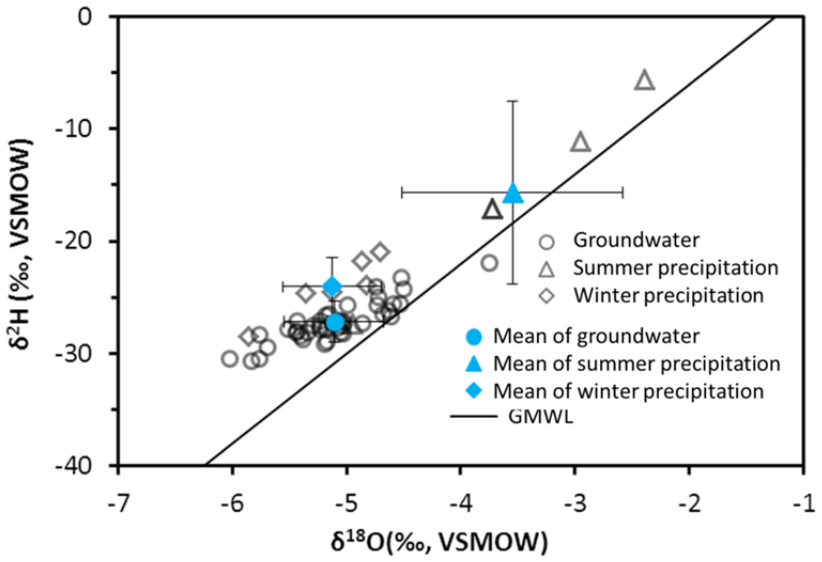

Figure 5.4 Water stable isotopic composition of groundwater (42 samples, open circles), summer precipitation (6 multiple-month samples, open triangles) and winter precipitation (5 multiple-month samples, open diamonds) in the study area. The blue fitted shapes with error bars are the mean value for the corresponding water body.

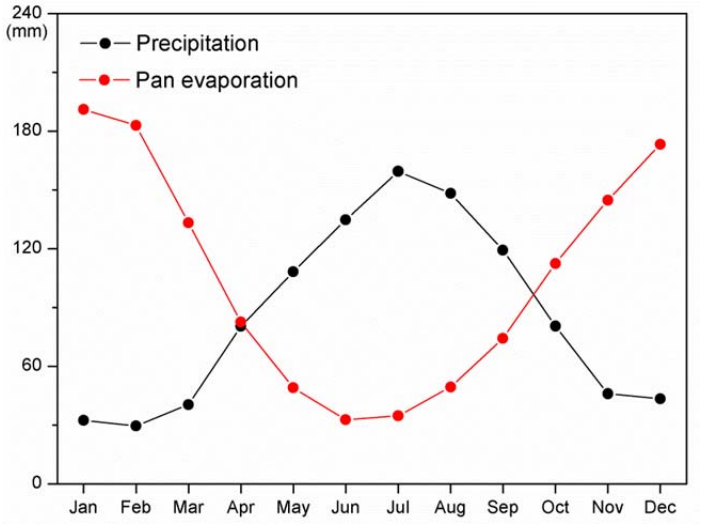

Figure 5.5 Long-term average precipitation and pan evaporation for each month at sample site 23801 (1967-2007, catchment 3 marked on figure 5.2) in the Mount Lofty Ranges.

5.4.2 Storage-discharge relationships and recharge estimation

The derived S-Q functions for the six catchments are shown in Table 2. Linear regressions of $\ln(-dQ/dt)$ *vs* ln*Q* for the catchments show very good coefficients of determination. They are all larger than 0.92, with small root mean square errors. Parameters *a* and *b* are similar among the catchments except for catchment 4. These two parameters are related to catchment hydraulic properties, particularly *b* plays the controlling role in the relationship between catchment storage and stream discharge.

Table 5.2 Derived storage-discharge functions for 6 catchments in the Mount Lofty Ranges. The values of *a* and *b* as in $-dQ/dt = aQ^b$ are estimated from the intercept (e.g. $a = e^{-2.05}$ for catchment 3) and slope (e.g. *b*=0.97 for catchment 3) of the linear fitting respectively.

Catchment No.	Catchment area (km^2)	a	b	S-Q Function	Adjusted R^2	RMSE
1	192.2	0.21	1.01	$S\text{-}S_0=4.81Q^{0.99}$	0.96	0.29
2	55.8	0.12	0.86	$S\text{-}S_0=7.31Q^{1.14}$	0.96	0.23
3	227.3	0.13	0.97	$S\text{-}S_0=7.47Q^{1.03}$	0.99	0.17
4	5.0	0.34	1.41	$S\text{-}S_0=4.99Q^{0.59}$	0.96	0.19
5	9.8	0.18	1.10	$S\text{-}S_0=6.17Q^{0.90}$	0.92	0.31

6	60.0	0.12	0.89	$S\text{-}S_0=7.51Q^{1.11}$	0.99	0.12

Based on the storage-discharge relationship and observed streamflow, we estimated direct water-table recharge and net groundwater recharge for each studied catchment (Table 5.3). Net groundwater recharge ranges from 0.38 mm yr^{-1} to 10.09 mm yr^{-1} which accounts for less than 25% of direct water-table recharge of each catchment. Storage changes in both dry season and wet season are almost equal to each other. Net recharge and net subsurface lateral outflow are equal to each other. Estimated baseflow in the wet season ranges from 9.43 mm yr^{-1} to 29.17 mm yr^{-1}. The amount of baseflow in the dry season is small (0.65 mm yr^{-1} to 4.93 mm yr^{-1}) but significant in comparison to the amount of net groundwater recharge.

Table 5.3 Annual average values for streamflow, storage changes, and base flow in the dry period and wet period respectively. The last three columns present net groundwater recharge (R_n), net subsurface lateral outflow (L) and direct water table recharge (R_w). It should be noticed that values of $Q_{\min}^{1or4}$ are all larger than zero but only two digits are shown here.

Catch-ment No.	$Q_{min}^{1\ or\ 4}$ (mm day^{-1})	Q_{max}^{3} (mm day^{-1})	ΔS_d (mm yr^{-1})	ΔS_w (mm yr^{-1})	B_d (mm yr^{-1})	B_w (mm yr^{-1})	R_n (mm yr^{-1})	L (mm yr^{-1})	R_w (mm yr^{-1})
1	0.00	0.80	-3.84	3.84	0.88	16.51	5.91	5.92	23.31
2	0.01	0.77	-5.62	5.61	2.97	23.5	5.30	5.30	31.77
3	0.00	0.55	-4.13	4.13	0.65	9.43	6.96	6.96	17.04
4	0.05	1.79	-5.61	5.58	4.93	26.59	1.28	1.32	33.33
5	0.01	1.63	-9.29	9.29	2.67	29.17	13.48	13.48	44.70
6	0.00	1.04	-8.00	8.00	1.93	15.73	11.86	11.86	30.07

For most catchments in our study, parameter *b* is close to one. In other words, these catchments have approximately linear relationship between catchment storage and stream discharge. This is consistent with the results in Brutsaert and Nieber (1977), Clark (2009), Harman (2009), and Rupp and Selker (2006) who applied streamflow recession analysis at the hillslope scale. However, the situation is different for catchment 4 which has the largest *a* and *b* compared to other catchments. A large *a* means that catchment 4 has a small CRT ($1/a*Q^{(1-b)}$). This is reasonable given that it is the wettest and smallest catchment of the six (Table 1). A large *b* suggests that a large recession of streamflow is related to a small depletion of catchment storage. Thus discharge in catchment 4 may be more sensitive than other catchments to the catchment storage depletion.

Although catchment 4 has the largest annual precipitation among the six examined ones, net recharge is very small in this catchment due to large baseflow in the dry season (Table 5.3). Contrary to catchment 4, catchment 5 is also small in size but has the least average precipitation and highest net recharge. Given the averaged value of $Q_{\min}^{1}$ and indicated

streamflow $Q^3_{\max}$ for catchment 4 (0.78 mm/day) and catchment 5 (0.61 mm/day) (Table 5.3), the CRT ($1/a*Q^{(1-b)}$) is calculated to be 3 days and 6 days for the two catchments, respectively. Thus, according to the CRT and net groundwater recharge estimates, catchment 4 may be good for water renewability while catchment 5 may have the advantage of storage capacity. But this inference is not conclusive without further verification. Especially, recursive digital filtering algorithm (Eckhardt, 2005; 2012) for baseflow estimation is based on the assumption that discharge is linearly proportional to catchment storage. This baseflow estimation may not be appropriate for catchment 4. Due to depleted water storage in the dry season, baseflow values become very small right before the start of the wet season. Average baseflow in catchment 1 and 3, is 0.001 mm d^{-1}, and for catchment 2 and 5, is 0.01 mm d^{-1}. Even for catchment 4 which has the largest baseflow, it is only 0.05 mm d^{-1}. These observed values of baseflow further support our conceptual model for the separation of different hydrologic periods.

Without quantifying catchment baseflow in a dry season, the recharge estimation from *Ajami et al.* (2011) approach only provides a lower bound estimates. Even though initial catchment storage is unknown (S_0 in equation (5.5)); dynamic storage change can be estimated by storage-discharge relationships using streamflow values before and after the raining season. The difference between the two provides the storage change resulting from direct water-table recharge, baseflow and net subsurface lateral outflow of the catchment. With little recharge in dry season, continuous baseflow and net subsurface lateral outflow in dry season are neglected in the algorithm of Ajami *et al.* (2011). From our results (Table 5.3), baseflow after the raining season is quantitatively important compared to net groundwater recharge.

To assume that net subsurface lateral outflow is the same between the wet period and dry period may cause some error in the estimation. However, larger uncertainties for recharge

estimation are surely induced if we totally neglect this process. Ajami *et al.* (2011) also suggested more evidence was needed about the overall flow path in the mountain bedrock. But knowledge of water flow path in mountainous areas is difficult to obtain in practice. Based on our assumption about the net subsurface lateral outflow, we have a rough quantitative understanding of how water distributes into each component of the catchment water balance (equation (5.1)). Taking catchment 3 as an example, under the multiple-year average condition, water storage change is almost zero and precipitation input is 921.4 mm; *ET* which is calculated from the residual of the balance consumes most of the water which is 92.4% (851.4 mm), while streamflow accounts for only 7.3% (67.2 mm) and net subsurface lateral outflow is only 0.3% (2.83 mm).

5.4.3 Comparison between the SQR and the CMB

The PCA results are summarized in Figure 6 and Table 5.4. The first four PCs account for 91% of the variance in the data and reflect major physical processes influencing hydrochemistry of the catchment 3. The related physical process(es) can be detected by the loadings of major ions in each PC. PC2 has significant positive loadings for Na^+ and Cl^-, and negative loadings for Ca^{2+} and Mg^{2+}. It represents the process(es) leading to changes in Ca^{2+} and Mg^{2+}concentration in an opposite direction as Na^+ and Cl^- concentration. In catchment 3, a large proportion of native vegetation cover has been replaced by orchards, grazing pasture and irrigated sown grasses (Radke *et al*., 2000). Thus PC2 is very likely related to the release of soil chloride after anthropogenic disturbance along with the exchange of cations. Groundwater samples with PC2 very close zero indicate that they are least influenced by forest clearance induced historical soil chloride release. They are chosen to calculate groundwater Cl^- concentration for CMB calculation. The averaged groundwater Cl^- concentration is 92.3 mg L^{-1}. Precipitation and discharge along with Cl^- concentrations in catchment 3 are presented in Table 5.5 and 5.6, respectively. Using the CMB method, we estimate net groundwater recharge of catchment 3 to be 3 mm/year

which is very close to 2.83 mm/year estimated from the SQR method. It should be noted that a different net groundwater recharge rate (27 mm/year) was reported for this catchment in Guan *et al.* (2010a). This difference is due to that a wrong stream gauge data was used for the CMB estimation in Guan *et al.* (2010a).

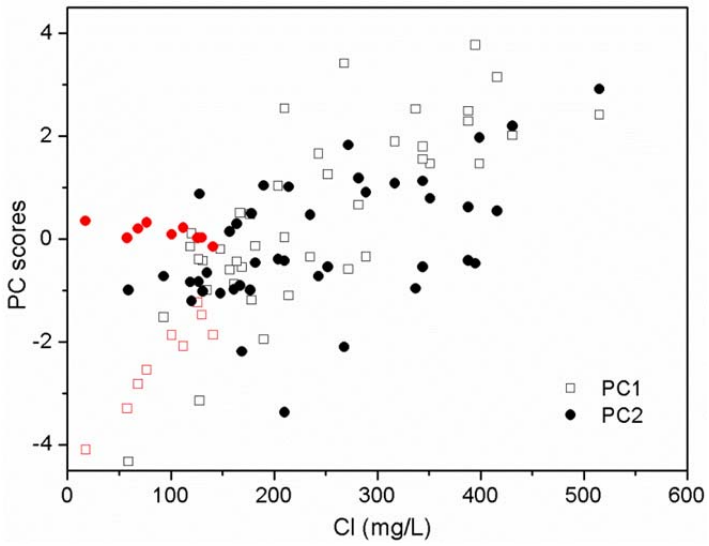

Figure 5.6 Selected PCA results of observed borehole hydrochemical data. Red dots are used to calculate groundwater Cl^- concentration for Hahndorf catchment (catchment 3).

Estimated recharge values from SQR and CMB are net groundwater recharge estimates and theoretically they should be equivalent. But the two methods represent different spatial and temporal aspects of groundwater recharge. While the S-Q method estimates annual net recharge values, the CMB estimate represents long term average recharge value ranging from years to decades. Streamflow is an aggregated measure of the entire catchment response (Kirchner, 2009). To what spatial extent the CMB estimation represents is dependent on the number and spatial distribution of valid groundwater chloride concentration data.

Table 5.4. Principle component loadings (correlation coefficients between principal component scores and original data) of the first four PC.

Principal Components	PC1	PC2	PC3	PC4

(variance interpreted)	(48%)	(17%)	(16%)	(10%)
Ca^{2+}	0.74	-0.51	-0.28	0.05
Mg^{2+}	0.80	-0.45	0.26	-0.06
Na^{+}	0.72	0.62	0.02	0.16
K^{+}	0.82	0.17	-0.06	0.19
HCO_3^{-}	0.57	-0.31	-0.71	-0.10
Cl^{-}	0.84	0.46	0.01	0.17
SO_4^{2-}	0.46	-0.36	0.78	0.10
NO_3^{-}	-0.46	-0.23	-0.13	0.84

Sources of uncertainties to estimate net groundwater recharge are also different for the two methods. For the CMB method, spatial variability of precipitation can affect the accuracy of the CMB method. Chloride deposition to catchment 3 was calculated from a previously published data (Guan *et al.,* 2010b) to account for this spatial variability. Groundwater chloride concentration has significant impact on the accuracy of net groundwater recharge estimation. We applied the PCA method (Guan *et al.*, 2013) to select the points which are more likely to have reached the steady state. Dry deposition of chloride which can be enhanced by vegetation (Deng *et al.*, 2013) also induces uncertainty in the chloride input to the catchment. Without considering canopy enhanced chloride deposition in the catchment, recharge may be underestimated but further investigation of this problem is beyond the scope of this study. Both streamflow measurements and its chloride concentration affect the accuracy of the CMB method. In catchment 3, the standard deviation of annual streamflow chloride load (over 9 years) is 2 g m^{-2} yr^{-1}. Adding this uncertainty to the CMB calculation, it gives a range of net recharge of 0~24 mm yr^{-1}. One can tell that a small change in the streamflow chloride load can result in quite different recharge estimation. For the SQR method, streamflow measurement error has an impact on the model fit especially for low flow rates. The impact of *ET* on streamflow recession

especially in the period we used to derive the sensitivity function can cause steeper recessions and decreases in parameter *b*. Uncertainty of baseflow estimation is another major source of uncertainty in net recharge estimates. More details of the uncertainties and limitations of the SQR will be discussed in section 5.5. Nevertheless, the good agreement between the recharge estimates from the two independent methods provides us some confidence to apply both net catchment recharge estimation methods in the study area.

Table 5.5 Water input (precipitation) and output (streamflow) of Onkaparinga River at Hahndorf (catchment 3).

Catchment No.	Catchment site	Catchment area (km^2)	Precipitation ($mm\ yr^{-1}$)	Streamflow ($mm\ yr^{-1}$)
3	Onkaparinga River at Hahndorf	227.3	921.4	67.2

Table 5.6 Chloride input (precipitation) and output (streanflow) of Onkaparinga River at Hahndorf (catchment 3) and annual groundwater recharge based on CMB method.

Catchment No.	Cl deposition ($g\ m^{-2}yr^{-1}$)	Stream Cl ($g\ m^{-2}yr^{-1}$)	Groundwater Cl ($mg\ L^{-1}$)	Groundwater recharge ($mm\ yr^{-1}$)
3	4.3	4.0	92.3	3

5.4.4 Dynamic recharge and climate

Catchments with long term observational records, 44 years for catchment 1 and 2, and 29 years for catchment 4, are chosen to reveal the relationship between dynamic recharge processes and climate conditions (Figure 5.7). To detect the time lag between precipitation and recharge, the windowed cross regression method (Boker *et al.*, 2002) was used to plot Figure 5.7. In this method, annual recharge and climate values from the same period (e.g. April to March of the next calendar year) were first used. Then annual climate values were

calculated by shifting the time window by one month backward each time, for three times. The best correlation was chosen from the four exercises, as shown in Figure 5.7.

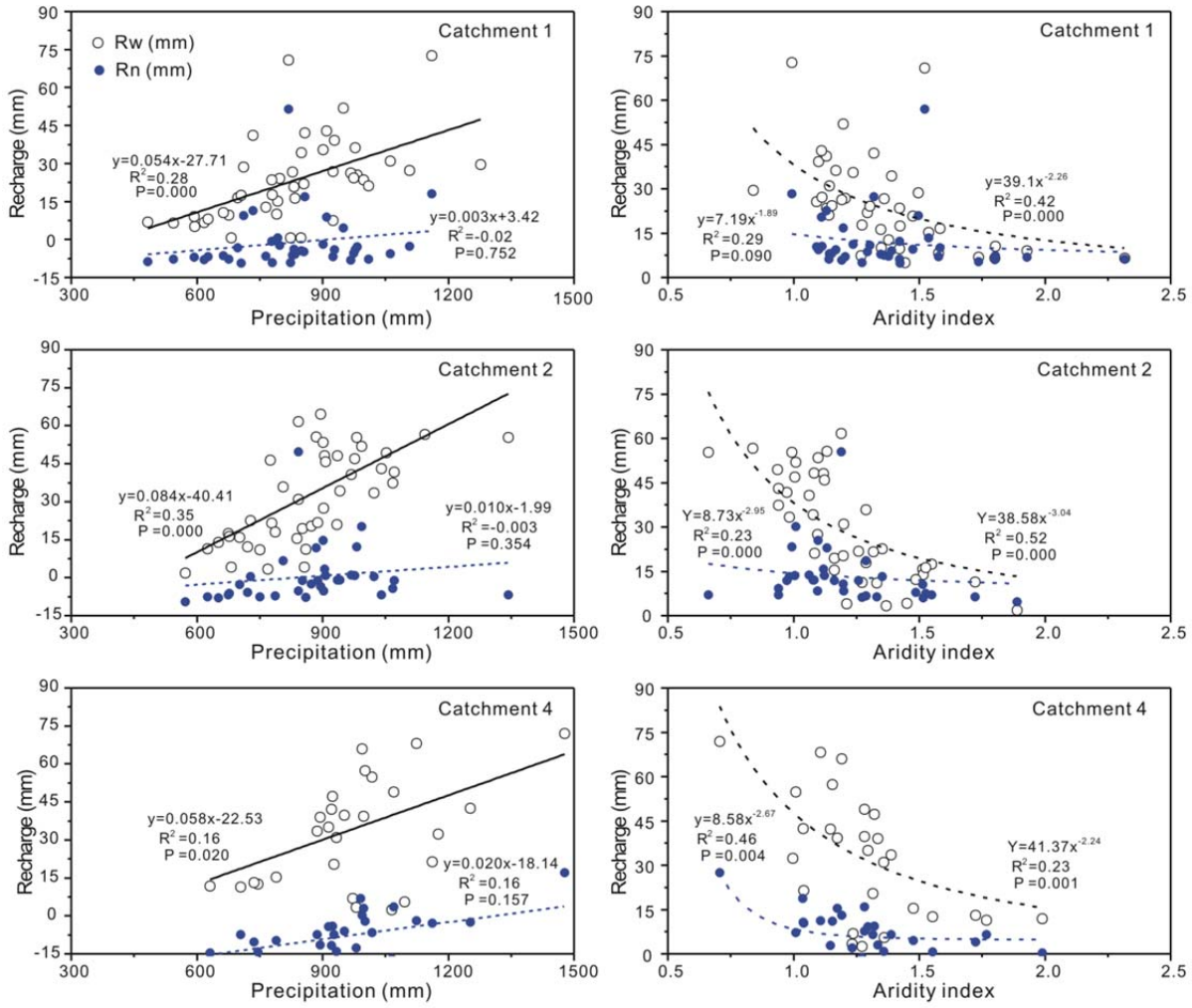

Figure 5.7. Inter-annual variability of direct water-table recharge and net recharge versus precipitation and aridity index for the three catchments with long time series data. The net recharge values (5 points) that are much smaller than -5 mm/year were excluded in the fitting of catchment 2 because of unreasonable high baseflow estimation in dry season.

Generally, larger annual recharge corresponds to larger annual precipitation although the rate of net groundwater recharge increase is much smaller than that of direct water-table recharge (Figure 5.7, left panel). Overall, relationships between recharge and aridity index (the ratio of annual potential evapotranspiration to annual precipitation, *PET*/*P*) are improved (higher R^2) compared to recharge and precipitation alone and it shows that more

severe drought condition can result in a rapid decrease in recharge (Figure 5.7, right panel). However, there are still scatter points of direct water-table recharge and net recharge deviated from the major trend, which may be associated with different antecedent catchment soil moisture conditions. Long term average relationship between recharge and climate conditions among catchments is shown in Figure 5.8. Precipitation solely cannot be used to explain recharge process while aridity index which combines *PET* and precipitation can be used to explain the recharge better.

Apparently, direct water-table recharge appears to be more sensitive than net recharge to the climate conditions. This is because net recharge is more controlled by the subsurface outflow from the catchment which is related to catchment hydrogeological properties, while direct water-table recharge is more controlled by the deep drainage process in the vadose zone which is related to water inputs to the catchment. The deep drainage is determined by the excess soil moisture left by *ET* and it depends on the climate conditions like solar radiation, air temperature, air humidity and wind speed.

Long term average of recharge and precipitation should eliminate the impact of antecedent moisture conditions and reveal the effect of climate conditions on different catchments (Figure 5.8). As can be seen in Figure 5.8, precipitation alone does not show significant effect on recharge, but aridity index shows good correlation with direct water-table recharge. Although precipitation plays a significant role in recharge process, the aridity index which lumps precipitation and potential evapotranspiration should better explain variability in recharge compared to precipitation alone.Net recharge, as mentioned earlier, is more likely to be determined by catchment hydrogeological properties like capacity of water storage, catchment hydraulic transmissivity, and topography-induced cross catchment hydraulic gradient, thus it shows a weaker association with the catchment aridity index than direct water-table recharge. The improved correlation from that between

direct water-table recharge and aridity index at an annual (Figure 5.7, right panel) to that of long term average (Figure 5.8, right panel) time scales, indicates the influences of antecedent moisture conditions on the inter-annual variability of recharge. The infiltrated water partly becomes potential recharge as it may or may not reach the water table because of unsaturated zone processes (e.g. *ET*) or the ability of the saturated zone to accept recharge (Scanlon *et al.*, 2002). The time lag from potential recharge to recharge is possible to be longer than a hydrological year. Thus, direct water-table recharge is better interpreted by the aridity index based on long term average data across catchments (Figure 5.8) than that based on multiple year data within a catchment (Figure 5.7).

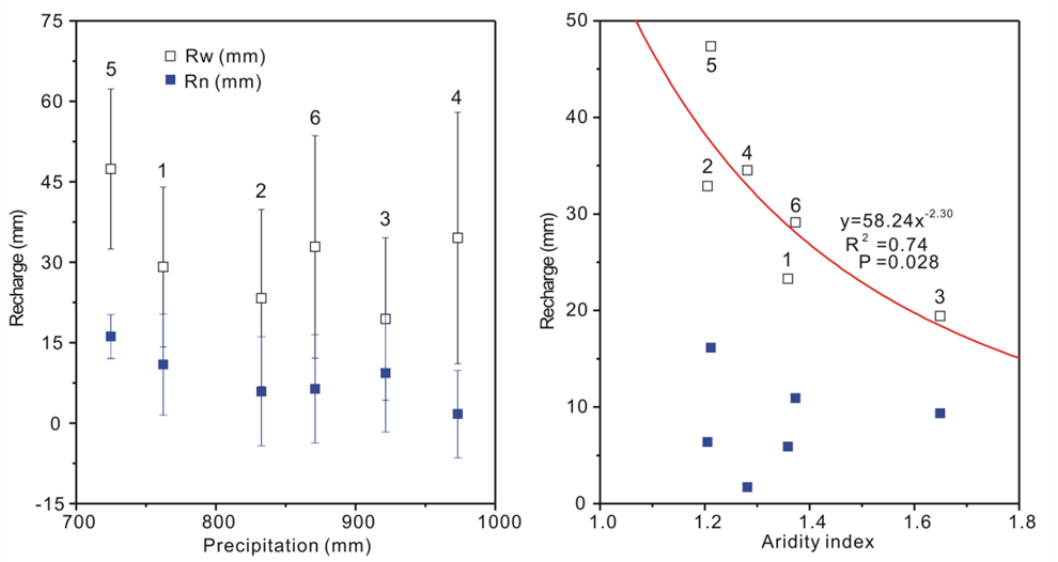

Figure 5.8 Inter-catchment variability of mean direct water-table recharge and net recharge versus precipitation and aridity index for the six catchments. Data labels show catchment numbers from Table 5.1.

5.5 Limitations and difficulties

Although the improved SQR method has potential to provide estimation for different water balance components (particularly groundwater recharges) on annual and seasonal time scales, limitations and difficulties applying this method should be noted. First, the effect of *ET* on the parameterization of the sensitivity functions cannot be completely avoided in the

SQR method. In order to check how *ET* affects the sensitivity functions, Kirchner (2009) re-estimated the sensitivity functions based on daily data under certain criteria, and got similar results as those data that were entirely based on rainless night-time data. Thus it is important to set the criteria according to the climate conditions such as days when $ET \ll Q$ and $P = 0$. To derive the storage-discharge relationships for the catchments in this study, only rainless data of dry periods were included, as dry season *ET* is often assumed to be much less than the baseflow itself.

Besides the limitation mentioned above, it is also difficult to accurately prescribe the parameters in the baseflow estimation equations (equation (5.13)). Both recession constant *c* and the maximum value BFI_{max} of the baseflow index are difficult to be calibrated due to the lack of catchment scale observations, e.g. tracer-based hydrograph separation (Gonzales *et al.*, 2009). Nonetheless, Eckhardt *et al.* (2012) proposed the method to evaluate the mean error of baseflow estimation by calculating the ratio between the relative error of *BFI* and the relative error of the parameter *c* or BFI_{max}. This method provides a preliminary idea of uncertainty in baseflow estimation using recursive digital filtering of hydrographs (Table 5.7). Of the two parameters, uncertainty in *c* is more significant in leading to the uncertainty in the baseflow estimation. For example, a 10% relative error in *c* for catchment 1 causes a relative error of -7.3% in baseflow estimation. But according to the analysis proposed by Eckhardt (2008), parameter *c* usually has only about 2% deviations from the theoretical value of 0.98 when the catchment follows the linear reservoir (parameter b=1 in storage-discharge function) and streamflow mainly composed by baseflow.

Table 5.7 The results of analytical sensitivity analysis of the two parameter recursive digital basflow separation filter. S (*BFI*|*c*) is the sensitivity index for the parameter *c*. In this notation, S stands for "sensitivity index", the first symbol in the parentheses (here *BFI*) indicates the output that is assessed, and the second symbol (here *c*) the uncertain input. Similarly as the sensitivity index S ($BFI|BFI_{max}$) for parameter BFI_{max}.

Catchment No.	c	BFI_{max}	BFI	S (BFI|c)	S (BFI|BFI_{max})
1	0.98	0.25	0.166	-0.73	0.04
2	0.98	0.25	0.200	-0.34	0.04
3	0.98	0.25	0.172	-0.65	0.04
4	0.98	0.25	0.220	-0.18	0.03
5	0.98	0.25	0.221	-0.18	0.03
6	0.98	0.25	0.206	-0.29	0.03

5.6 Conclusions

We improved the storage-discharge relationship method to estimate groundwater recharge in mountainous catchments. Compared to the Ajami *et al*. (2011) approach which provides lower-bound recharge estimates, the improved SQR method has two advantages: 1) it incorporates net subsurface lateral outflow in the recharge estimation; and 2) net groundwater recharge and direct water-table recharge are estimated on annual basis.

The application of the SQR method was performed over six catchments of various aridity, size and hydrogeological conditions in the Mount Lofty Ranges, and compared with an independent method (CMB) on one catchment. The net recharge estimated from the proposed methods (7.0 mm/year) is close to that from the CMB (3 mm/year). The results indicate that the improved SQR method provides an alternative solution for catchment recharge estimation in mountainous catchments. Good correlation between annual direct water-table recharge and aridity index has been found in this study, suggesting this method can also be used to examine dynamic responses of groundwater recharge to the climate conditions in mountainous regions.

References

Aishlin, P., J. P. McNamara., 2011. Bedrock infiltration and mountain block recharge

accounting using chloride mass balance. *Hydrol. Process.* 25(12), 1934-1948.

Ajami, H., P. A. Troch, T. Maddock, T. Meixner, C. Eastoe., 2011. Quantifying mountain block recharge by means of catchment-scale storage-discharge relationships, *Water Resour. Res.* 47(4), n/a-n/a.

Ajami, H., T. Meixner, F. Dominguez, J. Hogan, T. Maddock. 2012. Seasonalizing Mountain System Recharge in Semi-Arid Basins-Climate Change Impacts. *Ground Water*, 50(4), 585-597.

Banks, E., T. Wilson, G. Green, A. Love., 2007. Groundwater recharge investigations in the Eastern Mount Lofty Ranges, South Australia. *Rep.*, Department of Water, Land and Biodiversity Conservation, Adelaide.

Bazuhair, A. S., W. W. Wood., 1996. Chloride mass-balance method for estimating groundwater recharge in arid areas: examples from western Saudi Arabia. *J. Hydrol.* 186(1-4): 153-159.

Boker, S. M., J. L. Rotondo, M. Xu, K. King., 2002. Windowed cross-correlation and peak picking for the analysis of variability in the association between behavioral time series. *Psychol. Methods.* 7(3): 338-355.

Brutsaert, W., 2008. Long-term groundwater storage trends estimated from streamflow records: Climatic perspective. *Water Resour. Res.* 44(2), n/a-n/a.

Brutseart, W., J. L. Nieber., 1977. Regionalized drought flow hydrographs from a mature glaciated plateau. *Water Resour. Res.* 13(3), 637-643.

Clark, M. P., D. E. Rupp, R. A. Woods, H. J. Tromp-van Meerveld, N. E. Peters, and J. E. Freer., 2009. Consistency between hydrological models and field observations: linking processes at the hillslope scale to hydrological responses at the watershed scale. *Hydrol. Process.* 23(2): 311-319.

Cook, P. G., 2003. A guide to regional groundwater flow in fractured rock aquifers, Seaview Press, Adelaide.

Cook, P.G., Walker, G.R. Jolly, I.D., 1989. Spatial variability of groundwater recharge in a semiarid region. *J. Hydrol.* 111, 195-212.

Craig, H., L. Gordon., 1965. Deuterium and oxygen-18 in the ocean and the marine atmosphere. *Rep.*, 130 pp, Spoleto.

Creutzfeldt, B., P. A. Troch, A. Güntner, T. P. A. Ferré, T. Graeff, B. Merz., 2014. Storage-discharge relationships at different catchment scales based on local high-precision gravimetry, *Hydrol. Process.* 28(3): 1465-1475.

Dansgaard, W. (1964), Stable isotopes in precipitation, *Tellus*, 16, 436-468.

Deng, Z., S. C. Priestley, H. Guan, A. J. Love, C. T. Simmons., 2013. Canopy enhanced chloride deposition in coastal South Australia and its application for the chloride mass balance method. *J. Hydrol.* 497: 62-70.

Eckhardt, K., 2005. How to construct recursive digital filters for baseflow separation, *Hydrol. Process.* 19(2): 507-515.

Eckhardt, K., 2008. A comparison of baseflow indices, which were calculated with seven different baseflow separation methods. *J. Hydrol.* 352: 168-173.

Eckhardt, K., 2012. Technical Note: Analytical sensitivity analysis of a two parameter recursive digital baseflow separation filter. *Hydrol. Earth Syst. Sc.*16(2): 451-455.

Gan, R., Y. Luo., 2013. Using the nonlinear aquifer storage–discharge relationship to simulate the base flow of glacier- and snowmelt-dominated basins in northwest China, *Hydrol. Earth Syst. Sc.*17(9): 3577-3586.

Gee, G. W., Z. F. Zhang, S. W. Tyler, W. H. Albright, M. J. Singleton., 2005. Chloride mass balance: Cautions in predicting increased recharge rates. *Vadose Zone J.* 4(1): 72-78.

Gonzales, A. L., J. Nonner, J. Heijkers, S. Uhlenbrook., 2009. Comparison of different base flow separation methods in a lowland catchment. *Hydrol. Earth Syst. Sc.* 13: 2055-2068.

Green, G., E. Banks, T. Wilson, A. Love., 2007. Groundwater recharge and flow investigations in the Western Mount Lofty Ranges. *Rep.*, Department of Water, Land and Biodiversity Conservation, Adelaide.

Green, T. R., MakotoTaniguchi, H. Kooi, J. J. Gurdak, D. M. Allen, K. M. Hiscock, H. Treidel, A. Aureli., 2011. Beneath the surface of global change: Impacts of climate change on groundwater. *J. Hydrol.* 405(3-4): 532-560.

Guan, H., A. J. Love, C. T. Simmons, J. Hutson, Z. Ding., 2010. Catchment conceptualisation for examining applicability of chloride mass balance method in an area with historical forest clearance. *Hydrol. Earth Syst. Sc.*14(7): 1233-1245.

Guan, H., A. J. Love, C. T. Simmons, O. Makhnin, A. S. Kayaalp., 2010b. Factors influencing chloride deposition in a coastal hilly area and application to chloride deposition mapping. *Hydrol. Earth Syst. Sc.* 14(5): 801-813.

Guan, H., J. Hutson, Z. Ding, A. Love, C. T. Simmons, Z. Deng., 2013. Principal component analysis of watershed hydrochemical response to forest clearance and its usefulness for chloride mass balance applications. *Water Resour. Res.* 49(7): 4362-4378.

Harman, C. J., M. Sivapalan, P. Kumar., 2009. Power law catchment-scale recessions arising from heterogeneous linear small-scale dynamics. *Water Resour. Res.* 45(9), n/a-n/a.

Hassan, R.S., 2012. Nonlinearity in storage-discharge relationship and its influence on flood hydrograph prediction in mountainous catchments. *Int. J. Water Res. Environ. Eng.* 4(6).

Kao, Y.-H., C.W. Liu, S.W. Wang, C.H. Lee,. 2012. Estimating mountain block recharge to downstream alluvial aquifers from standard methods *J. Hydrol.* 426-427: 93-102.

Kendall, C., J. J. McDonnell (Eds.)., 1998. Isotope Tracers in Catchment Hydrology, 839 pp., Elsevier Science B.V., Amsterdam.

Kirchner, J. W., 2009. Catchments as simple dynamical systems: Catchment characterization, rainfall-runoff modeling, and doing hydrology backward. *Water Resour. Res.* 45(2), n/a-n/a.

Krakauer, N. Y., M. Temimi., 2011. Stream recession curves and storage variability in small watersheds. *Hydrol. Earth Syst. Sc.* 15(7): 2377-2389.

Likens, G. E., F. H. Bonnann, R. S. Pierce, W. A. Reiner., 1978. Recovery of a deforested ecosystem. *Science.* 199: 492–496.

Linsley, R.K., M.A. Kohler, J.L.H. Paulhus, 1982. Hydrology for engineers (3d ed.): New York, McGraw-Hill, 508 p.

Manning, A. H. 2002. Using noble gas tracers to investigate mountain block recharge to an intermountain basin, University of Utah.

Manning, A. H., D. K. Solomon., 2005. An integrated environmental tracer approach to characterizing groundwater circulation in a mountain block. *Water Resour. Res.* 41(12): n/a-n/a.

McMurray, D. 2003. Assessment of water use from farm dams in the Mount Lofty Ranges, South Australia. *Rep.*, Department of Water, Land and Biodiversity Conservation, Adelaide.

Ouimet, R., L. Duchesne. 2005. Base cation mineral weathering and total release rates from soils in three calibrated forest watersheds on the Canadian Boreal Shield. *Can. J. Soil Sci.* 85(2): 245–260.

Palmroth, S., G. G. Katul, D. Hui, H. R. McCarthy, R. B. Jackson, R. Oren. 2010. Estimation of long-term basin scale evapotranspiration from streamflow time series. *Water Resour. Res.* 46(10): n/a-n/a.

Peña-Arancibia, J. L., A. I. J. M. van Dijk, M. Mulligan, L. A. Bruijnzeel. 2010. The role of climatic and terrain attributes in estimating baseflow recession in tropical catchments, *Hydrol. Earth Syst. Sc.* 14(11): 2193-2205.

Preiss, W. V. (1987), The Adelaide Geosyncline: Late proterozoic stratigraphy, sedimentation, paleaontology and tectonics, Bulletin/Geological Survey of South Australia.

Price, J. R., C. R. Hardy, K. S. Tefend, D. W. Szymanski., 2012. Solute geochemical mass-balances and mineral weathering rates in small watersheds II : Biomass nutrient uptake, more equations in more unknowns, and land use/land cover effects, *Appl. Geochem*. 27(6): 1247–1265.

Radke, B. M., K. M. Ivkovic, K. L. Watkins, R. G. Cresswell, J. Bauld. 2000. A groundwater quality assessment of the upper Onkaparinga region, Southern Mount Lofy RangesRep., Bureau of Rural Sciences, South Australia.

Rupp, D. E., J. S. Selker., 2006. Information, artifacts, and noise in dQ/dt−Q recession analysis. *Adv. Water Resour.* 29(2): 154-160.

Scanlon, B. R., R. W. Healy, P. G. Cook., 2002. Choosing appropriate techniques for quantifying groundwater recharge. *Hydrogeol. J.* 10: 18-39.

Scanlon, B. R., K. E. Keese, A. L. Flint, L. E. Flint, C. B. Gaye, W. M. Edmunds, I. Simmers., 2006. Global synthesis of groundwater recharge in semiarid and arid regions. *Hydrol. Process.* 20(15): 3335-3370.

Somaratne, N., K. R. J. Smettem., 2014. Theory of the generalized chloride mass balance

method for recharge estimation in groundwater basins characterised by point and diffuse recharge. *Hydrol. Earth Syst. Sci. Discuss*. 11: 307-332.

Stoelzle, M., K. Stahl, M. Weiler., 2013. Are streamflow recession characteristics really characteristic? *Hydrol. Earth Syst. Sc.* 17(2): 817-828.

Taylor, R. G., B. Scanlon, P. Döll, M. Rodell, R. van Beek, Y. Wada, L. Longuevergne, M. Leblanc, J. S. Famiglietti, M. Edmunds, L. Konikow, T.R. Green, J. Chen, M. Taniguchi, M.F.P. Bierkens, A. MacDonald, Y. Fan, R.M. Maxwell, Y. Yechieli, J.J. Gurdak, D.M. Allen, M. Shamsudduha, K. Hiscock, P.J-F. Yeh, I. Holman, H. Treidel., 2012. Groundwater and climate change, *Nat. Clim. Change.* 3: 322-329.

van Dijk, A. I. J. M., 2010. Climate and terrain factors explaining streamflow response and recession in Australian catchments. *Hydrol. Earth Syst. Sc.*14(1): 159-169.

Viviroli, D., H. H. Dürr, B. Messerli, M. Meybeck, R. Weingartner., 2007. Mountains of the world, water towers for humanity: Typology, mapping, and global significance. *Water Resour. Res.* 43(7), n/a-n/a.

Vogel, R. M., C. N. Kroll., 1992. Regional geohydrologic-geomorphic relationships for the estimation of low-flow statistics. *Water Resour. Res.* 28(9): 2451-2458.

Wilson, J. L., H. Guan., 2004. Mountain-block hydrology and mountain-front recharge., in Groundwater Recharge in a desert Environment: The southweatern United States, edited by J. F. Hogan, F. M. Phillips and B. R.Scanlon, pp. 113-137, American Geophysical Union, Washington, D.C.

Xu, X., H. Guan, Z. Deng., 2014. Isotopic composition of throughfall in pine plantation and native *eucalyptus* forest in South Australia. *J. Hydrol.* 514: 150-157.

CHAPTER 6 CONCLUSIONS

Environmental stress on native vegetation, vegetation precipitation use, and groundwater recharge characteristics using isotopic tracers have been examined in this dissertation. The study is based on upland catchments in the Mount Lofty Ranges in South Australia. The summary of each chapter in the dissertation is given as follows, particularly showing the main findings, uniqueness or improvements, and recommendations for future work. I also emphasize the roles of $\delta^{13}C$, $\delta^{18}O$ and $\delta^{2}H$ in (eco)hydrological studies.

6.1 Leaf $\delta^{13}C$ and water stress

From the experiments we performed on the two contrasting hillslopes of the native vegetated catchment – Mount Wilson, Significant seasonal variations have been observed in leaf $\delta^{13}C$ for both studied C_3 tree genus up to 1.7‰ for *Eucalyptus* Leucoxylon and up to 2.7‰ for *Acacia pycnantha.* The difference in leaf $\delta^{13}C$ between the two hillslopes is around 2‰. These results suggest seasonal variations and slope effect due to aspects should be considered to examine the leaf $\delta^{13}C$ and ecosystem adaptions over a regional climate gradient.

Reasonable quantitative correlations have been obtained between leaf $\delta^{13}C$ and plant water stress in both temporally and spatially when we apply aridity index, which is the ratio of potential evapotranspiration to precipitation (PET/P), instead of the precipitation for environmental conditions. On the temporal axis, the correlation coefficients between leaf $\delta^{13}C$ and integrated aridity index can be as high as 0.44, and on the spatial axis, the correlation coefficients can be 0.36 for the examined *E*ucalyptus trees. These results suggest that PET/P may be a good indicator to quantify the relationship between leaf $\delta^{13}C$ and plant water stress. This index has the potential to be the indicator for further studies to relate C_3 vegetation and water stress in different regions.

As drought induced tree mortality has been found all around the world (Allen *et al*., 2010), it is worth to 'documenting' the vegetation responses to the environmental conditions through leaf $\delta^{13}C$. The success in associating the aridity index with leaf $\delta^{13}C$ in this study suggest leaf $\delta^{13}C$ can be used as a good dynamic water stress indicator, and to identify spatial niche for vegetation survival over a prolong drought. Future study to explore this potential should focus on more tree species in different climate zones.

6.2 Canopy alteration of throughfall isotopic composition

In vegetated catchments, the input water isotopic composition is altered from precipitation. Based on one year throughfall monitoring and using both ^{18}O and *d*-excess at two vegetated surfaces in Kuitpo Forest we have synthesized a conceptual framework for studying throughfall isotopic composition. The framework works as a useful tool to understand the effects of intra-event selection, partial evaporation and inter-event selection.

The results indicate that in summer, one or both of intra-event selection and inter-event selection is/are very likely to be the major control of the isotopic composition in throughfall at plantation (P) site and native vegetation (N) site. In winter intra-event selection is possible the major control of the isotopic composition of throughfall at P site and N site. Partial evaporation is also observed at both sites, but not as important as intra-event selection or inter-event selection. P site has more significant effect on isotopic composition of throughfall than N site because of its much denser vegetation cover.

Our results show the vegetation effects on isotopic input can be significant in densely vegetated catchments and is important for hydrograph separation studies but can be negligible for paleoclimate reconstruction and tracing groundwater recharge sources, which supports our conceptual model of groundwater recharge in the Mount Lofty Ranges (Chapter 5). Simply, the importance of the isotopic alteration highly depends on the density

of vegetation cover.

6.3 Ecohydrological processes of two contrasting hillslopes

Based on the evidence of previous studies that ^{2}H can have fractionation or not during root water uptake, I have generalized two typical patterns of $\delta^{18}O$ and $\delta^{2}H$ of tree (twig) water. With this background, I compared one-year $\delta^{18}O$ and $\delta^{2}H$ of throughfall and twig water on two contrasting hillslopes in a native vegetation catchment. The slope of twig water line on pole facing slope is much lower than that on the equator facing slope in the wet season (5.4 to 6.0) and particularly in the dry season (2.7 to 5.0) suggests that it is very likely that hydrogen isotopic fractionation takes place during root water uptake. This result calls for caution in using water isotope (particularly $\delta^{2}H$) to study the sources of plant water use. We should also keep in mind that the lower slope of twig water line from that of throughfall may not necessarily resulted from soil evaporation. This also calls for attention in using both $\delta^{18}O$ and $\delta^{2}H$ for evaporation and transpiration partitioning over vegetated surfaces.

$\delta^{18}O$ and $\delta^{2}H$ of twigs are also able to be the indicators to understand the root zone moisture replenishment. The response of $\delta^{18}O$ and $\delta^{2}H$ of twig water to the rain events indicates that only part of the event can be used by the study trees. The timing of the events with respect to the soil moisture condition determines its efficiency as the sources of soil moisture. The similar results of the $\delta^{18}O$ and $\delta^{2}H$ of groundwater with a mean value -5.1‰ and -27.5‰ respectively and that of throughfall in the wet season with a mean value -5.1(±1.7)‰ and -23.4(±13.3)‰ correspondingly indicate that groundwater recharge of the study area is dominated by events in the wet season.

$\delta^{18}O$ and $\delta^{2}H$ of twigs show a good potential to examine the root zone moisture replenishment. With this advantage, continuous observations for a specific site will provide useful information for (eco)hydrological processes. Further applications, like how long it takes for root zone moisture to be replenished can be explored with a careful experiment

design.

6.4 Groundwater recharge estimation for catchments of complex topography and vegetation cover

Based on the understanding of groundwater recharge gained from the above water isotopic study and more isotopic data of precipitation and groundwater of the catchments we are interested, we conclude that the groundwater recharge is dominated by precipitation in the wet season for six catchments in the Mount Lofty Ranges. The isotopic compositions of groundwater are close to that of the precipitation in the wet season. The alteration of isotopic composition of precipitation due to vegetation cover can be neglected for recharge studies as we addressed in Chapter 3 and Chapter 4. This seasonality helps us to construct the conceptual model of groundwater recharge and to improve the storage-discharge relationship method to quantify groundwater recharge in mountainous catchments. Compared to the *Ajami et al*. (2011) approach which provides lower-bound recharge estimates, the improved method (named as SQR) has two more advantages that it incorporates net subsurface lateral outflow in the recharge estimation and net groundwater recharge and direct water-table recharge are estimated on annual basis.

Our application of the improved method have been performed over six catchments of various aridity, size and hydrogeological conditions, and compared with an independent method (CMB) on one catchment. The net recharge estimated from the proposed methods (2.8 mm/year) agrees fairly well with that from the CMB (3 mm/year). The results indicate that the improved SQR method provides an alternative solution for catchment recharge estimation in mountainous catchments. Good correlation between annual direct water-table recharge and aridity index has been found in this study, suggesting this method can also be used to examine dynamic responses of groundwater recharge to the climate conditions in mountainous regions.

The SQR method is relative easily for application of groundwater recharge estimation as it mainly uses daily streamflow records. But it has difficulty to accurately prescribe the parameters in the baseflow estimation which is worth for further improvements. Nevertheless, more applications of this method in mountainous catchments will be very helpful for their water resources management.

6.5 Recommendations for future work

There are several major challenges which are also the good opportunities in ecohydrology studies (Asbjornsen *et al*., 2011; Wang *et al*., 2012). First, a central research topic in ecohydrological is scaling plant water use data from individual leaves and whole trees to stands and landscapes. Leaf $\delta^{13}C$ seems to be a powerful tool in this area. As it shown in our study (chapter 2), the good correlation between leaf $\delta^{13}C$ and water stress which can be quantified as aridity index has the potential for upscaling from plot scale to landscape scale.

Second, interactions and feedbacks between plant water use and soil moisture can have certain ecohydrological triggers such as the shifts of ecosystem states with different ecohydrological functions. The regime behind these shifts has not been well understood. It is necessary to have a long term monitoring to trace the plant water use and the dynamic of soil moisture changes. $\delta^{18}O$ and $\delta^{2}H$ of twig water provide one choice for these studies similarly as I applied in Mount Wilson (chapter 4).

More systematic understanding of upland vegetation and groundwater recharge and its interactions needs more studies like how plant water use, streamflow and groundwater table fluctuations affect or response to each other. These studies require diurnal, seasonal and annual dynamics of different time scales and stands, catchment and landscape spatial explorations in those three components.

Reference

Ajami, H., P. A. Troch, T. Maddock, T. Meixner, C. Eastoe., 2011. Quantifying mountain block recharge by means of catchment-scale storage-discharge relationships. *Water Resour. Res.* 47(4), n/a-n/a.

Allen, C.D., A.K. Macalady, H. Chenchouni, D. Bachelet, N. McDowell, M. Vennetier, T. Kitzberger, A. Rigling, D.D. Breshears, E.H. Hogg, P. Gonzalez, R. Fensham, Z. Zhang, J. Castro, N. Demidova, J-H. Lim, G. Allard, S.W. Running, A. Semerci, N. Cobb., 2010. A global overview of drought and heat-induced tree mortality reveals emerging climate change risks for forests. *Forest Ecol. Manag.* 259: 660–684.

Asbjornsen, H., G.R. Goldsmith, M.S. Alvarado-Barrientos, K. Rebel, F.P. Van Osch, M. Rietkerk, J. Chen, S. Gotsch, C. Tobon, D.R. Geissert, A. Gomez-Tagle, K. Vache, T.E. Dawson., 2011. Ecohydrological advances and applications in plant–water relations research: a review. *J. Plant Ecol.* 4(1-2): 3-22.

Wang, L., P. D'Odorico, J. Evans, D. Eldridge, M. McCabe, K. Caylor, E. King., 2012 Dryland ecohydrology and climate change: critical issues and technical advances. *Hydrol. Earth Syst. Sc*. 16: 2585-2603.

APPENDIX I

Table A.1 Leaf $\delta^{13}C$ [‰ VPDB] data of all the tree species at Mount Wilson site. These data have been used in Chapter 2. S is for south in direction, W is for west in direction, E is for East, N is for north and N/A is for not available in Direction column.

Date	Tree ID	Direction	$\delta^{13}C$ [‰ VPDB]
20120831	*a*	S	-30.26
20120831	*a*	W	-30.56
20120831	*b*	E	-30.89
20120831	*b*	N	-29.54
20120831	*d*	E	-30.97
20120831	*d*	S	-31.39
20120831	*d*	W	-31.01
20120831	*g*	E	-30.33
20120831	*g*	N	-29.09
20120831	*i*	N/A	-32.39
20120831	*i*	N/A	-30.92
20121003	*a*	E	-30.45
20121003	*a*	N	-30.40
20121003	*a*	W	-30.17
20121003	*b*	E	-30.83
20121003	*b*	W	-30.69
20121003	*d*	W	-31.64
20121003	*g*	E	-29.94
20121003	*g*	N	-30.38
20121003	*i*	E	-31.00
20121003	*i*	W	-30.63
20121030	*a*	N/A	-30.21
20121030	*a*	N/A	-30.37
20121030	*b*	E	-30.93
20121030	*g*	N/A	-30.55
20121121	*a*	N/A	-29.94
20121121	*a*	N/A	-29.98
20121121	*b*	E	-29.97
20121121	*b*	N	-30.02
20121121	*b*	W	-29.82
20121121	*d*	E	-28.62
20121121	*d*	N	-30.69
20121121	*d*	W	-30.89
20121121	*g*	N/A	-30.93
20121121	*g*	N/A	-29.41
20121121	*i*	N/A	-30.03
20121121	*i*	N/A	-30.71
20121218	*b*	E	-29.63
20121218	*d*	E	-29.56
20121218	*d*	N	-28.62
20121218	*g*	E	-29.79
20121218	*g*	N	-29.30

20121218	*i*	E	-30.49
20121218	*i*	S	-31.57
20130126	*a*	E	-29.49
20130126	*a*	N	-29.56
20130126	*a*	S	-30.16
20130126	*a*	W	-30.37
20130126	*b*	E	-29.54
20130126	*b*	W	-28.85
20130126	*d*	E	-29.79
20130126	*d*	N	-29.27
20130126	*d*	W	-28.74
20130126	*g*	E	-29.13
20130126	*g*	N	-29.12
20130126	*i*	N	-31.23
20130409	*b*	E	-29.41
20130409	*d*	N	-29.25
20130409	*d*	W	-29.28
20130409	*g*	E	-30.44
20130409	*i*	E	-31.69
20130501	*a*	E	-29.37
20130501	*a*	N	-29.03
20130501	*a*	S	-30.04
20130501	*a*	W	-28.97
20130501	*b*	E	-29.20
20130501	*b*	W	-29.10
20130501	*d*	E	-28.33
20130501	*d*	W	-30.61
20130501	*g*	E	-29.40
20130501	*g*	W	-29.89
20130501	*i*	E	-31.90
20130501	*i*	N	-31.25
20130517	*a*	E	-29.29
20130517	*a*	N	-29.57
20130517	*a*	S	-28.44
20130517	*a*	W	-29.15
20130517	*b*	E	-29.56
20130517	*b*	N	-29.02
20130517	*d*	S	-29.62
20130517	*d*	W	-28.16
20130517	*g*	E	-30.09
20130517	*g*	W	-29.09
20130517	*i*	E	-32.03
20130517	*i*	S	-31.86
20130619	*a*	E	-31.57
20130619	*a*	N	-29.43
20130619	*a*	S	-30.66
20130619	*b*	N	-29.40
20130619	*d*	E	-29.96
20130619	*d*	S	-28.94

20130619	*d*	W	-29.33
20130619	*i*	E	-32.01
20130619	*i*	S	-30.95
20130711	*a*	E	-29.11
20130711	*a*	N	-29.11
20130711	*a*	S	-29.53
20130711	*a*	W	-29.51
20130711	*b*	E	-29.72
20130711	*b*	N	-29.62
20130711	*d*	N	-30.03
20130711	*d*	W	-28.93
20130711	*g*	E	-30.31
20130711	*g*	W	-29.84
20130711	*i*	E	-31.38
20130711	*i*	S	-30.85
20130726	*a*	E	-29.05
20130726	*a*	N	-30.17
20130726	*a*	W	-30.07
20130726	*b*	N	-30.09
20130726	*b*	W	-29.87
20130726	*d*	N	-28.81
20130726	*d*	S	-29.52
20130726	*d*	W	-28.75
20130726	*g*	E	-30.03
20130726	*g*	N	-29.87
20130726	*i*	E	-31.37
20130815	*a*	E	-29.22
20130815	*a*	W	-30.34
20130815	*b*	E	-29.62
20130815	*g*	N	-29.99
20130815	*i*	N	-31.99
20130815	*i*	S	-32.46
20130827	*a*	E	-29.04
20130827	*a*	S	-29.56
20130827	*b*	E	-29.26
20130827	*d*	N	-28.89
20130827	*d*	S	-29.82
20130827	*g*	E	-30.57
20130827	*i*	E	-32.34
20130827	*i*	S	-31.75

Table A.2 Water stable isotopic compositions of soil water samples which were collected daily at depths of 20 cm and 50 cm on NFS and 30 cm and 50 cm on SFS, respectively. N/A for data is not available.

Sampling Date	$\delta^{18}O$ VSMOW	$\delta^{2}H$ VSMOW	$\delta^{18}O$ VSMOW	$\delta^{2}H$ VSMOW	$\delta^{18}O$ VSMOW	$\delta^{2}H$ VSMOW	$\delta^{18}O$ VSMOW	$\delta^{2}H$ VSMOW
	At NFS_20 cm	At NFS_20 cm	At NFS_50 cm	At NFS_50 cm	At SFS_30 cm	At SFS_30 cm	At SFS_50 cm	At SFS_50 cm
20130716	N/A	N/A	-0.87	-5.77	N/A	N/A	-4.03	-22.09
20130801	N/A	N/A	N/A	N/A	N/A	N/A	-5.50	-27.60
20130815	N/A	N/A	N/A	N/A	N/A	N/A	-5.66	-29.72
20130827	-3.53	-17.30	N/A	N/A	-3.41	-12.27	-5.70	-26.48
20130828	-4.57	-20.86	-4.65	-21.82	-4.55	-20.55	-5.57	-28.19
20130830	-4.82	-22.25	-4.61	-23.21	-4.75	-20.31	-5.60	-27.34
20130831	-4.80	-23.64	-4.65	-22.17	-4.87	-20.67	-5.37	-27.48
20130901	-4.90	-23.42	-4.71	-23.28	-4.73	-20.22	-5.56	-27.85
20130902	-4.82	-22.99	-4.79	-22.81	-4.70	-18.86	-5.39	-27.43
20130903	-4.91	-24.74	-4.87	-23.33	-4.66	-20.90	-5.53	-26.54
20130904	-4.95	-24.89	-4.82	-24.32	-4.63	-20.34	-5.39	-26.87
20130911	N/A	N/A	-4.74	-23.77	-4.69	-20.35	-5.46	-27.41
20130919	N/A	N/A	N/A	N/A	-4.62	-21.02	-5.45	-28.29
20130922	-4.86	-24.94	-5.03	-26.74	-4.39	-19.82	-5.35	-27.47
20131003	N/A	N/A	N/A	N/A	-4.33	-18.95	-5.33	-27.16
20131014	N/A	N/A	N/A	N/A	-4.32	-18.52	-5.36	-27.12
20131019	N/A	N/A	N/A	N/A	-4.31	-18.63	-5.40	-27.50
20131024	N/A	N/A	N/A	N/A	-4.32	-18.73	-5.39	-27.67
20131031	N/A	N/A	N/A	N/A	-4.39	-19.10	-5.45	-28.12
20131103	N/A	N/A	N/A	N/A	-4.24	-19.27	-5.31	-28.15

APPENDIX II

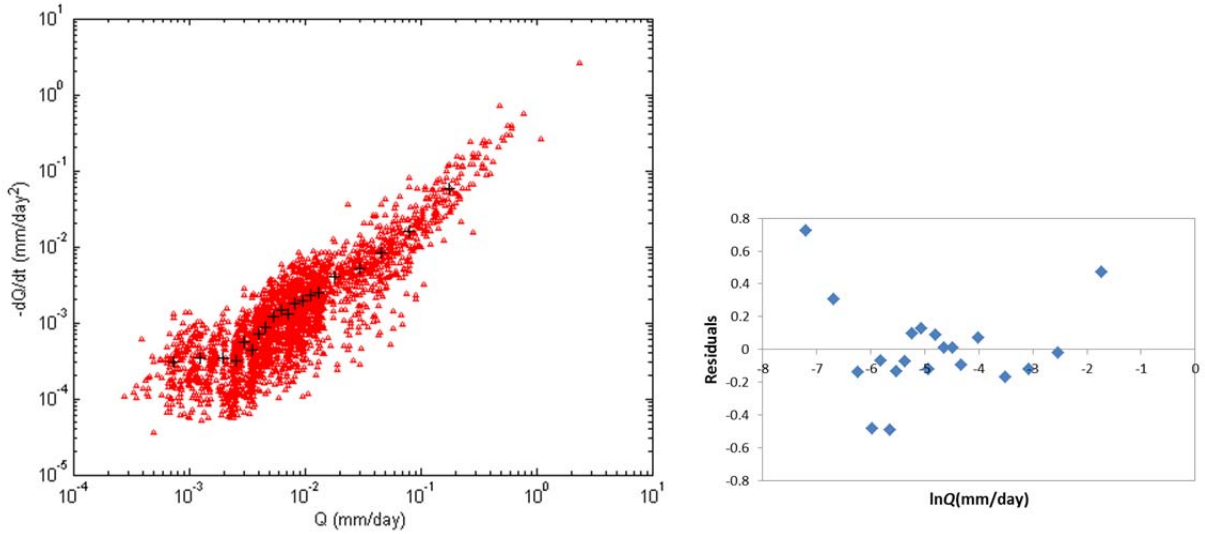

Figure A.1 Recession plot of the Finniss River catchment near Yundi (catchment 1) based on daily streamflow data of January to mid-April and mid-October to December from 1969 to 2012. Black crosses represent binned values obtained using the quantile method. Residuals are shown for the linear fit of *ln*(-d*Q*/d*t*) and *Q*.

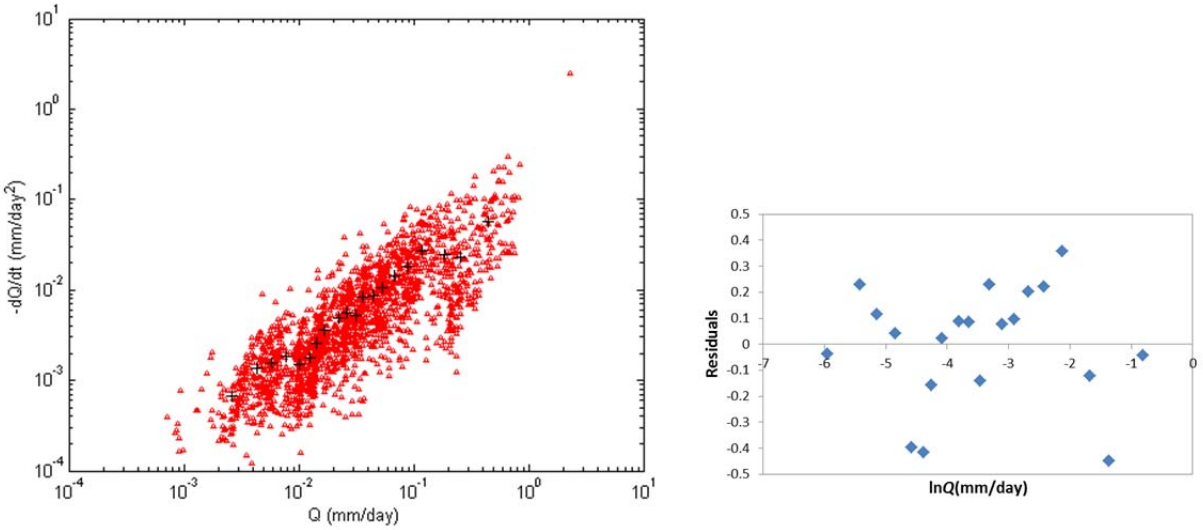

Figure A.2 Recession plot for the catchment of Hindmarsh River at Hindmarsh Valley (catchment 2) based on daily streamflow data of January to mid-April and mid-October to December from 1969 to 2012. Black crosses represent binned values obtained using the quantile method. Residuals are shown for the linear fit of *ln*(-d*Q*/d*t*) and *Q*.

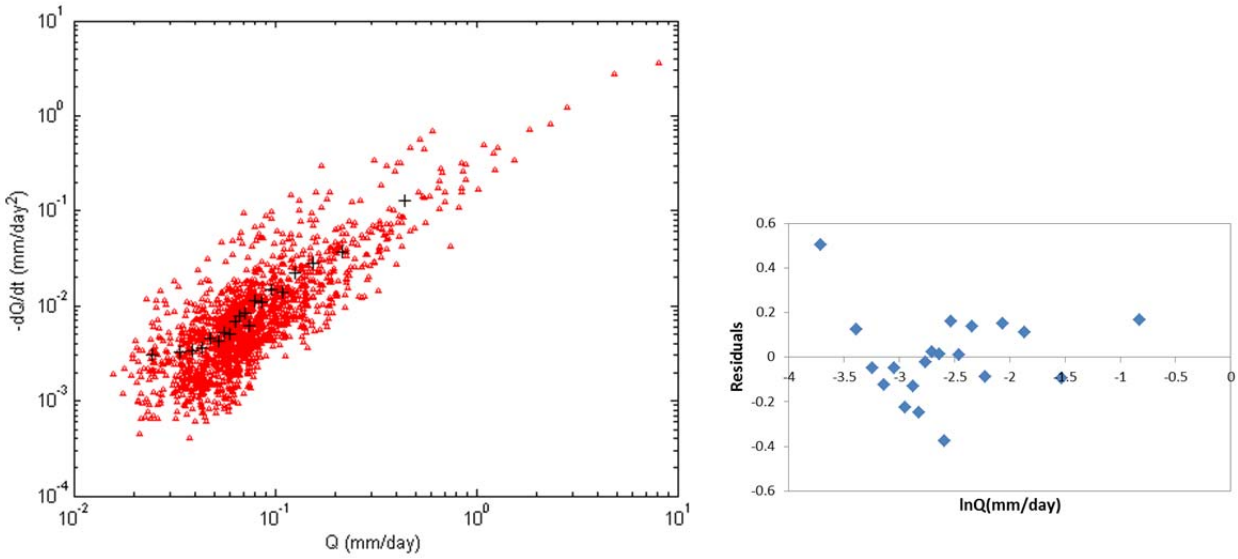

Figure A.3 Recession plot of the First Creek catchment at Waterfall Gully (catchment 4) based on daily streamflow data of January to mid-April and mid-October to December from 1977 to 2005. Black crosses represent binned values obtained using the quantile method. Residuals are shown for the linear fit of *ln*(-d*Q*/d*t*) and *Q*.

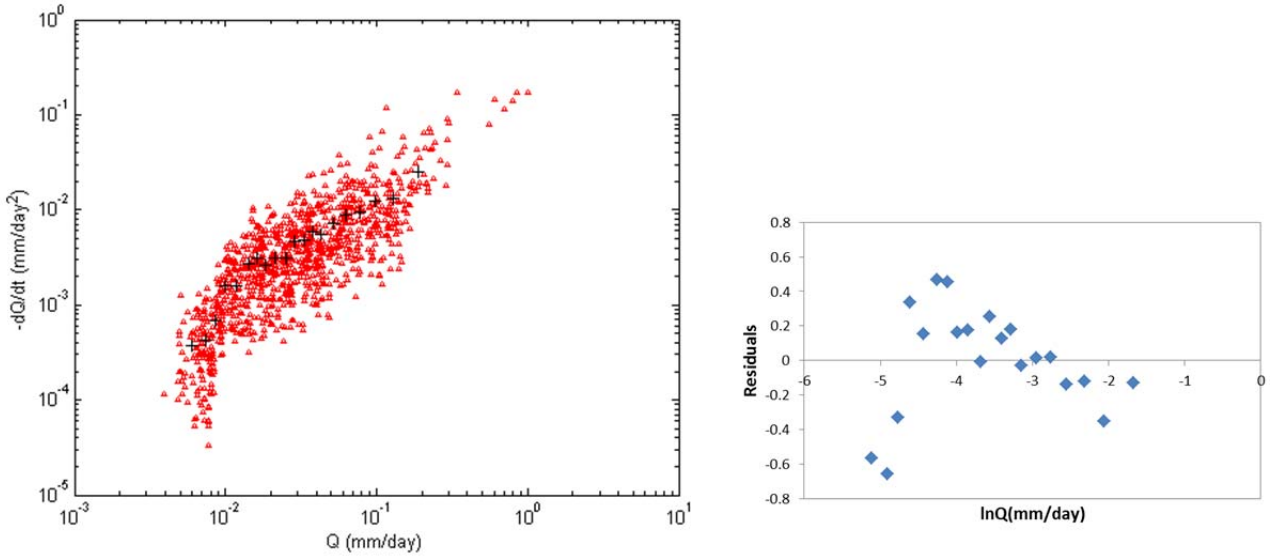

Figure A.4 Recession plot of the Chambers Creek catchment at Coromandel Valley (catchment 5) based on daily streamflow data of January to mid-April and mid-October to December from 1979 to 1988. Black crosses represent binned values obtained using the quantile method. Residuals are shown for the linear fit of *ln*(-d*Q*/d*t*) and *Q*.

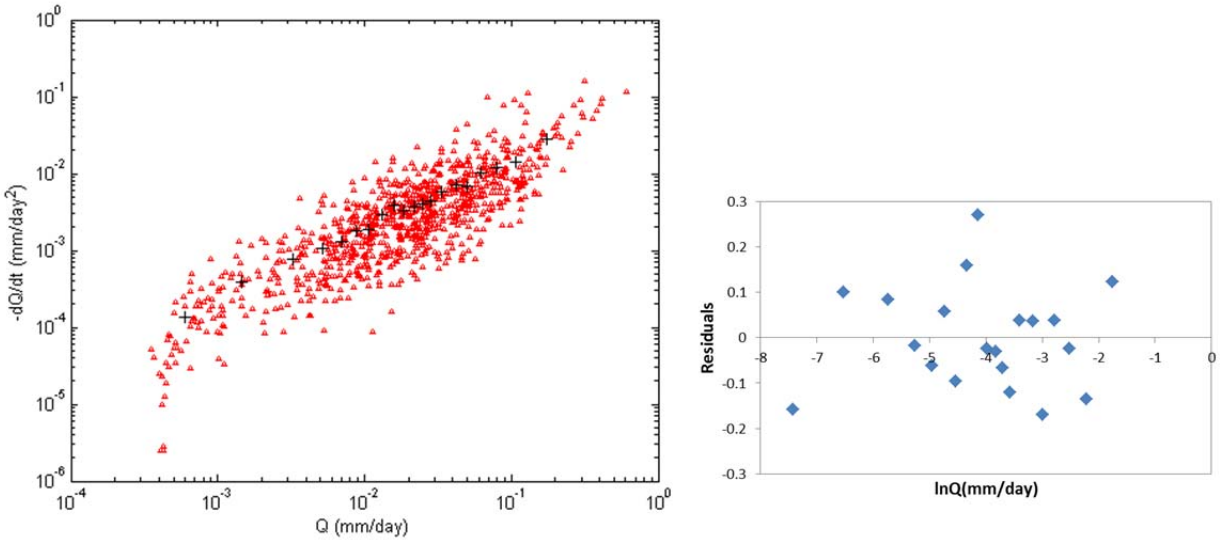

Figure A.5 Recession plot of the Chambers Creek catchment at Coromandel Valley (catchment 6) based on daily streamflow data of January to mid-April and mid-October to December from 1980 to 1988. Black crosses represent binned values obtained using the quantile method. Residuals are shown for the linear fit of *ln*(-d*Q*/d*t*) and *Q*.